

**BIOCHEMICAL CHARACTERIZATION OF NUCLEOTIDE AND  
PROTEIN INTERACTIONS OF HUMAN MULTIDRUG  
RESISTANCE PROTEIN 1 (MRP1/ABCC1)**

by

Xiaoqian Wang

A thesis submitted to the Department of Pathology and Molecular Medicine

In conformity with the requirements for  
the degree of Master of Science

Queen's University

Kingston, Ontario, Canada

(December, 2008)

Copyright ©Xiaoqian Wang, 2008

## Abstract

Multidrug resistance protein 1 (MRP1) is an integral membrane protein belonging to the ATP-binding cassette (ABC) superfamily that utilizes ATP binding and hydrolysis to transport various endogenous substrates and/or xenobiotics across membranes against a concentration gradient. The overall goal of my research was to examine the nucleotide and protein interactions of MRP1 using various biochemical methods. In the first study,  $\text{Cu}^{2+}(\text{Ph})_3$  which promotes cross-linking of two nearby Cys residues and limited proteolysis were used to study conformational changes of MRP1 at different stages of ATP binding and hydrolysis at the nucleotide binding domains (NBDs). The limited trypsin digestion patterns indicated that some Cys residues of MRP1 could be cross-linked in the nucleotide-free state and that the Cys cross-linked MRP1 was more susceptible to trypsinolysis. Furthermore, binding of ATP, AMP-PNP, and trapping of ADP by MRP1 prevented the cross-linking events from occurring, but binding of  $\text{ATP}\gamma\text{S}$  did not. However, the  $\text{ATP}\gamma\text{S}$ -bound MRP1, like nucleotide-free MRP1, showed enhanced sensitivity towards trypsinolysis. These studies show that the two ATP analogs, AMP-PNP and  $\text{ATP}\gamma\text{S}$ , interact with MRP1 in different ways. In the second study, the interaction of MRP1 with other cellular proteins was examined. An *in vivo* chemical cross-linking approach combined with affinity purification and MS analysis was initially used to identify protein partners directly interacting with MRP1. When this approach proved unsuccessful, a second approach involving immunoaffinity purification of MRP1-containing complexes followed by MS analysis was adopted. Six potential candidate interacting protein partners of MRP1 were identified via this approach and two

of them, FUS and drebrin, were further characterized by co-immunoprecipitation and colocalization experiments. FUS seems unlikely to be an important binding partner of MRP1 since confocal and subcellular fractionation studies showed it to be exclusively localized in the nucleus. On the other hand, drebrin depletion by siRNA knock-down resulted in a moderate decrease in MRP1 overall expression levels although the membrane localization of MRP1 remained unchanged.

## **Co-Authorship**

This thesis was written by the author with critical reading and corrections by Dr. Susan P.C. Cole. All of the work described within this thesis is the original work of the author under the supervision of Dr. Susan P.C. Cole, except for the mass spectrometry experiments and data analysis which were performed by Dr. Yi-min She in the Department of Chemistry (Queen's University, Kingston).

## Acknowledgements

I would like to thank my supervisor, Dr. Susan P.C. Cole, for giving me this wonderful opportunity to study with her. She has given me valuable insights and guidance in my research as well as understanding and support in everything. The whole learning and researching journey was a memorable and meaningful experience to me, and she really has had a huge influence on me. I would also like to thank my supervisory committee members, Drs. Peter A. Greer, David P. LeBrun and Roger G. Deeley, for their helpful suggestions on my project.

I would like to thank everyone in the Cole lab for providing such a warm and friendly work environment. They are always willing to offer help whenever I needed. Especially, Drs. Tozammel Hoque, Gwenaëlle Conseil and Alice Rothnie, who provided technical input and valuable insights into my research. I also thank Kathy Sparks for her patient and excellent technical assistance.

I am grateful to Dr. Yi-min She in the Department of Chemistry (Queen's University, Kingston) for his exceptional mass spectrometry work. This project would have not been possible without his help. He has not only answered all my questions about protein mass spectrometry but also offered his expertise to my research. It really has been a thought provoking experience working with him.

Last but not least, I would like to thank my parents for their unconditional love and support. They have tried their best to make sure that I have the best opportunities and happiest life. I will be forever grateful for everything they have done for me.

# Table of Contents

Abstract.....	ii
Co-Authorship.....	iv
Acknowledgements.....	v
Table of Contents.....	vi
List of Figures.....	ix
List of Tables.....	xi
List of Abbreviations.....	xii
Chapter 1 Introduction.....	1
1.1 Multidrug resistance in cancer and the discovery of MRP1.....	1
1.2 The ATP-binding cassette (ABC) superfamily.....	2
1.3 Membrane topology and structure of MRP1.....	3
1.4 Expression and localization of MRP1.....	8
1.5 Substrate profiles of MRP1.....	9
1.6 Physiological and pathological aspects of MRP1.....	12
1.7 Structure and function of NBDs of MRP1.....	14
<i>1.7.1 NBD Structure</i> .....	14
<i>1.7.2 Functional characteristics of NBDs of MRP1</i> .....	15
1.8 Proposed transport cycle of MRP1.....	19
1.9 Regulation of MRP1 expression.....	20
1.10 Protein-protein interaction studies in ABCC proteins.....	23
<i>1.10.1 CFTR and its interacting partners</i> .....	23
<i>1.10.2 Other ABCC proteins</i> .....	26

1.11 Research objectives.....	27
Chapter 2 Nucleotide-induced Conformational Changes in MRP1 .....	29
2.1 Introduction.....	29
2.2 Materials and Methods.....	32
2.2.1 Materials.....	32
2.2.2 Transfection of HEK293T Cells .....	33
2.2.3 Membrane Vesicle Preparations .....	34
2.2.4 Disulfide Cross-linking and Nucleotide Binding Assays .....	34
2.2.5 Limited Trypsin Digestion and Immunoblotting of MRP1 .....	35
2.3 Results.....	36
2.3.1 Limited Proteolysis Pattern of MRP1.....	36
2.3.2 Limited Proteolysis of MRP1 with or without Nucleotides .....	38
2.4 Discussion.....	39
Chapter 3 Identification and Characterization of Protein Interacting Partners of Human MRP1 .....	45
3.1 Introduction.....	45
3.2 Materials and Methods.....	47
3.2.1 Materials.....	47
3.2.2 Chemical Cross-linking of Cultured Cells.....	49
3.2.3 Immunoprecipitations .....	50
3.2.4 Immunoblotting and Coomassie Blue Staining .....	51
3.2.5 In-gel Digestion and Peptide Extraction .....	52
3.2.6 Mass Spectrometry Analysis and Protein Identification .....	52

3.2.7 NanoLC-ESI MS/MS Analysis and Data Processing .....	53
3.2.8 Preparation of Subcellular Fractions and Whole Cell Lysates.....	54
3.2.9 siRNA Knockdown of Drebrin .....	55
3.2.10 Confocal Fluorescence Microscopy .....	56
3.3 Results.....	57
3.3.1 In vivo chemical cross-linking of H69AR cells.....	57
3.3.2 Identification of proteins co-immunoprecipitated with MRP1 by MS.....	62
3.3.3 Protein-protein association by reciprocal co-immunoprecipitation .....	64
3.3.4 Cellular localization of FUS.....	71
3.3.5 Consequences of Drebrin siRNA knock-down .....	71
3.4 Discussion.....	77
References.....	86

## List of Figures

Figure 1.1 Sequence alignment of the NBDs of MRP1 and a cartoon representation of the NBD dimer.....	4
Figure 1.2 Dendrograms and topologies of full-length ABCC proteins.....	5
Figure 1.3 Predicted topology model and tryptic fragment pattern of human MRP1 .....	7
Figure 1.4 Chemical structures of selected substrates of MRP1 .....	10
Figure 1.5 Schematic of binding and hydrolysis cycle of ATP and vandate-induced trapping of ADP by an ATPase .....	16
Figure 1.6 Chemical structures of ATP and ATP analogs used in the present study .....	17
Figure 1.7 Proposed transport cycle of MRP1 .....	21
Figure 1.8 Molecular switches that regulate CFTR activity at the plasma membrane ....	25
Figure 2.1 Schematic illustration of endogenous Cys residues in MRP1 (ABCC1) and Pgp (ABCB1).....	31
Figure 2.2 Immunoblots of limited trypsin digests of wild-type MRP1 chemically cross-linked in the absence and presence of nucleotides.....	37
Figure 3.1 Schematic outlining experimental approach of identifying interacting protein partners of MRP1 .....	48
Figure 3.2 Reaction scheme of NHS-ester and chemical structure of NHS-ester cross-linkers.....	58
Figure 3.3 <i>In vivo</i> cross-linking of H69AR cells with DSP.....	60
Figure 3.4 Immunoaffinity purification of MRP1 and potential interacting proteins from H69, H69AR, and H69AR cells treated with DSP .....	61

Figure 3.5 SDS-PAGE and Coomassie staining of proteins obtained by co-immunoprecipitation with MRP1 .....	63
Figure 3.6 MALDI-MS spectrum of drebrin E tryptic fragments .....	65
Figure 3.7 Co-immunoprecipitations of MRP1 and potential interacting proteins in H69 and H69AR cells .....	69
Figure 3.8 Co-immunoprecipitations of MRP1 and its potential interacting proteins in H69 and H69AR cell lysates containing 1% Triton X-100 .....	70
Figure 3.9 Domain structures of FUS, and drebrin E and A proteins.....	72
Figure 3.10 Subcellular localization of FUS in various MRP1 expressing cell lines.....	73
Figure 3.11 Expression of MRP1 in H69AR cells treated with drebrin siRNA .....	75
Figure 3.12 MRP1 expression and localization in H69AR cells treated with drebrin siRNA .....	76

## List of Tables

Table 3.1 Summary of LC- MS/MS analysis of proteins co-immunoprecipitated with

MRP1 ..... 66

## List of Abbreviations

ABC	ATP-binding cassette
ABCC	ATP-binding cassette C subfamily transporters
ACN	acetonitrile
AMP-PNP	5'-adenylyl- $\beta$ - $\gamma$ -imidodiphosphate
ATP $\gamma$ S	adenosine-5'- <i>O</i> -(3-thiotriphosphate)
ATR-FTIR	attenuated total reflection-Fourier transform infrared
BSA	bovine serum albumin
CHAPS	3-[(3-cholamidopropyl)-dimethyl- ammonio]-1-propane sulfonate
CFTR	cystic fibrosis transmembrane conductance regulator (ABCC7)
CL	cytoplasmic loop
CLL	chronic lymphoblastic leukemia
Cx43	connexin-43
DAPI	4',6-diamidino-2-phenylindole dihydrochloride
DCC	diphenylcarbonyl chloride
DMEM	Dulbecco's modified Eagle medium
DOX	doxorubicin
DSP	dithiobis (succinimidyl propionate)

DSS	disuccinimidyl suberate
DTT	dithiothreitol
E <sub>2</sub> 17βG	β-estradiol 17-(β-D-glucuronide)
ER	endoplasmic reticulum
FBS	fetal bovine serum
FUS	fusion protein
GSH	reduced glutathione
GSSG	glutathione disulfide
GS-X	glutathione conjugate
HA	hemagglutinin A
HEK	human embryonic kidney cell
IP	immunoprecipitation
LC	liquid chromatography
LTC <sub>4</sub>	leukotriene C <sub>4</sub>
mAb	monoclonal antibody
MDR	multidrug resistance
MRP1	multidrug resistance-associated protein 1 (ABCC1)
MALDI-TOF	matrix-assisted laser desorption ionization time-of-flight
MS	mass spectrometry

MSD	membrane spanning domain
MudPIT	multidimensional protein identification technology
NBD	nucleotide binding domain
NBS	nucleotide binding site
NEM	<i>N</i> -ethylmaleimide
NSCLC	non-small cell lung cancer
PBS	phosphate buffered saline
Pgp	P-glycoprotein (ABCB1)
PMSF	phenylmethylsulfonyl fluoride
ROS	reactive oxygen species
SCLC	small cell lung cancer
SCX	strong cation exchange
SDS-PAGE	sodium dodecyl sulfate-polyacrylamide gel electrophoresis
SUR	sulfonylurea receptor (SUR1/ABCC8 and SUR2/ABCC9)
TM	transmembrane
TSB	Tris-sucrose buffer
Vi	vanadate

## **Chapter 1 Introduction**

### **1.1 Multidrug resistance in cancer and the discovery of MRP1**

Chemotherapy is a common strategy used in the treatment of malignant tumors. However, successful drug treatment in cancer patients is often confounded by the acquisition of chemoresistance by the tumor cells. Multidrug resistance (MDR) can be induced *in vitro* by repeatedly exposing tumor cells to a single chemotherapeutic drug, such as doxorubicin (DOX) (which targets topoisomerase II) or docetaxel (which targets tubulin). Frequently, the cells become resistant to not only the original drug used for selection but also to other structurally and functionally unrelated agents [1]. Patients with certain types of cancer, such as non-small cell lung cancer (NSCLC) [2] and chronic lymphoblastic leukemia (CLL) [3], show intrinsic or natural resistance to many chemotherapy agents. In contrast, some tumors, such as small cell lung cancer (SCLC) [4] and gastric carcinoma [5], are initially sensitive to chemotherapy but then acquire resistance after extensive drug treatments.

The very first membrane transporter shown to be directly associated with the emergence of a drug resistant phenotype was identified in several drug-selected Chinese hamster ovary cell lines in 1976 [6]. This 170 kDa cell surface glycoprotein, named P-glycoprotein (Pgp), was further characterized as an energy-dependent efflux pump that actively transports various xenobiotics (including many anticancer drugs) out of cells by utilizing the energy from ATP binding and hydrolysis [7].

Pgp remained the only known multidrug efflux transporter responsible for MDR until the late 1980s. At that time, a human SCLC cell line (NCI-H69) variant obtained by culture in gradually increasing doses of DOX displayed a MDR phenotype without increased expression of Pgp [8, 9]. This MDR variant of NCI-H69, designated H69AR, not only showed resistance to DOX but was also cross-resistant to a broad range of anticancer drugs, including anthracycline analogues, *Vinca* alkaloids and epipodophyllotoxins [9, 10]. This non-Pgp-mediated MDR phenomenon was subsequently found to be associated with a novel membrane protein, named multidrug resistance protein 1 (MRP1), which was cloned from H69AR cells in 1992 [11]. This finding not only confirmed that drug resistance could occur in a Pgp-independent manner, but also facilitated the subsequent discovery of a whole new family of membrane proteins, namely the MRP-related transporters, with significant physiological, pharmacological and pathological roles [12].

## **1.2 The ATP-binding cassette (ABC) superfamily**

The ATP-binding cassette (ABC) superfamily proteins are characterized by three highly conserved motifs found in their cytoplasmic nucleotide binding domains (NBDs). The Walker A motif (with consensus sequence *GXXGXGK(S/T)* where *X* can be various amino acids), and the Walker B motif (with consensus sequence *HHHHD(E/D)* where *H* is a hydrophobic residue) are found in many ATPases and they have been demonstrated to be essential for binding and hydrolysis of ATP [13-15]. In addition, ABC proteins possess a unique ABC signature sequence LSGGQ (known as 'C' signature), which is

just upstream of the Walker B motif (Fig. 1.1A) [14]. ABC proteins that carry out very diverse cellular functions can be found in organisms ranging from prokaryotes to humans [16].

The human ABC superfamily is now known to be comprised of 48 genes and these have been classified into 7 subfamilies (ABCA to ABCG) [17]. The ABC C subgroup consists of 12 members, including MRP1 through MRP9, the cystic fibrosis transmembrane conductance regulator (CFTR/ABCC7) and two sulfonylurea receptors (SUR1/ABCC8 and SUR2/ABCC9) (Fig. 1.2). Almost all of the MRPs (except MRP9) have been associated with drug resistance, at least *in vitro*, by the demonstration that they can transport certain types of endo- and xenobiotics across membranes [18]. However, three ABCC proteins are not directly involved in active transport. Thus CFTR functions as a cAMP regulated chloride ion channel that mediates the transepithelial salt and water transport down a concentration gradient [19]. The SURs are regulators of the inwardly rectifying K<sup>+</sup> channels Kir6.2 and Kir6.1 that couple changes in plasma glucose concentration to insulin release [20].

### **1.3 Membrane topology and structure of MRP1**

MRP1 contains 1,531 amino acids and the fully glycosylated form has an apparent molecular weight of 190 kDa. The initial computer-assisted analysis of the predicted sequence of MRP1 revealed that this protein consists of multiple transmembrane (TM) helices and two cytoplasmic domains containing the ABC motifs [11]. Subsequent biochemical studies, such as identification of utilized *N*-glycosylation

**Figure 1.1: Sequence alignment of the NBDs of MRP1 and a cartoon representation of the NBD dimer.** (A) The amino acid sequence alignment of NBD1 and NBD2 of human MRP1 was performed using ClustalW2 (EBI). The Walker A and Walker B sequences are highlighted in grey whereas the C signature motif is in bold. The Q-, D- and H-loops are underlined, and conserved Q, D and H residues are in boldface and italics. The catalytic base Glu (E) is indicated by an arrow. The consensus sequences of Walker A, Walker B and 'C' signature motifs are shown underneath the sequence alignment. (B) The cartoon representation of the closed NBD dimer. Each NBS consists of Walker A motif ( $W_A$ ) and Walker B motif ( $W_B$ ) from one NBD together with the 'C' signature motif from the other NBD. The Q-, D- and H-loops are in white and italics. NBS1 is considered as 'non-consensus' due to the lack of catalytic Glu residue from Walker B of NBD1 as well as the presence of non-conserved 'C' signature motif from NBD2.

# A

		Walker A		Q-Loop
NBD1	672	ALVAVVGQVGC	SSLLSALLAEMDKVEGHVAIKGS-----	VAYVPPQAWIQNDSLRENILFGCQLEE
NBD2	1321	EKVGIVGRTGAGKS	SLTLGLFRINESAEGEIIIDGINIAKIGLHDLRFKITIIP	QDPVLFSGSLRMNLDPFSQYSD
Consensus		GXXGXGKS		
		C signature		Walker B D-Loop
NBD1	735	PYYRSVIQACALLPDLEILPSGDRTEIGEKGVN	<b>LSGGQ</b> KQRVSLARAVYSNADIYLFDDPLSAVD	DAHVGKHIFENV
NBD2	1397	EEVWTSLELAHLKDFVSALPKLDHECAEGGEN	<b>LSVGQ</b> RQLVCLARALLRKT	ILVLDEATAAVDLETDDLIQSTI
Consensus		LSGGQ HHHHD↑		
		H-Loop		
NBD1	810	IGPKGMLKNKTRILV	<b>TH</b> SMSYLPQVDVIIVMSGGKISEMGSYQELLARDGAFAEFLRITYAST	
NBD2	1474	R---TQFEDCTVLTIA	<b>HR</b> LNTIMDYTRVIVLTKGEIQEYGAPSDLLQQRGLFYMAKDAGLV	

# B

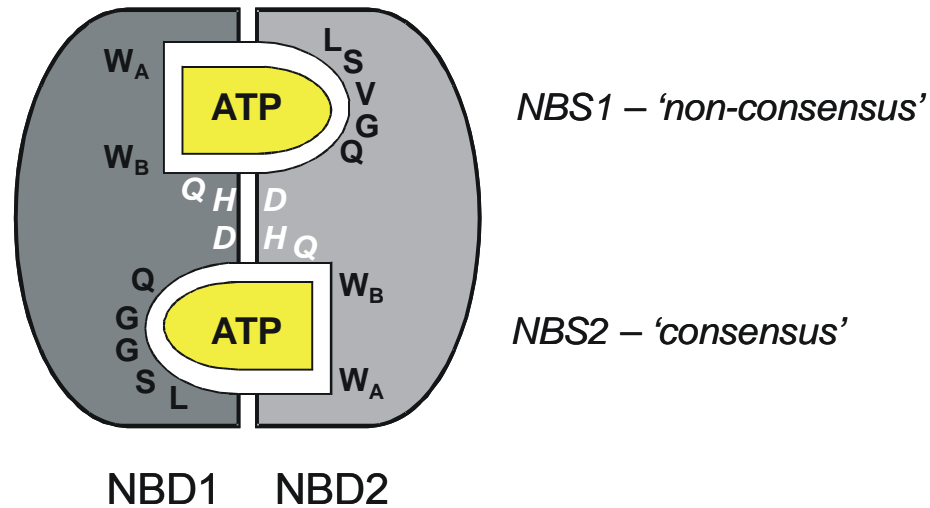


**Figure 1.2: Dendrograms and topologies of full-length ABCC proteins. (A)**

Dendrogram representation of the relative similarities among members of the ABCC subfamily based on the sequence alignment of full-length proteins using ClustalW2

(EBI). Swiss-Prot accession numbers: MRP1/ABCC1, P33527; MRP2/ABCC2, Q92887;

MRP3/ABCC3, O15438; MRP4/ABCC4, O15439; MRP5/ABCC5, O15440;

MRP6/ABCC6, O95255; CFTR/ABCC7, P13569; SUR1/ABCC8, Q09428;

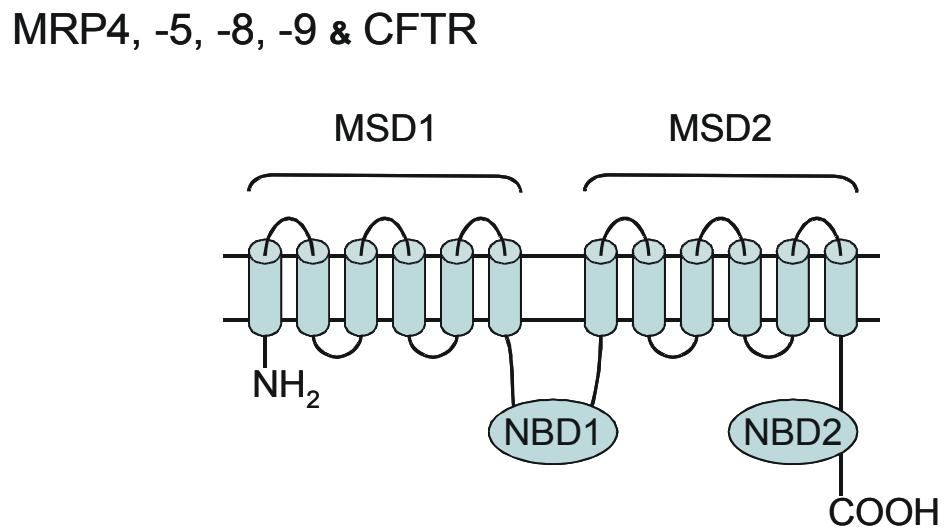
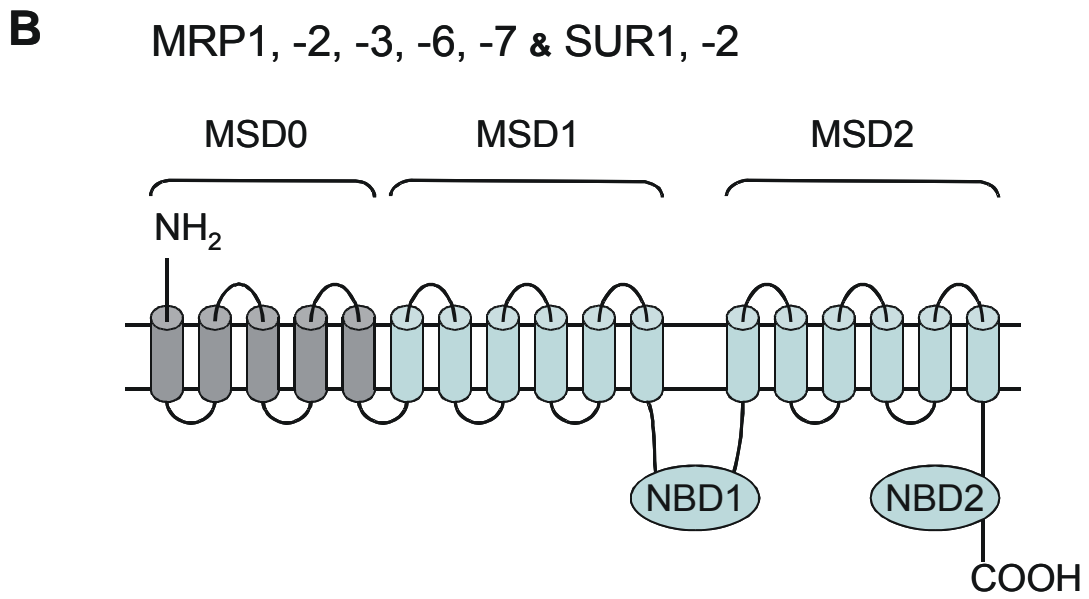
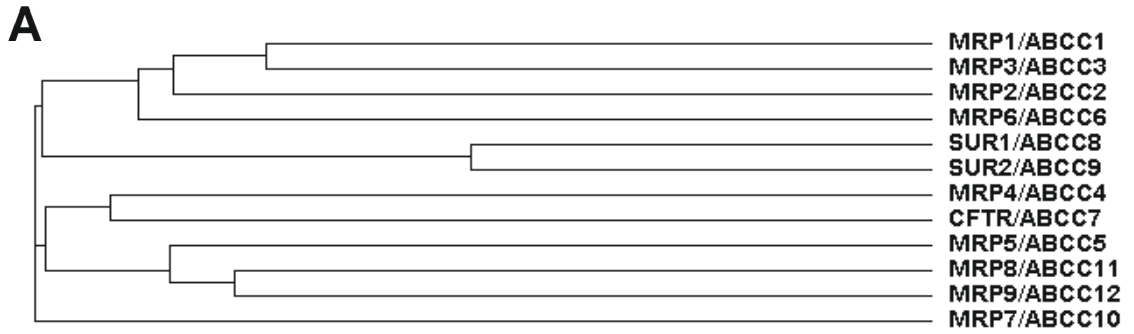
SUR2/ABCC9, O60706; MRP7/ABCC10, Q5T3U5; MRP8/ABCC11, Q96J66;

MRP9/ABCC12, Q96J65. (B) Topology of long and short ABCC proteins. Long ABCC

proteins (MRP1, -2, -3, -6, -7 and SUR1, -2) have three polytopic MSDs and two NBDs.

Short ABCC proteins (MRP4, -5, -8, -9 and CFTR) have only two polytopic MSDs and

two NBDs.



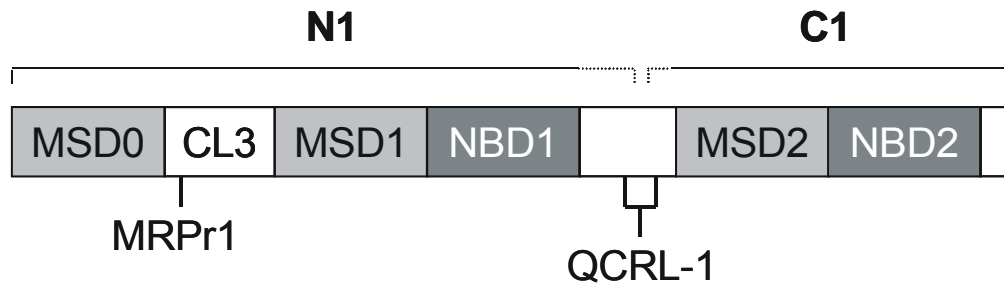
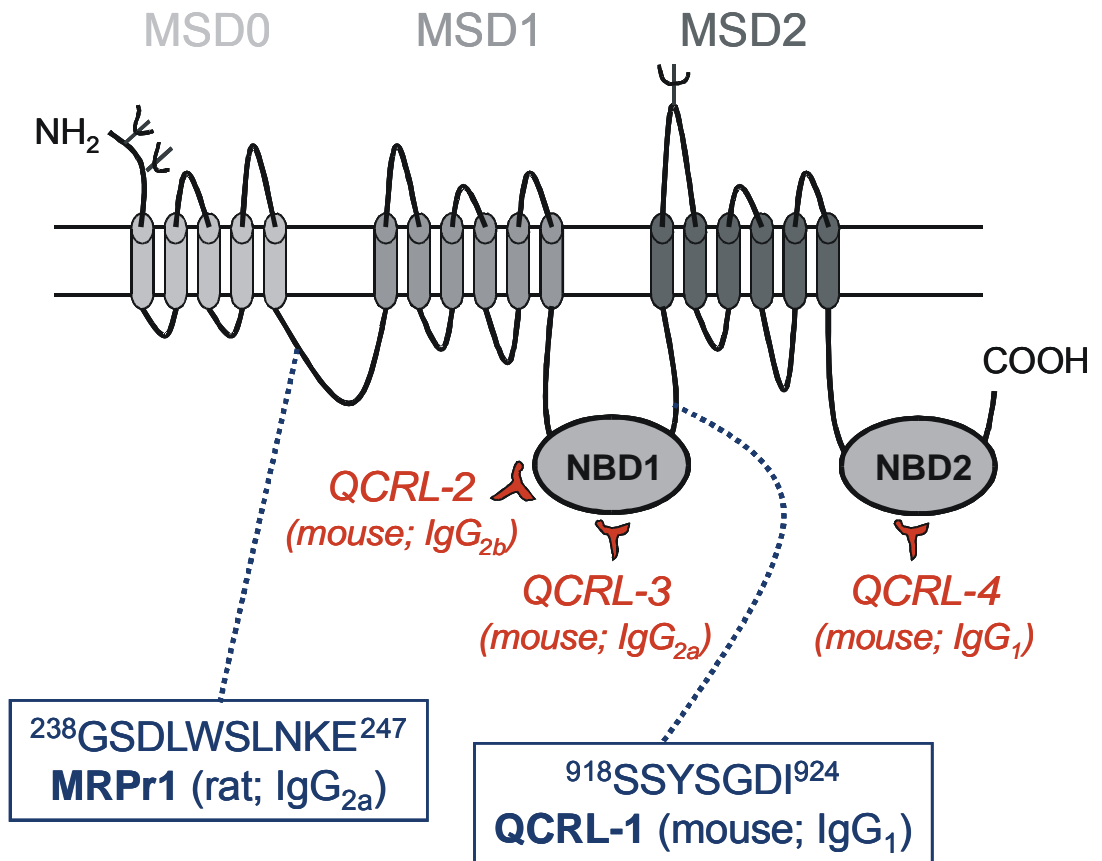
sites [21, 22], epitope mapping of MRP1-specific monoclonal antibodies (mAb) [23-26], and hemagglutinin A (HA) epitope insertion analyses [27, 28], are consistent with an overall membrane topology of 17 TM helices arranged into three polytopic membrane spanning domains (MSD) and two cytosolic NBDs (Fig. 1.3B).

In addition to the conventional 4-domain core structure of an ABC protein (NH<sub>2</sub>-MSD-NBD-MSD-NBD-COOH), MRP1 (a so-called 'long' MRP) has an extra NH<sub>2</sub>-terminal domain comprising five TM helices with an extracellular NH<sub>2</sub>-terminus [21, 22]. The functional significance of this additional MSD, which is now designated MSD0, is currently unknown. However, several studies have shown that deletion of MSD0 has no effect on protein trafficking to the plasma membrane of mammalian cells and is not required for the transport of some MRP1 substrates (e.g., leukotriene C<sub>4</sub> (LTC<sub>4</sub>)) [29, 30]. Instead, cytoplasmic loop 3 (CL3) which links MSD0 to MSD1 contains a sequence between Cys<sup>208</sup> and Lys<sup>270</sup> that is critical for MRP1 trafficking and activity [31, 32].

The first but very limited set of 3D structural data for MRP1 was obtained at 22 Å resolution by electron microscopy of single particles of the purified protein [33]. The MRP1 monomer, similar to CFTR [34] and Pgp [35], showed a 2-fold pseudosymmetry with a ring of protein around a 35 Å diameter pore. This may correspond to the substrate translocation "pore" of MRP1 [33]. Atomic models of MRP1 (i.e., the core structure lacking MSD0) [36] have been derived by comparative homology modeling using the crystal structure of a bacterial ABC transporter (Sav1866) from *Staphylococcus aureus* at 3.0 Å resolution as template [37]. The homology models are in an ADP-bound conformation in which the transporter is open to the extracellular space (another crystal

**Figure 1.3: Predicted topology model and tryptic fragment pattern of human**

**MRP1.** (A) Schematic representation of MRP1 fragments generated by limited trypsin proteolysis [23]. (B) Predicted secondary structure of human MRP1 based on various computer-assisted algorithms and considerable experimental data. In this model, the protein has 17 predicted TMs that are organized into three MSDs. The two cytoplasmic NBDs are responsible for binding and hydrolyzing ATP. The three “tree” symbols indicate the utilized *N*-glycosylation sites at Asn<sup>19</sup>, Asn<sup>23</sup> and Asn<sup>1006</sup> [22]. The locations of the epitopes of five MRP1 specific mAbs (isotypes indicated) are shown. mAbs MRPr1 [24] and QCRL-1 [23] recognize linear epitopes (sequence indicated) where as mAbs QCRL-2, QCRL-3 and QCRL-4 recognize conformational epitopes within the two NBDs [25].

**A****B**

structure has been reported for Sav1866 in complex with AMP-PNP, but the two structures are virtually identical with only minor conformational differences at the NBDs [38]). The 12 TM helices exhibit considerable twist and each NBD is in contact with the opposite MSD (i.e., NBD1-MSD2; NBD2-MSD1) [36]. Sav1866 is a homodimeric multidrug exporter that shows significant sequence similarity to human ABC transporters of the B subfamily (Pgp NBD1 is 50% identical to the Sav1866 NBD; Pgp MSD1 is 16% identical plus 19% similar and Pgp MSD2 is 15% identical plus 20% similar to the Sav1866 MSD [39]), and the Sav1866 structure is consistent with cysteine (Cys)-scanning mutagenesis and chemical cross-linking data for Pgp (ABCB1) [39, 40]. The Sav1866 monomer has approximately 22% sequence identity to MSD1-NBD1 (amino acids 300-871) and MSD2-NBD2 (amino acids 971-1531) of MRP1 [36]. However, similar tertiary structures are likely to be conserved among these large transmembrane ABC exporters. Therefore, the homology models provide possible dispositions of the 12 TM helices and 2 NBDs of the core structure of MRP1.

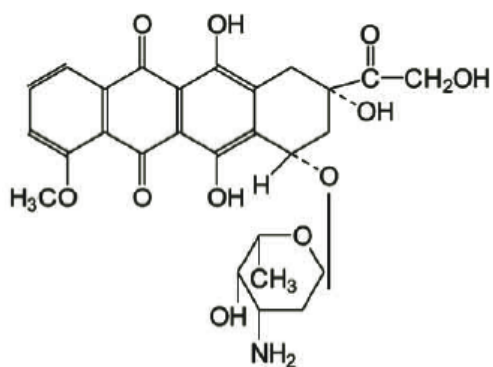
#### **1.4 Expression and localization of MRP1**

MRP1 is ubiquitously expressed in all tissues in the body with high levels of expression reported in lung, testis, kidney, placenta, and cardiac muscles [11, 41, 42]. MRP1 is barely detectable in normal human liver; however, its expression is elevated during liver regeneration and in some severe liver diseases, such as primary biliary cirrhosis, chronic hepatitis C virus infection and submassive cell necrosis [43, 44].

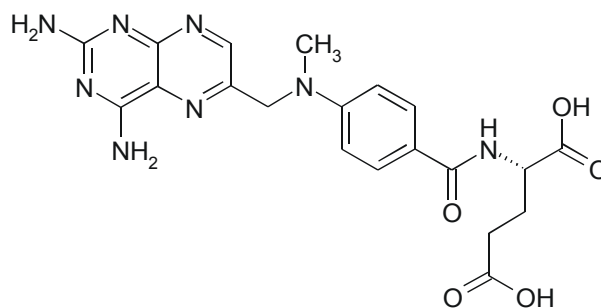
Immunocytochemical studies have demonstrated that MRP1 is predominantly localized on the basolateral membrane of polarized cells, including transfected cells and in normal tissue samples [42-47]. However, MRP1 is reported to localize to the apical membrane of the brain capillary endothelial cells in adult human brain tissue samples [48] and primary cultured bovine brain cells [49]. This suggests that MRP1 may limit the entry of various endogenous organic anions and xenobiotics to the brain. Moreover, MRP1 protein is also present in various physiological barriers, including the blood-brain barrier [48], blood-cerebrospinal fluid barrier [48], the placenta [42], and the blood-testis barrier [41]. With the exception of blood-brain barrier, MRP1 is expressed in the basolateral membrane of these physiological barriers [41, 42, 48]. MRP1 is believed to contribute to the barrier function and protect various 'sanctuary' sites by extruding toxic compounds back into the bloodstream.

### **1.5 Substrate profiles of MRP1**

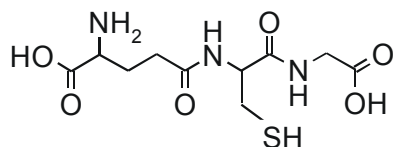
Initially, the substrate specificities of MRP1 were examined by *in vitro* drug accumulation assays, which revealed many anticancer drugs as substrates of MRP1, such as anthracycline, plant alkaloids, methotrexate and certain heavy metal oxyanions (Fig. 1.4) [8-11, 50]. Later on, many endogenously formed organic anion substrates of MRP1 were discovered by vesicular transport experiments. Many of these are glutathione (GSH), glucuronate, and sulfate conjugates (Fig. 1.4) [51, 52]. The GSH-conjugated pro-inflammatory mediator LTC<sub>4</sub> [53] and the cholestatic estrogen conjugate  $\beta$ -estradiol 17-( $\beta$ -D-glucuronide) (E<sub>2</sub>17 $\beta$ G) [54] are two well-known substrates for MRP1 and are



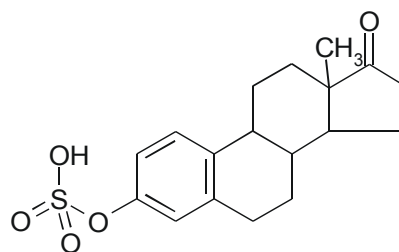
Doxorubicin



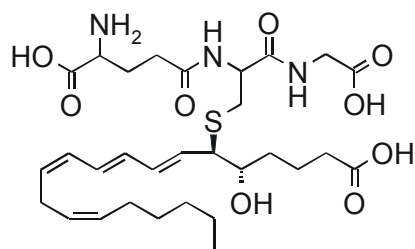
Methotrexate



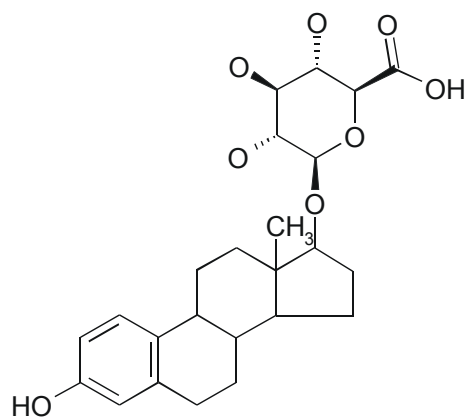
Glutathione (GSH)



Estrone 3-sulfate



Leukotriene C<sub>4</sub>



$\beta$ -estradiol 17-( $\beta$ -D-glucuronide)

Figure 1.4: Chemical structures of selected substrates of MRP1.

commonly used in standard vesicle transport assays *in vitro*. Thus MRP1 is a conjugated organic anion transporter as well as a multidrug transporter.

The mechanisms of substrate transport are rather complicated in MRP1. Some drug substrates, such as vincristine and mitoxantrone, are effluxed through a co-transport or reciprocal-stimulated mechanism with GSH [55, 56]. In other circumstances, GSH can stimulate substrate transport (e.g., estrone 3-sulfate ( $E_13SO_4$ ), 4-(methylnitrosamino)-1-(3-pyridyl)-1-butanol-*O*-glucuronide (NNAL-*O*-gluc) and glutathionyl-quinolineoxide (QO-SG)) without itself being transported [57-59]. GSH itself is a relatively poor substrate for MRP1, but its transport can be enhanced by some xenobiotics, such as verapamil and apigenin, by increasing the apparent affinity of the transporter for GSH [60, 61]. Lastly, some substrate transport by MRP1, such as the antifolate methotrexate and  $E_217\beta G$ , occurs independently of GSH [54, 62]. Techniques, such as photoaffinity labeling with radioactive substrates and nucleotides together with site-directed mutagenesis, have been used extensively to determine regions that are important for substrate binding and transport activity. However, there are still a lot of unanswered questions regarding the substrate selectivity and translocation pathway, such as the number and exact region of substrate binding and/or modulating site(s), as well as the translocation mechanism for substrates moving from one side of the membrane to the other.

## 1.6 Physiological and pathological aspects of MRP1

The contribution of MRP1 to the protection of normal mammalian tissues has been investigated in knockout mice. *Mrp1/Abcc1*-deficient mice generated independently by two groups were found to be both viable and fertile indicating that this transporter is not essential to life [63, 64]. *Mrp1*<sup>-/-</sup> mice show an impaired LTC<sub>4</sub>-mediated inflammatory response, presumably due to a reduced secretion of LTC<sub>4</sub> from mast cells during inflammation, which confirms that LTC<sub>4</sub> is an endogenous substrate for MRP1 [64]. Furthermore, these mice are hypersensitive to the damaging effects of etoposide in tissues that normally express high levels of *Mrp1*, such as the bone marrow, the epithelium of the oropharynx, the testicular tubules, and the urinary-collection duct cells [64, 65]. The predominantly basolateral membrane location of MRP1 protein contrasts with the apical membrane localization of other ABC transporters, such as Pgp [66], MRP2 [67], ABCG2 [68], which is thought to be crucial in tissue defense. Therefore, MRP1 likely protect these vital organs against endo- and xenobiotics through a basolateral cellular defense mechanism rather than the elimination of the metabolites from the body through the urine or bile [47].

MRP1 also exports antioxidant GSH and the pro-oxidant GSSG, and thus it may play a role in regulating cellular GSH/GSSG homeostasis. Studies have shown that the cellular GSH levels are decreased in at least some cell lines overexpressing MRP1 [69], whereas increased levels of GSH are observed in tissues of *Mrp1*<sup>-/-</sup> mice that normally have high levels of the protein [63]. Furthermore, the levels of MRP1 in certain tissues can be enhanced upon exposure to some agents that induce oxidative stress [70]. This

presumably is one of the cell's mechanisms of self-defense since MRP1 can efflux the toxic lipid peroxidation products (e.g., 4-hydroxynonenal-GS) that are formed during periods of oxidative stress [71]. Taken together, MRP1 seems to have multiple functions in cells, and not only plays a role in mediating inflammatory responses involving LTC<sub>4</sub> but also has a role in protecting cells from chemical toxicity and oxidative stress.

Clinical MDR is studied by analyzing the tissue samples from cancer patients. Increased expression of MRP1 has been reported in a wide range of solid and hematological tumors, such as lung, breast, prostate, as well as leukemia and childhood neuroblastoma [2-4, 72-77]. MRP1 is often overexpressed in NSCLC, and its expression has been shown to be predictive of poor response to chemotherapy and poor overall survival [72, 73]. MRP1 expression also correlates with relapse and the reduction in overall survival in breast cancer [74] and neuroblastoma [77].

Direct evidence for a causative role of MRP1 in clinical drug resistance has to date been difficult to prove, which may be due to several factors. First, apart from MRP1 (ABCC1), two other ABC transporters, Pgp (ABCB1) and breast cancer resistance protein (BCRP/ABCG2), have been demonstrated to contribute to MDR in tumors, and they often are co-expressed in many cancer types [78]. Secondly, the mechanisms of MDR found in tumor cells are indeed multifactorial, and can involve alterations in drug uptake, drug detoxification processes, DNA damage repair systems, and apoptosis pathways [79]. Thirdly, variations in clinical validation (e.g., tissue processing methodologies, detection methods and scoring criteria) contribute to the difficulty of uncovering the mechanisms of MDR for these multidrug transporters in clinical tumors.

## 1.7 Structure and function of NBDs of MRP1

### 1.7.1 NBD Structure

The high resolution crystal structures of both dimeric NBDs of Rad50 from *Pyrococcus furiosus* [80] and the complete bacterial ABC transporter Sav1866 [37] reveal that the two ATP-binding sites are very close together when nucleotide is bound, and each ATP-binding site is made up of residues from both NBDs. The two NBDs present in a 'head-to-tail' arrangement, and each nucleotide binding site (NBS) is composed of the Walker A and Walker B motifs from one NBD together with the 'C' signature motif from the other NBD (Fig. 1.1B) [37, 80-82]. Other than the two Walker motifs and ABC signature motif, the Q, D and H loops are also remarkably conserved among all ABC transporters (Fig. 1.1A) [83]. Furthermore, the crystal structures of NBDs from a number of bacterial ABC proteins reveal a conserved fold in each NBS. ATP binding is mainly stabilized by interactions of the three phosphate groups with residues of the Walker A motif [84]. Highly conserved serine (Ser) and glycine (Gly) residues from the 'C' motif also contact the  $\gamma$ -phosphate, but only in the dimeric ATP-bound state [85]. Both the terminal aspartate (Asp) in the Walker B motif and the glutamate (Glu) immediately following the Walker B motif coordinate the  $Mg^{2+}$  ion through water [81, 82, 86, 87]. The Q loop contains a highly conserved glutamine (Gln) that binds to the  $Mg^{2+}$  ion and the attacking water, and is thought to have an important role in coupling hydrolysis to transport [82, 87]. The Asp and Histidine (His) in the D and H loop, respectively, stabilize the nucleotide through the contact of water [82, 85].

### *1.7.2 Functional characteristics of NBDs of MRP1*

The ATP binding and hydrolysis characteristics of the individual NBSs of MRP1 have been investigated using various radioactive and non-radioactive ATP and ATP analogs [88-96]. The individual steps of the catalytic cycle have been characterized under different conditions (Fig. 1.5) [97]. ATP analogs, such as AMP-PNP (nonhydrolyzable) and ATP $\gamma$ S (poorly hydrolyzable) (Fig. 1.6), are commonly used instead of the more labile ATP to study the nucleotide binding properties of various ATPases during the pre-hydrolysis steps of their catalytic cycle [90, 98]. The transition state of an ATPase during ATP hydrolysis can be examined by “trapping” ADP in the protein. This involves the use of a phosphate-mimicking anion, orthovanadate, where the geometry of such ADP-trapped protein complexes is thought to resemble that of the transient transition state complex (MRP1·Mg·ADP·Pi) [99, 100]. ATPases such as Pgp and MRP1 are trapped in an inhibitory complex state and their catalytic cycle and transport process is arrested at the post-ATP hydrolysis state [88, 100].

The NBDs of all ABC transporters share extensive amino acid sequence identity. However, some structural features present in the NBDs of MRP1 and related ABCC transporters (e.g., CFTR/ABCC7) are different from proteins in other subfamilies of ABC proteins (e.g., Pgp/ABCB1). The two NBSs of MRP1 have been proven to be functionally non-equivalent and the transport requires both NBSs to be functional [88-96]. The photolabeling of MRP1 by 8-azido- $[\gamma^{32}\text{P}]$ ATP and 8-azido- $[\alpha^{32}\text{P}]$ AMP-PNP occurred predominantly at NBS1 whereas trapping of 8-azido- $[\alpha^{32}\text{P}]$ ADP in the presence of orthovanadate occurs predominantly at the more hydrolytically active NBS2 [88-96].

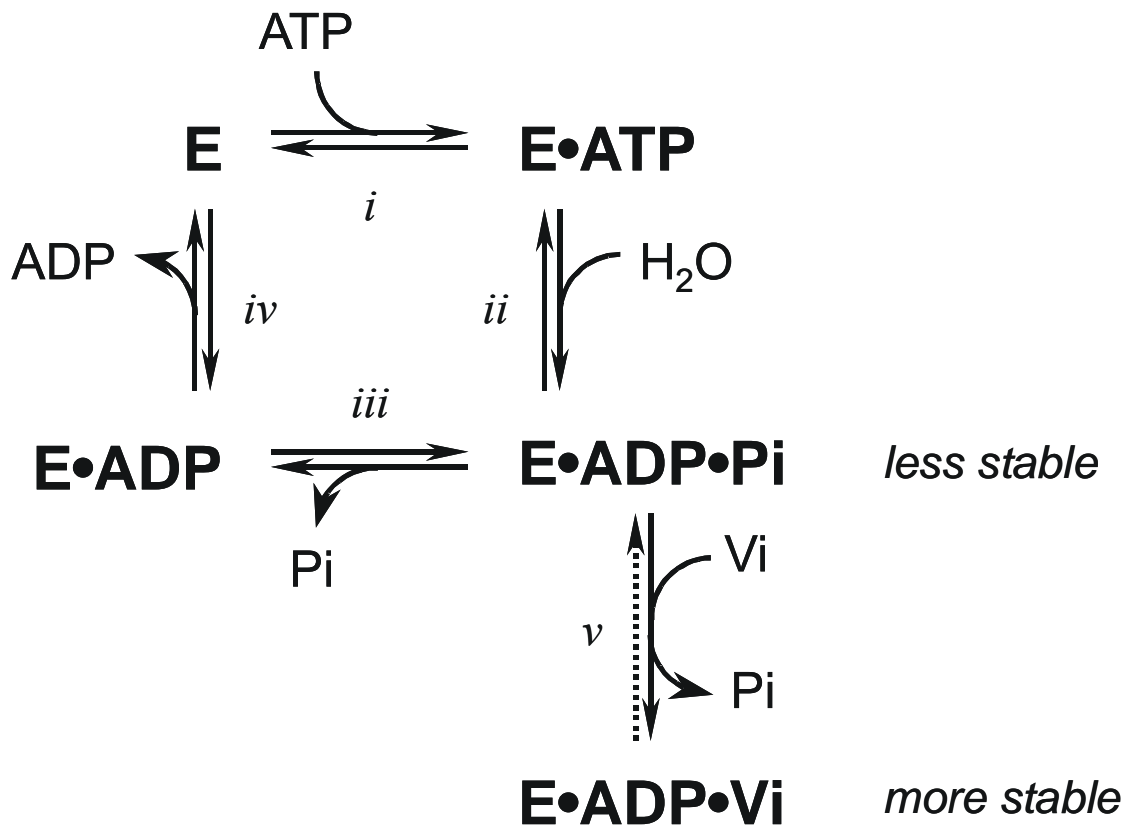


**Figure 1.5: Schematic of binding and hydrolysis cycle of ATP and vandate-induced trapping of ADP by an ATPase.** Shown are four steps of the catalytic cycle of an ATPase. Step *i*) ATP binds to the active site of the ATPase; step *ii*) ATP is hydrolyzed to form a transition state with  $Mg^{2+}$ , ADP and organic phosphate ( $P_i$ ) bound; step *iii*)  $P_i$  is released; step *iv*) ADP dissociates and the ATPase is reset to its original state. For trapping of ADP (step *v*), a phosphate-mimicking anion, orthovanadate, replaces  $P_i$  to form a more stable, non-covalent  $Mg^{2+}\cdot ADP\cdot Vi$  complex at the active site. Adapted from Senior *et al.*, 1995 [97].

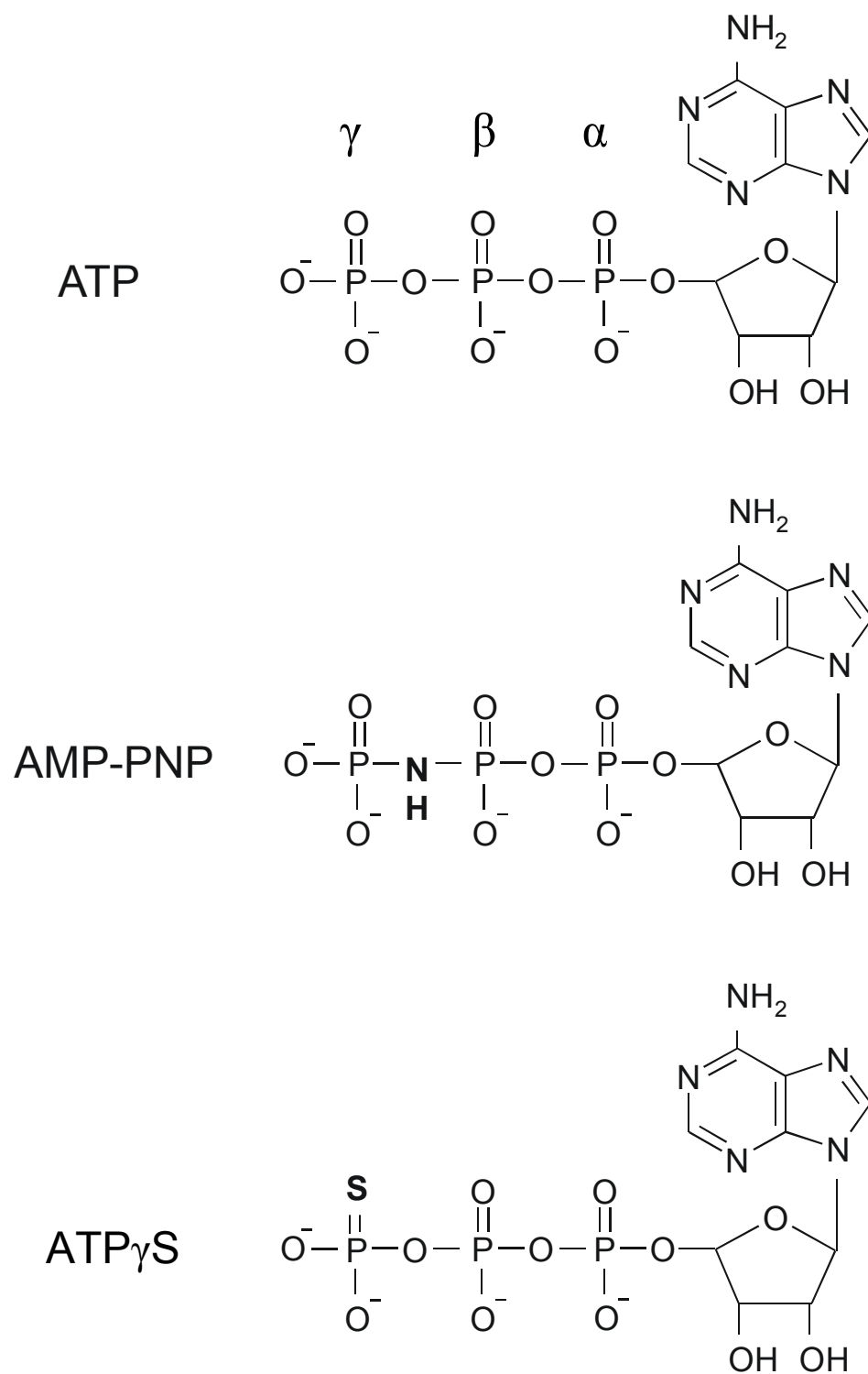


Figure 1.6: Chemical structures of ATP and ATP analogs used in the present study.

This may be due to the structural differences present in the two NBDs. MRP1 has a relatively atypical NH<sub>2</sub>-proximal NBD (NBD1) with the presence of an Asp residue instead of a Glu residue following the Walker B motif (Fig. 1.1A) [11]. This Glu residue has shown to be essential for the  $\beta$ - $\gamma$  phosphodiester bond cleavage of ATP as its mutation completely inhibits the ATPase activity of the bacterial ABC transporter MJ0796 [81, 82]. The absence of Glu in NBD1 may be responsible for the low hydrolytic activity of NBS1 compared with NBS2 [88, 89]. Mutating this Asp<sup>793</sup> to Glu in NBD1 enhanced the ATPase activity of NBS1, whereas the reciprocal Glu<sup>1455</sup> in NBD2 to Asp mutation inactivated the protein and decreased the rate of ADP release from NBS2 [91, 92]. Similar to other MRP-related transporter proteins and CFTR, the NBD1 of MRP1 has a 13 amino acid “deletion” between the Walker A motif and ‘C’ signature motif which is not present in NBD2 nor in NBD1 of ABCB family members (Fig. 1.1A) [11]. Insertion of 13 amino acids “corresponding” to the sequence in NBD1 of human Pgp into MRP1 caused a major conformational change at that region since a conformation-dependent mAb (QCRL-3) specific for that region of MRP1 failed to recognize the mutant protein [25, 88]. The insertion not only abolished high affinity ATP binding by NBS1 but also arrested the transport cycle [88]. Compared with NBD1, the COOH-terminal NBD2 includes the consensus Walker A and B motifs as well as the catalytic Glu<sup>1455</sup> residue (Fig. 1.1A). However, its signature motif is not strictly conserved, a feature also found in some other ABCC proteins (e.g., CFTR and SUR1) (Fig. 1.1A) [19, 20]. As revealed by the ‘head-to-tail’ folding of the NBD dimer, the NBD2 signature sequence is associated with the NBS1. The mutation of conserved

glycine (Gly<sup>1433</sup>) residue at the fourth position of LSVGQ signature motif to Asp in NBD2 of MRP1 enhanced 8-azido- $[\gamma\text{-}^{32}\text{P}]\text{ATP}$  labeling of NBS2 but completely inhibited the 8-azido- $[\alpha\text{-}^{32}\text{P}]\text{ADP}$  trapping at NBS1 [93].

Like other ABC-ATPases, the two NBSs of MRP1 show allosteric interaction and they function cooperatively. The binding of ATP at NBS1 increases the ATP binding and hydrolysis at NBS2 [94]. Meanwhile, NBS1 is able to bind ATP with high affinity independently of NBS2 [88]. However, the ATP binding at NBS1 could be enhanced by vanadate-induced trapping of ADP at NBS2 [89]. Moreover, mutations in the Walker A motif of NBD1 (Lys<sup>684</sup> to Leu, Met, Arg or Glu) which significantly reduced ATP binding at mutated NBS1 result in decreased ATP-dependent solute transport [30, 88, 89, 94-96]. On the other hand, impairing the ATP binding and hydrolysis functions of NBS2 by mutating Lys<sup>1333</sup> (to Leu, Met, Arg or Glu) in the Walker A motif of NBD2 result in complete loss of transport activity [30, 88, 89, 94-96].

### **1.8 Proposed transport cycle of MRP1**

Several studies support the idea that MRP1, as well as Pgp, alternate between high- and low-affinity substrate binding states during the substrate transport cycle [30, 91, 96]. Studies using photoactive substrates (e.g., LTC<sub>4</sub>) have shown that the photolabeling of MRP1 by [<sup>3</sup>H]-LTC<sub>4</sub> was strongly attenuated in the presence of ATP and vanadate under conditions permitting hydrolysis [30]. Similar results were obtained using ATP or poorly hydrolysable ATP analog ATP $\gamma$ S [91, 96]. This suggests that ATP binding rather than hydrolysis converts the protein from a high to low affinity substrate

binding state, and the occupancy of both NBSs with ATP locks the protein in a low affinity substrate binding state.

The transport cycle of MRP1 is still under investigation, but a model is proposed based on current structural and biochemical data (Fig. 1.7) [101, 102]. First, substrate binds to a high affinity binding site that induces a conformational change of the protein and facilitates the binding of ATP to NBS1. The initial binding of ATP promotes the binding of a second ATP as well as the formation of the NBD dimer. Upon the binding of second ATP, the closed NBD dimer configuration forces the protein into a low-affinity binding state and the substrate is released into extracellular medium. After ATP hydrolysis at NBS2, the inorganic phosphate and ADP are released from NBS2. Whether the release of ADP from NBS2 alone is enough to reset the protein for another cycle or the dissociation of ATP from NBS1 is also required is still speculative. Indeed, not all MRP1 substrates transport the same way, especially those that involve co-transport and allosteric transport mechanisms.

### **1.9 Regulation of MRP1 expression**

Regulation of MRP1 is complicated and not well understood. It may require different regulatory mechanisms in normal tissues and in cancer cells. The human *MRP1* gene is mapped to chromosome 16p13.11-13.12 [11]. In some drug resistant cancer cell lines, elevated MRP1 expression is due to the amplification of the gene rather than transcriptional activation [11, 103], while in others, an increased transcription occurs without gene amplification [104, 105].

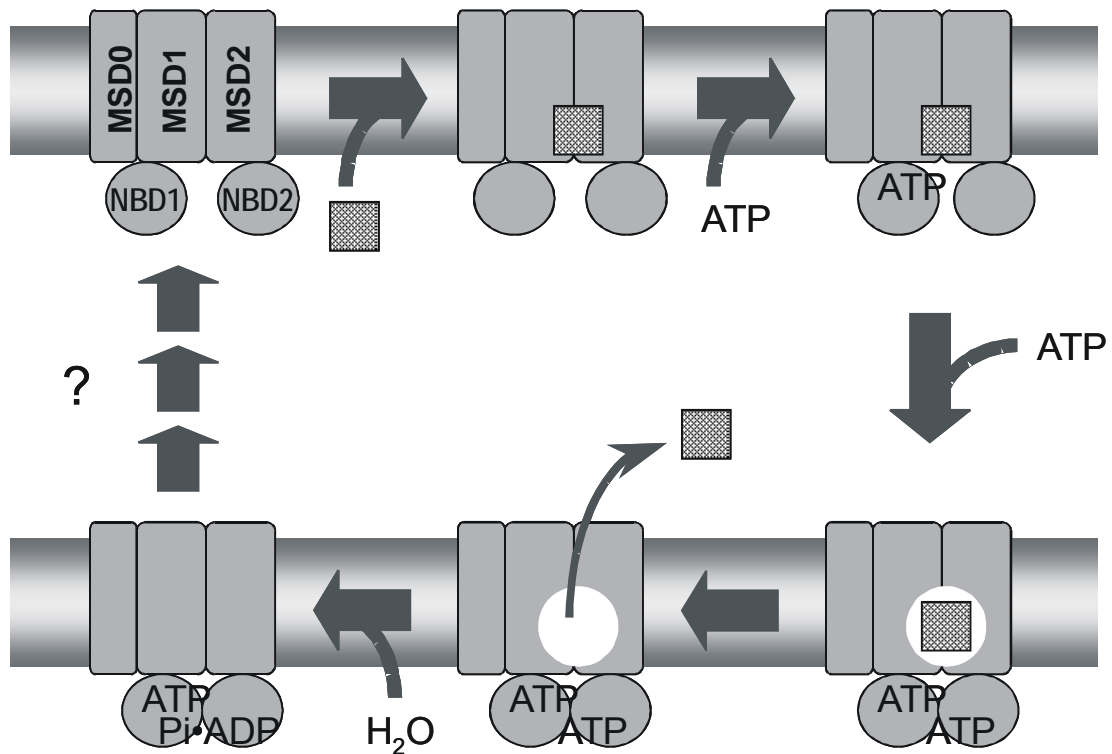


**Figure 1.7: Proposed transport cycle of MRP1.** A schematic illustration of substrate transport by MRP1. The binding of substrate to the high-affinity binding site of MRP1 causes a conformational change, which promotes the binding of first ATP molecule. This stimulates the binding of second ATP molecule by MRP1 and the close NBD dimer formation. When ATP is bound to both NBDs, the protein is in a low-affinity binding state, which allows the release of the substrate into the extracellular medium. Then, ATP is hydrolyzed at the more hydrolytically active NBS2. The protein resets for another cycle through some unknown steps. Adapted from Higgins *et al.*, 2004 [101].

Studies have shown that *MRP1* has a TATA-less and CAAT-less proximal promoter, and the basal promoter activity was localized to a GC-rich region (-91 to +103) [106-108]. This GC-rich region contains several putative binding sites for the transcription factor Sp1 that modulates the basal promoter activity of *MRP1* [109]. The tumor suppressor protein p53 has been shown to suppress *MRP1* promoter activity *in vitro*, which may be caused by disrupting the binding of Sp1 since there is no canonical p53 binding site within the promoter region of *MRP1* [110]. Therefore, there seems to be a link between a loss of p53 function and/or an increase in Sp1 activity and the up-regulation of *MRP1* expression found in some drug resistant tumors [72, 111]. The *MRP1* promoter region also presents an AP-1 site (-498 to -492) which interacts with a complex containing oncogenes *c-jun* and *junD* [107]. Moreover, in HL-60/ADR cells transfected with mutant *c-jun*, MRP1 expression was reduced as revealed by immunofluorescence detection [112].

The induction of MRP1 expression by various chemicals is not easily achieved, at least after short-term exposure. However, in some cell types, MRP1 expression is induced after exposure to some prooxidants that generate reactive oxygen species (ROS), such as *tert*-butylhydroquinone, 2,3-dimethoxy-1,4-naphthoquinone, menadione and sulindac [113, 114]. The mechanisms of upregulation are not so clear. However, one group has reported the co-induction of other redox sensitive genes such as glutamate-cysteine lyase (GCL), which is the rate-limiting enzyme in GSH biosynthesis [113, 114]. Presumably, the upregulation of both GSH biosynthesis and MRP1 expression ensures that the GSH-dependent detoxification mechanism by MRP1 is functional. Currently,

there is no report of MRP1 regulation by other proteins within the cell. Although MRP1 has shown serine/threonine phosphorylation *in vivo* [115], the phosphorylation sites have not been revealed.

### **1.10 Protein-protein interaction studies in ABCC proteins**

Proteins seldom carry out their function in isolation. Rather, they operate through a number of interactions with other cellular macromolecules, such as the multi-protein complexes found during DNA replication and RNA transcription, and the transient interactions found in signal transduction networks. Therefore, mapping of proteome-wide protein interactions is essential for understanding the processes of biological systems. The study of protein-protein interactions of large amphipathic membrane proteins could be quite a challenge. Most proteomic methods commonly used for probing protein-protein interactions in soluble proteins cannot be used directly for membrane proteins since they require the presence of detergent at all times which may interfere with certain physical associations. Nevertheless, some regulatory protein interactions have been characterized in several ABCC proteins including CFTR (ABCC7) and SURs (ABCC8 and 9). Protein-protein interactions of CFTR and some other ABCC proteins are discussed briefly below.

#### *1.10.1 CFTR and its interacting partners*

CFTR is best known for its role in human disease. Thus the trafficking mutant ( $\Delta F508$ ) form of CFTR is the major cause of cystic fibrosis (CF) [116]. CFTR channel activity can be enhanced by phosphorylation at its regulatory (R) domain which is unique

among ABC proteins [117]. At the plasma membrane, most direct protein-protein interactions occur at the two terminal tails of CFTR (Fig. 1.8) [118]. The NH<sub>2</sub>-terminus of CFTR (amino acids 1-79) is reported to bind to two t-SNARE (soluble *N*-ethylmaleimide-sensitive factor attachment protein receptor on the target membrane) proteins, namely SNAP23 (soluble NSF attachment protein of 23 kDa) and SYN1A (syntaxin 1A), which down-regulate its function by cooperatively reducing the capacity of PKA (protein kinase A) to activate the R domain [119, 120]. On the other hand, binding of Munc-18a, a syntaxin-binding protein, abolishes the SYN1A effect on CFTR [121].

There are four protein-protein interaction domains reported at the COOH-terminus of CFTR so far – a PDZ (PSD-95/Disc-large/ZO-1) binding motif (amino acids 1478-1480), a protein phosphatase-2A (PP2A)-binding domain (amino acids 1451-1476), an AMP kinase (AMPK)-binding domain and two endocytic motifs (the tyrosine-based motif YDSI, and the dileucine motif LL) [118]. The recruitment of PKA and PKC via PDZ-domain proteins enhances CFTR activity, whereas dephosphorylation through binding of PP2A or AMPK reduces CFTR-mediated Cl<sup>-</sup> secretion across the apical plasma membrane in epithelial cells (Fig. 1.8) [118, 122].

Sophisticated network interactions also have been found in other cellular processes, such as endoplasmic reticulum (ER) quality control, molecular chaperones, intracellular trafficking, as well as the endocytic retrieval/exocytic insertion of CFTR [118]. The identification of the CFTR-binding partners has shown how CFTR functions as an ion channel and as a regulator of other transporters. Although the ultimate goal of

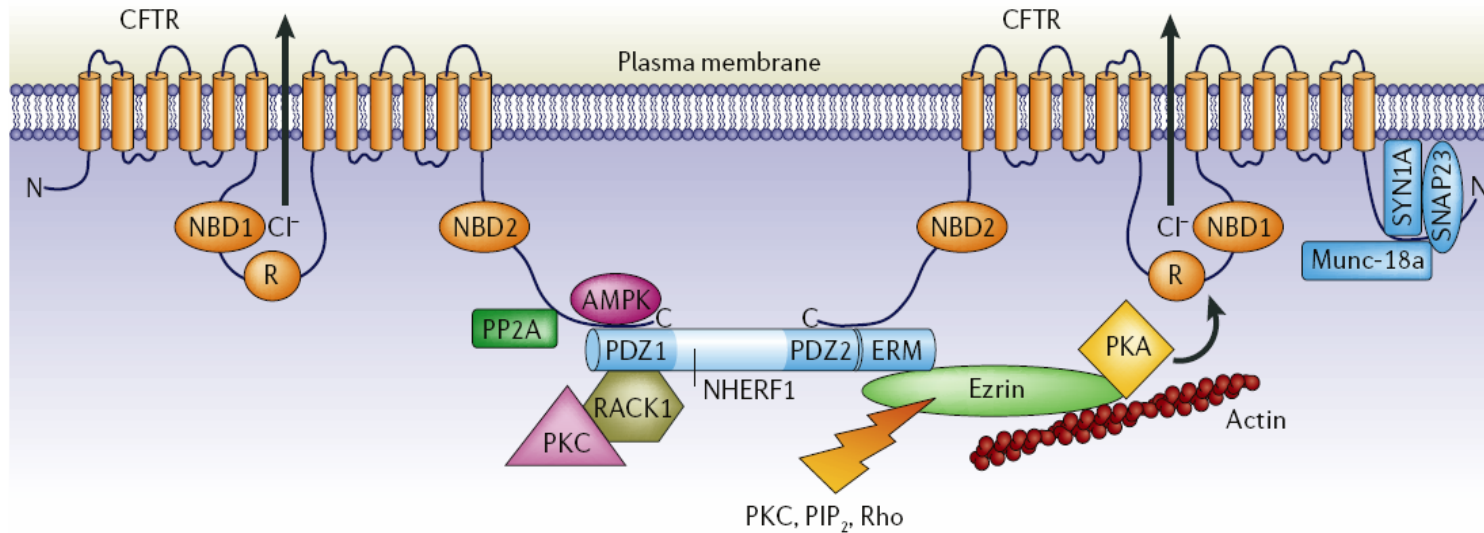


**Figure 1.8: Molecular switches that regulate CFTR activity at the plasma membrane.** Proteins that inhibit channel activity and reduce CFTR-mediated Cl<sup>-</sup> secretion across the apical plasma membrane in epithelial cells include phosphatase-2A (PP2A), AMP kinase (AMPK), syntaxin-1A (SYN1A) and synaptosome-associated protein, 23 kDa (SNAP23). CFTR-interacting proteins that enhance CFTR activity via either direct or indirect interaction include Na<sup>+</sup>/K<sup>+</sup> exchanger regulatory factor isoform-1 (NHERF1), receptor for activated C-kinase-1 (RACK1), protein kinase C (PKC), protein kinase A (PKA), Munc-18a and ezrin. ERM, ezrin, radixin, moesin binding domain; NBD, nucleotide binding domain; PIP<sub>2</sub>, phosphatidylinositol bisphosphate; R, regulatory domain. Adapted from Guggino *et al.*, 2006 [118].

CFTR investigation is to provide a cure or more effective treatment for CF patients by targeting these modulators, these types of studies can also provide some insights into dynamic macromolecular regulation of other ABC transporters.

### 1.10.2 Other ABCC proteins

Compared with CFTR, the protein-protein interaction studies in other ABC proteins are relatively few in number or in some cases, have not yet been explored. Sequence analyses have revealed that among the currently known 48 human ABC proteins, CFTR, MRP2, MRP4, ABCA1, and ABCA7 possess classical PDZ binding motifs at their COOH-termini [123]. Several typical PDZ domain-containing proteins have been demonstrated to interact at the COOH-terminal region of MRP2 by *in vitro* peptide binding assays (e.g., EBP50, IKEPP) [123] and yeast two-hybrid analysis (e.g., PDZK1) [124]. ABCA1, a putative cholesterol transporter, binds to the modular adapter protein  $\beta$ 2-syntrophin, which may anchor ABCA1 in specific micro-membrane domains [125]. Moreover, the internalization of MRP4 and thus its efflux function is found to be regulated by NHERF1 via direct interaction at its PDZ motif [126]. Another ABC C subfamily protein worth mentioning here is SUR, which acts as a regulatory subunit of  $K_{ATP}$  channel [20]. A site within the COOH-terminal domain of rat SUR2A (amino acids 1294-1358) is crucial for the assembly of functional  $K_{ATP}$  channels with full-length Kir6.2 [127]. Moreover, the SNARE protein SYN1A acts as an endogenous inhibitor of  $K_{ATP}$  channels by binding to both NBDs of rat SUR1 [128]. Nevertheless, G-protein  $\beta\gamma$ 2-subunits (G  $\beta\gamma$ 2), which also directly interact with the NBDs of SUR1 and SUR2A,

activates the Kir6.2/SUR channel by reducing the ATP-induced inhibition of the channel [129].

### **1.11 Research objectives**

Crystal structural analysis and photolabeling studies have shown that ATP binding rather than hydrolysis mediates a major conformational change both in NBDs and the MSDs of MRP1, which not only promotes the formation of closed NBD dimer, but also shifts the protein from a high-affinity drug-binding state to a low-affinity configuration. However, these structure and function studies have proven to be expensive and technically difficult to manipulate. Here, two commonly used biochemical approaches for studying structural changes of protein, chemical cross-linking by sulfhydryl reagents followed by limited trypsin digestion, were used to deduce the conformational states of MRP1 induced by binding of various nucleotides and by ATP hydrolysis. The results of this study are described in Chapter 2.

Previous studies have revealed that some ABC C subfamily members, specifically CFTR, MRP2, MRP4 and SUR, functionally interact with other proteins either directly or through adaptor proteins within the cell. No comparable studies have yet been reported for MRP1. However, the extensive functional characterization studies done earlier along with the availability of several reliable and well-characterized MRP1-specific antibodies make this approach possible at this stage. To address the hypothesis that MRP1 synthesis, folding, trafficking, plasma membrane expression and/or transport activity can be modulated by interactions with other cellular proteins, an *in vivo* cross-linking

proteomics approach was applied on intact MRP1 overexpressing cells. Putative MRP1 binding partners captured by this method were identified by protein mass spectrometry (MS), and the preliminary functional studies of MRP1-protein interactions were carried out. The results of these studies are described in Chapter 3.

## **Chapter 2 Nucleotide-induced Conformational Changes in MRP1**

### **2.1 Introduction**

The lack of high resolution crystal structures makes it quite difficult to fully understand certain structural and functional aspects of ABC proteins, such as the packing of the TM helices and the arrangements of the different domains, as well as domain movements and interactions during the substrate transport process. Several biophysical methods, including attenuated total reflection-Fourier transform infrared (ATR-FTIR) spectroscopy, hydrogen/deuterium (H/D) exchange and tryptophan (Trp) fluorescence quenching have been used as alternative tools to investigate the structure and conformational changes in the MSDs of ABC proteins upon nucleotide and substrate binding, including Pgp [130-132] and MRP1 [133-135]. Specifically, in reconstituted MRP1-containing lipid vesicles, the binding of ATP, ATP $\gamma$ S and ADP and Pi induce conformational changes in the MSDs that increase the protein's accessibility to the aqueous environment. ATP hydrolysis, revealed by addition of ADP, apparently does not cause significant changes to the conformational state of the transporter [133]. However, these biophysical approaches require highly purified protein samples, and only the global restructuring of the protein upon ligand binding is reported and the location of the helices or domains, and/or the contribution of specific amino acids can not be identified.

Several biochemical techniques such as protease sensitivity [22, 23, 136-142], photoaffinity labeling [88-96], and sulfhydryl modification [39, 143-148] have been widely used to probe local conformational changes in ABC proteins caused by

interactions with nucleotides and substrates. These biochemical approaches are relatively simple and can be carried out in membrane preparations. However, the sulfhydryl modification studies require Cys-less forms of the protein as templates. Two Cys-less mutants of human Pgp (ABCB1) have been constructed by two independent research groups where all seven endogenous Cys were replaced with alanine (Ala) [143] or serine (Ser) [144] (Fig. 2.1). The mutant forms of Cys-less Pgp still retained their correct folding and transport of certain substrates [143, 144]. Then pairs of Cys residues were re-introduced into the Cys-less templates followed by treatment with thiol-reactive reagents and substrates. A rapid and simple assay was used to detect for the presence of cross-linking, based on an upward shift in the electrophoretic mobility of Pgp due to the slower migration of its cross-linked moieties on SDS gels [39, 145, 148]. This method, namely Cys-scanning mutagenesis, has been used quite extensively to examine the topology, TM helix packing and conformational changes that occur during the transport process of Pgp [39, 143-148].

MRP1 contains substantially more Cys residues than Pgp (25 versus 7). Furthermore, certain Cys residues in MRP1 (e.g., Cys<sup>43</sup> (TM1) and Cys<sup>265</sup> (CL3) (Fig. 2.1)) seem to be critical for maintaining its proper folding and transport function [139]. Also the Cys<sup>682</sup> to Ala mutation in Walker A motif of NBD1 decreases the  $K_d$  value for ATP by ~2.4 fold [149]. However, there is one report for a NH<sub>2</sub>-truncated (lacking MSD0) Cys-less MRP1 (i.e., MRP1<sub>204-1531</sub>) expressed in *Saccharomyces cerevisiae* membranes, in which all 18 Cys residues were substituted with Ala [150]. The resultant

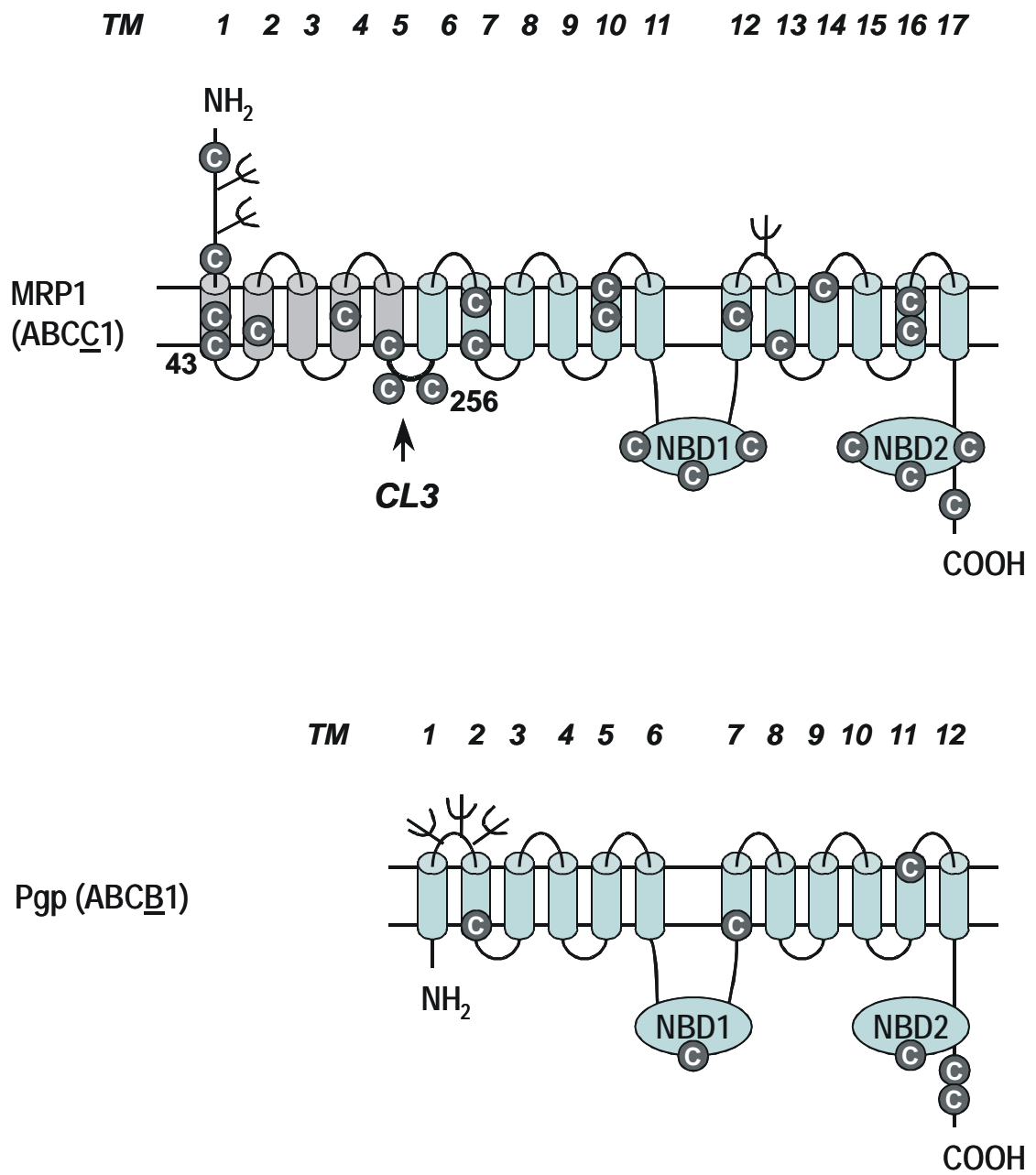


**Figure 2.1: Schematic illustration of endogenous Cys residues in MRP1 (ABCC1) and Pgp (ABCB1).**

protein displayed a 3-fold increase in  $K_m$  and unchanged  $V_{max}$  for LTC<sub>4</sub> transport [150]. Therefore, using the Cys-scanning mutagenesis strategy to study the structural aspect and transport mechanism, which has been done in Pgp, may not be feasible in MRP1.

In this study, the reagent copper phenanthroline ( $Cu^{2+}(Ph)_3$ ), which promotes cross-linking of two nearby Cys residues [151], was used together with immunoblotting of limited trypsin digests to study both the native structure of MRP1 and the conformational changes in the transporter induced by binding of various nucleotides and by ATP hydrolysis. MRP1-enriched membranes were used in this study and immunoblotting of limited trypsin digests of MRP1 with well-characterized antibody was used to deduce the conformational states of MRP1 induced by the binding of different nucleotides.

## **2.2 Materials and Methods**

### *2.2.1 Materials*

ATP, 5'-adenylyl- $\beta$ - $\gamma$ -imidodiphosphate (AMP-PNP), adenosine-5'-*O*-(3-thiotriphosphate) (ATP $\gamma$ S), copper sulfate, diphenylcarbonyl chloride (DCC)-treated trypsin, sodium orthovanadate, phenylmethylsulfonyl fluoride (PMSF), *N*-ethylmaleimide (NEM) and 1,10-phenanthroline were purchased from Sigma Chemical Co. (St. Louis, MO). Complete EDTA-free protease inhibitor cocktail was purchased from Roche Diagnostics (Indianapolis, IN). Leupeptin was purchased from MP Biomedicals (Irvine, CA). Lipofectamine<sup>TM</sup> 2000 was from Invitrogen (Carlsbad, CA). BioTrace<sup>TM</sup>PVDF (polyvinylidene fluoride) membranes (0.45  $\mu$ m pore size) were from

Pall Corporation (Pensacola, FL). Horseradish peroxidase-conjugated goat anti-mouse IgG was from Pierce (Edmonton, AB). Western Lightning<sup>TM</sup> chemiluminescence reagent Plus was from Perkin Elmer Life Science, Inc. (Boston, MA). Progene<sup>®</sup> Scientific autoradiographic film was from Ultident Scientific (St. Laurent, QC).

### *2.2.2 Transfection of HEK293T Cells*

Human embryonic kidney (HEK293T) cells were transfected with the wild-type pcDNA3.1(-)MRP1<sub>k</sub> expression vector [152] and cultured in DMEM medium supplemented with 4 mM L-glutamine and 7.5% fetal bovine serum (FBS) at 37 °C in a humidified atmosphere of 5% CO<sub>2</sub> and 95% air. For large scale transient transfections, approximately 18 x 10<sup>6</sup> cells were seeded in each 150 mm plate and incubated under the above conditions until 90% confluent. HEK293T cells were transfected with 20 µg of DNA (A<sub>260</sub>/A<sub>280</sub> ratio between 1.7 and 1.8) using 75 µl Lipofectamine<sup>TM</sup> 2000 according to the manufacturer's instructions. For each 150 mm plate, 75 µl Lipofectamine<sup>TM</sup> 2000 and 20 µg of DNA were first diluted in 2 ml of serum-free DMEM medium separately and left at room temperature for 5 min. Then the diluted DNA was added to the diluted Lipofectamine<sup>TM</sup> 2000, mixed gently and incubated at room temperature for 30 min. The mixture was then added to the 150 mm plate dropwise and dispersed evenly by gently rocking the plate back and forth. Four h after transfection, the medium was replaced with 20 ml fresh DMEM/FBS medium. Cells were collected 48 h after transfection and snap frozen in liquid nitrogen until needed for membrane vesicle preparation.

### *2.2.3 Membrane Vesicle Preparations*

MRP1-containing membrane vesicles were prepared according to procedures described previously [53] and are summarized briefly here. All steps were performed at 4 °C. HEK293T cells transfected with wild-type pcDNA3.1(-)MRP1<sub>k</sub> expression vector were washed and resuspended in homogenization buffer (50 mM Tris-HCl, pH 7.4/250 mM sucrose/0.25 mM CaCl<sub>2</sub>) with 1 x protease inhibitors added. Cells were then disrupted by argon cavitation (300 psi, 5 min) and the solution of exploded cells was centrifuged at 800 x g for 10 min. Enriched membrane fractions were prepared by layering the supernatant on top of a solution containing 35% sucrose and 50 mM Tris-HCl (pH 7.4), followed by centrifugation at 100,000 x g for 1 h. The membranes at the interface between the supernatant and the sucrose cushion were collected, and then mixed with 50 mM Tris-HCl, pH 7.4/25 mM sucrose buffer solution. After centrifugation at 100,000 x g for 30 min, the membranes were washed and resuspended in 100 µl Tris-sucrose buffer (TSB) (50 mM Tris-HCl, pH 7.4/250 mM sucrose). The membrane vesicles were formed by passing the suspension through a 27-gauge needle 10 times, and then stored in 15 µl aliquots at -80 °C. The protein concentration of each membrane vesicle preparation was determined using a Bradford assay kit (Bio-Rad).

### *2.2.4 Disulfide Cross-linking and Nucleotide Binding Assays*

Cross-linking reactions using Cu<sup>2+</sup>(Ph)<sub>3</sub> as an oxidation reagent were carried out as described previously [145]. Briefly, freshly prepared Cu<sup>2+</sup>(Ph)<sub>3</sub> complex (6.7 µl) containing 10 mM CuSO<sub>4</sub> and 30 mM phenanthroline was added to membranes enriched

for wild-type MRP1 (70 µg protein) diluted in ~150 µl Tris-HCl buffer (50 mM, pH 7.4) and then incubated at room temperature for 10 min. The reaction was stopped by adding 20 µl of 0.5 M EDTA and 20 µl of 100 mM NEM.

For some cross-linking reactions, MRP1-containing membrane vesicles were first incubated with nucleotides before cross-linking with  $\text{Cu}^{2+}(\text{Ph})_3$ . For ATP, AMP-PNP, and  $\text{ATP}\gamma\text{S}$ , the membranes (70 µg protein) were incubated in a solution containing 10 mM  $\text{MgCl}_2$  and 4 mM nucleotide at room temperature for 15 min. For ADP-trapping assays, the membranes were mixed with 10 mM  $\text{MgCl}_2$ , 4 mM ATP and 1 mM freshly prepared sodium orthovanadate (100 mM stock solution, boiled to get rid of the yellow color, and adjusted the pH to 10) at 37 °C for 15 min [153]. Then the cross-linking reactions were carried out as described above.

#### *2.2.5 Limited Trypsin Digestion and Immunoblotting of MRP1*

Limited trypsin digestion of MRP1 was performed as previously described [23] with some modifications. Specifically, membrane vesicles containing solutions (70 µg of protein in 240 µl) (with or without chemical and nucleotide treatments) were divided into 14 microcentrifuge tubes (7 tubes as one group) with 16 µl per tube. For each group, 4 µl trypsin were added to each tube such that the trypsin to protein ratio ranged from 1:500 to 1:2.5; as a control one tube had no trypsin added. The tubes were incubated at 37 °C for 15 min, and the digestions were stopped by adding Laemmli sample buffer containing 15 µg/ml leupeptin and 10 mM PMSF. Dithiothreitol (DTT) was then added to the samples in one of the group to a final concentration of 62.5 mM. All the samples were

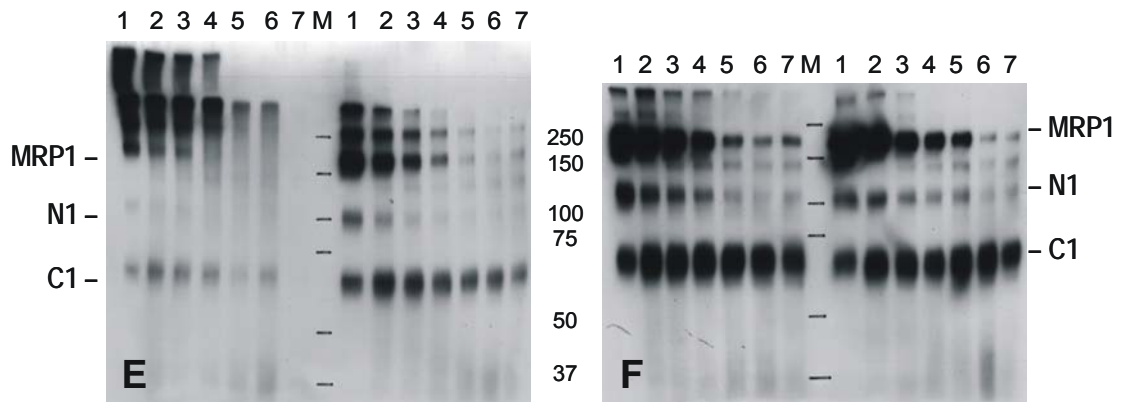
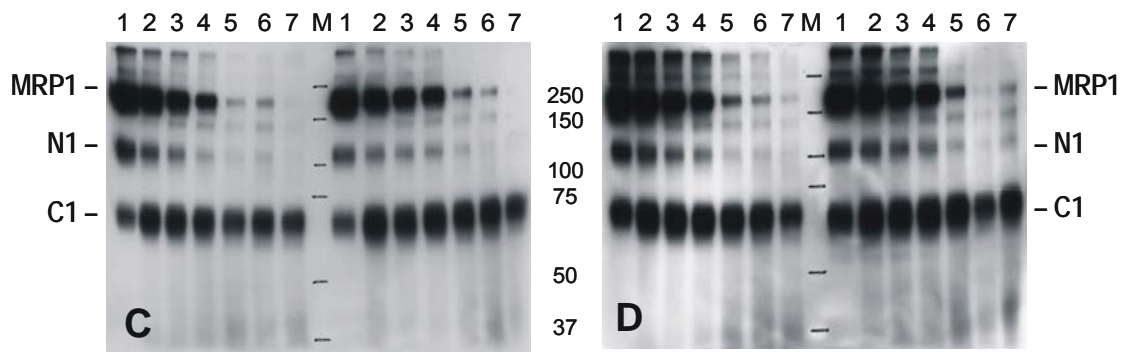
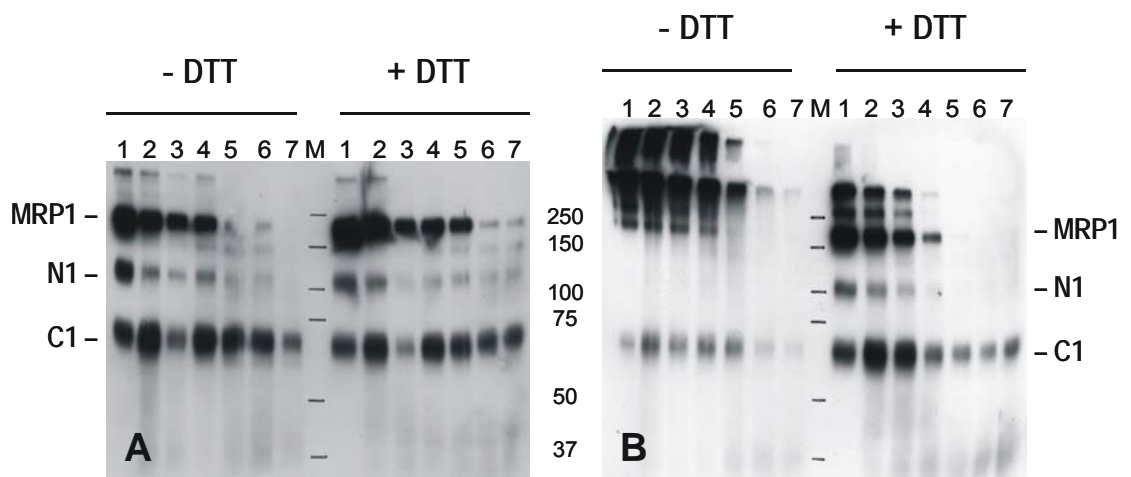
electrophoresed on 7% SDS-polyacrylamide gels and electrotransferred (200 mA, overnight) to PVDF membranes. Blots were blocked by incubating with 4% (w/v) skim milk at room temperature for 1 h followed by incubation with human MRP1-specific murine mAb QCRL-1 (1:10,000) which recognizes a linear epitope between NBD1 and TM12 (amino acids 918-924) [23] in blocking solution at room temperature for 1 h. After several washes with TBS-Tween solution (150 mM NaCl and 0.5% (v/v) Tween 20 in 10 mM Tris, pH 7.5), the blot was incubated for 1 h with horseradish peroxidase-conjugated goat anti-mouse IgG. Binding of the conjugates was detected using Western Lightning<sup>TM</sup> chemiluminescence reagent and exposure of the blot to Progene<sup>®</sup> Scientific autoradiographic film.

## 2.3 Results

### 2.3.1 Limited Proteolysis Pattern of MRP1

Trypsin cleavage site accessibility has been successfully applied to assess ligand-induced conformational changes of various proteins, including ABC transporters (e.g., Pgp and MRP1) [22, 23, 136-142]. Limited trypsin digestion patterns of human MRP1 have been well characterized previously by using antibodies against defined regions of MRP1 [22, 23, 138, 139]. As expected and as shown in Fig. 2.2A, incubation of MRP1-enriched membranes with increasing concentrations of trypsin resulted in a gradual disappearance of full-length MRP1 (190 kDa) and a concomitant appearance of peptide fragments with approximate molecular masses of 120 and 70 kDa as detected by mAb QCRL-1 [23]. The 120 and 70 kDa fragments correspond to the NH<sub>2</sub>-proximal (N1,

**Figure 2.2: Immunoblots of limited trypsin digests of wild-type MRP1 chemically cross-linked in the absence and presence of nucleotides.** Trypsin digests were carried out on membranes prepared from HEK293T cells transfected with wild-type MRP1 at 37 °C for 15 min with the following trypsin:protein ratios (w:w) (1) control (no trypsin), (2) 1:500, (3) 1:100, (4) 1:50, (5) 1:10, (6) 1:5, (7) 1:2.5. The reactions were stopped by adding Laemmli sample buffer and half of the samples were reduced by adding DTT. The samples were then resolved by SDS-PAGE and immunoblotted with mAb QCRL-1. The N1 and C1 fragments are labeled on the sides of each blot whereas the molecular markers are indicated in the centre. (A) Untreated MRP1-enriched membranes in the absence of nucleotide; (B) MRP1-enriched membranes treated with  $\text{Cu}^{2+}(\text{Ph})_3$ ; (C) MRP1-enriched membranes pre-incubated with ATP (4 mM) and then treated with  $\text{Cu}^{2+}(\text{Ph})_3$ ; (D) MRP1-enriched membranes pre-incubated with AMP-PNP (4 mM) and then treated with  $\text{Cu}^{2+}(\text{Ph})_3$ ; (E) MRP1-enriched membranes pre-incubated with  $\text{ATP}\gamma\text{S}$  (4 mM) and then treated with  $\text{Cu}^{2+}(\text{Ph})_3$ ; (F) MRP1-enriched membranes pre-incubated with ATP (4 mM) and sodium orthovanadate (1 mM) at 37 °C (ADP-trapped) and then treated with  $\text{Cu}^{2+}(\text{Ph})_3$ .



MSD0-MSD1-NBD1) and COOH-proximal (C1, MSD2-NBD2) regions of MRP1, respectively (Fig. 1.3A) [23]. The fragments generated by trypsin cleavage at less sensitive sites can be detected using these and other MRP1-specific mAbs but were not included in this study [22, 138, 139].

### *2.3.2 Limited Proteolysis of MRP1 with or without Nucleotides*

The oxidation reagent  $\text{Cu}^{2+}(\text{Ph})_3$  promotes the formation of a covalent disulfide bond between two Cys residues that are in close proximity. The cross-linked proteins or peptides will consequently have altered mobilities through SDS polyacrylamide gels. To examine the structural changes of MRP1 associated with nucleotide binding, wild-type MRP1 membrane vesicle preparations were treated with  $\text{Cu}^{2+}(\text{Ph})_3$  followed by limited trypsin digestion under various conditions. In the nucleotide-free state, the addition of  $\text{Cu}^{2+}(\text{Ph})_3$  caused the aggregation of MRP1 in the stacking gel and the upper part of the separating gel. Under these conditions, the 120 kDa N1 fragment was no longer detectable and the 70 kDa C1 fragment was only weakly detected (Fig. 2.2B, -DTT panel). The distinctive bands corresponding to full-length MRP1 and the N1 and C1 fragments were only resolvable by adding the thiol-reducing reagent DTT (Fig. 2.2B, +DTT panel). This observation suggested that reversible cross-linking had occurred. Moreover, the whole protein appeared more susceptible to trypsinolysis as revealed by the rapid and total disappearance of the 190 kDa (MRP1) and 120 kDa (N1) bands on the blot (Fig. 2.2B, lanes 4-7 of +DTT panel).

After incubation of MRP1-enriched membranes with ATP and AMP-PNP, as well as ATP and orthovanadate under conditions permitting hydrolysis, the limited trypsin digestion profiles of MRP1 appeared similar to that of MRP1 in the absence of nucleotide (Fig. 2.2A). Thus the full-length MRP1, and the N1 and C1 fragments were clearly resolved, both with and without DTT treatment (Fig. 2.2C, D, F). This suggests that none of the Cys residues in MRP1 were able to cross-link in the presence of these nucleotides. Furthermore, the digestion efficiency of trypsin was unchanged, which suggests that the ATP bound, AMP-PNP bound and ADP-trapped conformations of MRP1 exhibited no differences in the accessibility of their trypsin cleavage sites. In contrast, the digestion pattern after incubation with ATP $\gamma$ S was substantially different. Thus, similar to the cross-linking pattern of MRP1 in the nucleotide-free state, massive aggregation of proteins without DTT treatment was observed and the limited trypsin digest pattern showed enhanced sensitivity to trypsin (Fig. 2.2E). This observation suggests that ATP $\gamma$ S binding induces a conformational change in MRP1 that not only permits some Cys residues positioned in close proximity to be cross-linked, but also makes the cytoplasmic loop linking NBD1 to MSD2 more accessible to trypsin. Together, these data indicate that the conformational changes induced by ATP and AMP-PNP are not the same as those induced by ATP $\gamma$ S.

## **2.4 Discussion**

The transport function of MRP1 relies on ATP binding and hydrolysis at its NBDs but the mechanism by which the energy generated is coupled to substrate

translocation across the membrane is so far not fully understood. Information about the structural consequences of nucleotide binding to MRP1 at different stages of its catalytic cycle (Fig. 1.5) is likely to be helpful in understanding this complex process. In this study, different biochemical approaches were combined to gain structural information about nucleotide-induced conformational changes of MRP1. Chemical cross-linking was used to gain information about local movement of certain Cys residues while limited trypsin digestion permitted investigation of structural changes in the cytosolic regions of MRP1. These experiments were performed using MRP1-enriched membranes in the absence of substrates.

There are certain geometric requirements for disulfide bridge formation between two Cys residues. Conformational analysis of disulfide bridges in high resolution crystal structures indicates that the distance between the  $\alpha$ -carbons of each Cys (N-C $_{\alpha}$ -C $_{\beta}$ -S $_{\gamma}$ ) can be no more than 7.0 Å whereas  $\beta$ -carbons need to be within 4.7 Å of each other [154]. Furthermore, for a standard disulfide bond, the S $_{\gamma}$ -S $_{\gamma}$  distance is less than 3 Å and the average C $_{\beta}$ -S $_{\gamma}$ -S $_{\gamma}$ -C $_{\beta}$  dihedral angle is approximately 90° [154]. Therefore, the cross-linking event is relatively specific and does not occur randomly. This has been demonstrated in Cys-scanning mutagenesis studies of Cys-less Pgp [39, 143-148].

Cys cross-linking of MRP1 in the nucleotide-free state showed multimeric aggregates of the transporter in the stacking gel as well as the upper part of the separating gel (Fig. 2.2B, -DTT panel). This is not surprising given that MRP1 contains 25 endogenous Cys residues (Fig. 2.1). The aggregates are likely the result of various inter- and intra-chain disulfide bonds formed at different regions of MRP1 which alter the

mobility of the polypeptide fragments in the gel. Reduction of disulfide bonds with DTT resolved the trypsin digest pattern (Fig. 2.2B, +DTT panel), which suggests that the cross-linking does not alter the trypsin sensitive site between NBD1 and TM12. Instead, the cross-linking of certain Cys residues seems to constrain the protein in a conformation that is more accessible to trypsin since its tryptic digest profile showed a rapid disappearance of both the full-length MRP1 and N1 fragments compared with the untreated control (Fig. 2.2A). The current methodology does not allow the exact sites of Cys cross-linking to be identified. A reliable homology model of MRP1 may help to probe the Cys residues that are involved in the cross-linking in the future.

The crystal structures of the isolated NBDs as well as full-length ABC transporters have shown that the binding of ATP or its analog AMP-PNP induces major conformational changes in the NBDs and causes the monomeric NBDs to dimerize [38, 80, 82]. Biophysical studies using reconstituted MRP1-containing liposomes have shown that binding of ATP rather than its hydrolysis drives a major structural reorganization in the MSDs of MRP1 [133]. The results of the present study indicate that the binding of ATP (Fig. 2.2C) or AMP-PNP (Fig. 2.2D) under non-hydrolytic conditions, as well as the trapping of ADP in the presence of orthovanadate (post-hydrolysis state) (Fig. 2.2F), force conformational changes in MRP1 that prevent Cys cross-linking as indicated by the fact that the tryptic digestion patterns were similar to those of untreated control (Fig. 2.2A). Whether or not MRP1 possesses exactly the same conformation in these three nucleotide bound conditions is not known. Nevertheless, it is clear that the trypsin digest pattern is different after ATP $\gamma$ S binding to MRP1 (Fig. 2.2E), where the tryptic digestion

profiles are comparable to those of MRP1 in the nucleotide-free state (Fig. 2.2B).

Whether or not the ATP $\gamma$ S-bound and the nucleotide-free conformations of MRP1 have the same numbers and sites of Cys cross-linking is also not known.

The structures of both ATP $\gamma$ S and AMP-PNP closely resemble that of ATP (Fig. 1.6) and are commonly used instead of the more labile ATP to study the nucleotide binding properties of various ATPases during the pre-hydrolysis steps of their catalytic cycle. AMP-PNP contains a nitrogen atom between the  $\beta$ - and  $\gamma$ -phosphate moieties while the  $\beta\gamma$ -phosphodiester bond is unchanged in ATP $\gamma$ S (Fig. 1.6). Therefore, AMP-PNP is considered a nonhydrolyzable ATP analog whereas ATP $\gamma$ S is still hydrolysable but at a much slower rate [155]. Hopfner *et al.* [80] have shown that the crystal structure of the DNA repair ABC ATPase Rad50 dimer in complex with AMP-PNP has the same conformation as its ATP-bound crystal form. On the other hand, there is no ATP $\gamma$ S-bound crystal structure of any ABC protein reported thus far. However, in the periodic table, the sulfur atom (S) is in the same group as oxygen (O), and their electronegativity properties are similar (O is 3.44 and S is 2.58). Thus, at the active site of NBS, the binding of ATP $\gamma$ S should be closely mimicking the binding of ATP. Whether or not these two ATP analogs are interchangeable is still a matter of debate. Previous photolabeling studies using membranes from an insect cell expression system have shown that ATP $\gamma$ S but not AMP-PNP is able to substitute for ATP in driving the transition from high- to low-affinity LTC<sub>4</sub>-binding state of MRP1 [91, 96]. In another study, the affinity of MRP1 for estrone sulfate was decreased in the presence of either AMP-PNP or ATP $\gamma$ S when MRP1-enriched human lung cancer cell membranes were

used [141]. On the other hand, in the present study, AMP-PNP and ATP $\gamma$ S binding seem to exert different effects on MRP1 as revealed by Cys cross-linking and limited trypsin digestion using membrane preparations from HEK293T cells transfected with MRP1. Thus, there are some apparent differences between the current results and previous findings. These potential discrepancies may be due to differences in experimental setup and detection methods. Nevertheless, the current data provide additional evidence that significant structural changes occur during the catalytic cycle of MRP1. They also demonstrate that the two ATP analogs, AMP-PNP and ATP $\gamma$ S, do not interact with MRP1 in an equivalent fashion, although the reasons for this are not yet clear.

It is known that substrate binding to the MSDs induces a conformational change in ABC transporters, such as Pgp (ABCB1) [131, 132] and TAP (ABCB2/3) [156]. GSH is known to induce substantial conformational changes in MRP1 [88, 134, 135, 140-142]. H/D exchange [134] and Trp fluorescence quenching [135] studies suggest that GSH binding reorganizes the MSDs of MRP1 in a way that the protein accessibility to the aqueous environment is decreased and the percentage of Trp residues exposed to the hydrophobic quencher is increased, which can not be achieved by binding of drug substrate DOX alone. Furthermore, binding of ATP or AMP-PNP in the presence of GSH increases the accessibility of the transporter towards the aqueous environment and decreases Trp exposure [134, 135]. Some biochemical studies also have shown that binding of GSH can protect against digestion of MRP1 by trypsin [134, 140, 141], but not other MRP1 substrates, such as DOX [134], estrone sulfate and vincristine [142]. Also, the labeling of MRP1 by 8-azido- $[\gamma^{32}\text{P}]\text{ATP}$  is increased significantly in the presence of

*S*-methyl GSH (non-reducing analog of GSH), whereas substrates (i.e., estrone sulfate, vincristine) or modulators (i.e., verapamil, apigenin) have no effect on the level of 8-azido- $[\gamma^{32}\text{P}]$ ATP labeling [88]. Therefore, the effect of GSH binding on MRP1 can be investigated in the future by looking at its Cys cross-linking pattern in the presence of GSH.

Several conclusions can be drawn from this study. First, some Cys residues within MRP1 can be cross-linked when the transporter is in the nucleotide-free state and the chemically cross-linked MRP1 becomes more susceptible to trypsin digestion than untreated control indicating conformation change caused by the cross-linking. Second, binding of ATP and AMP-PNP, and trapping of ADP prevented chemical cross-linking, indicating that conformational changes in MRP1 involving the accessibility of Cys residues are induced by these nucleotides. In contrast, MRP1 appears to adopt a different conformation after binding of ATP $\gamma$ S as is evident from its unchanged Cys cross-linking pattern and its enhanced sensitivity towards trypsinolysis. More detailed work is clearly needed to fully understand the structural changes that occur during binding, hydrolysis and release of nucleotide, and how the energy released at each stage is coupled to the substrate transport process of MRP1.

## Chapter 3 Identification and Characterization of Protein Interacting Partners of Human MRP1

### 3.1 Introduction

As discussed in Chapter 1, the plasma membrane expression and/or activity of some ABC C subfamily members, specifically CFTR, MRP2 and MRP4, can be regulated through their interaction with other cellular proteins [116-122, 123, 124, 126, 157, 158]. The protein-protein interactions reported for these ABCC proteins, either directly or through adaptor proteins, have thus far been mediated by certain well-defined protein binding motifs (e.g., PDZ motif). MRP1 has no canonical protein interacting motifs present in its amino acid sequence based on a PROSITE analysis (<http://www.ebi.ac.uk/Tools/ppsearch/index.html>). There are also presently no reports of protein-protein interactions for MRP1. Therefore, an unbiased screening seems a reasonable approach to identifying proteins that might interact with MRP1 in a structural and/or functional manner. Initially, surface plasmon resonance (trade name Biacore) spectroscopy was used in attempts to detect the binding between MRP1 and potential binding partners (C. Moreau, Q. Mao and S.P.C. Cole, unpublished data). However, the amount of bound proteins recovered from a MRP1-coated sensor chip was not sufficient for MS-based identification. Therefore, a more conventional approach, combining *in vivo* chemical cross-linking, immunoaffinity purification and protein MS techniques, was used in the present study to investigate the association of MRP1 with other proteins in the cell.

Chemical cross-linking in combination with MS techniques is a commonly used approach for studying protein-protein interactions and topological structures of protein complexes [159]. The cross-linking allows noncovalent protein-protein interactions, which may be transient or dependent on specific physiological conditions, to be stabilized in long-lived covalent complexes that retain structural information during subsequent purification, enrichment, and analysis. Modern MS techniques with enhanced sensitivity, mass accuracy and tolerance towards sample heterogeneity is widely recognized as a powerful tool for identification of interacting proteins [160].

Membrane proteins are intrinsically difficult to study because of their relatively large size and highly hydrophobic nature. Most proteomic methods commonly used for the analysis of soluble proteins cannot be used directly for the study of membrane proteins, since most of the time, detergents are required for solubilization which may potentially adversely affect the proper folding and function of the protein. Nevertheless, we have had some success in immunoaffinity purification and MS analysis of MRP1 previously [161-163]. In particular, native MRP1 has been immunoaffinity purified to homogeneity from H69AR lung cancer cells using a well-defined MRP1-specific mAb [161, 162]. The proteoliposome reconstituted MRP1 exhibited modest substrate-stimulated ATPase activity and ATP-dependent transport of several substrates [161, 162]. In addition, matrix-assisted laser desorption ionization time-of-flight (MALDI-TOF) MS technique was used for peptide mapping of purified recombinant human MRP1 expressed in *Pichia pastoris*, and sequence coverage of > 98% was achieved [163].

In this study, a proteomic approach initially involving *in vivo* chemical cross-linking followed by affinity purification and MS analysis was taken to identify proteins that have direct interactions with MRP1 in H69AR cells (Fig. 3.1). When the direct cross-linking approach proved unsuccessful, a second approach involving immunoaffinity purification of MRP1-containing complexes followed by MS analysis was adopted. In this way, several candidate protein partners of MRP1 were identified. The interactions of two of these proteins, FUS and drebrin, with MRP1 were then further investigated.

## **3.2 Materials and Methods**

### *3.2.1 Materials*

Triton X-100, PMSF, 4',6-diamidino-2-phenylindole dihydrochloride (DAPI), murine anti-actin mAb (clone AC-40) and murine anti- $\alpha$ -tubulin mAb (clone T6074) were purchased from Sigma Chemical Co. (St. Louis, MO). CHAPS was purchased from MP Biomedicals, LLC (Solon, OH). GammaBind<sup>TM</sup> Plus Sepharose<sup>TM</sup> was purchased from GE Healthcare Bio-Sciences AB (Uppsala, Sweden). Dithiobis (succinimidyl propionate) (DSP) was from Pierce (Rockford, IL). Protease inhibitor cocktail and phosphatase inhibitor cocktail were purchased from Roche Diagnostics (Indianapolis, IN). Rat anti-MRP1 mAb MRPr1 was a kind gift from Drs. R. J. Scheper and G. L. Scheffer (Amsterdam, Netherlands). Murine anti-MRP1 mAbs QCRL1-4 ascites were as described previously [23, 25, 164]. Murine anti-FUS/TLS (clone 4H11) mAb and normal mouse/rat IgGs were from Santa Cruz Biotechnology (Paso Robles, CA). Murine anti-

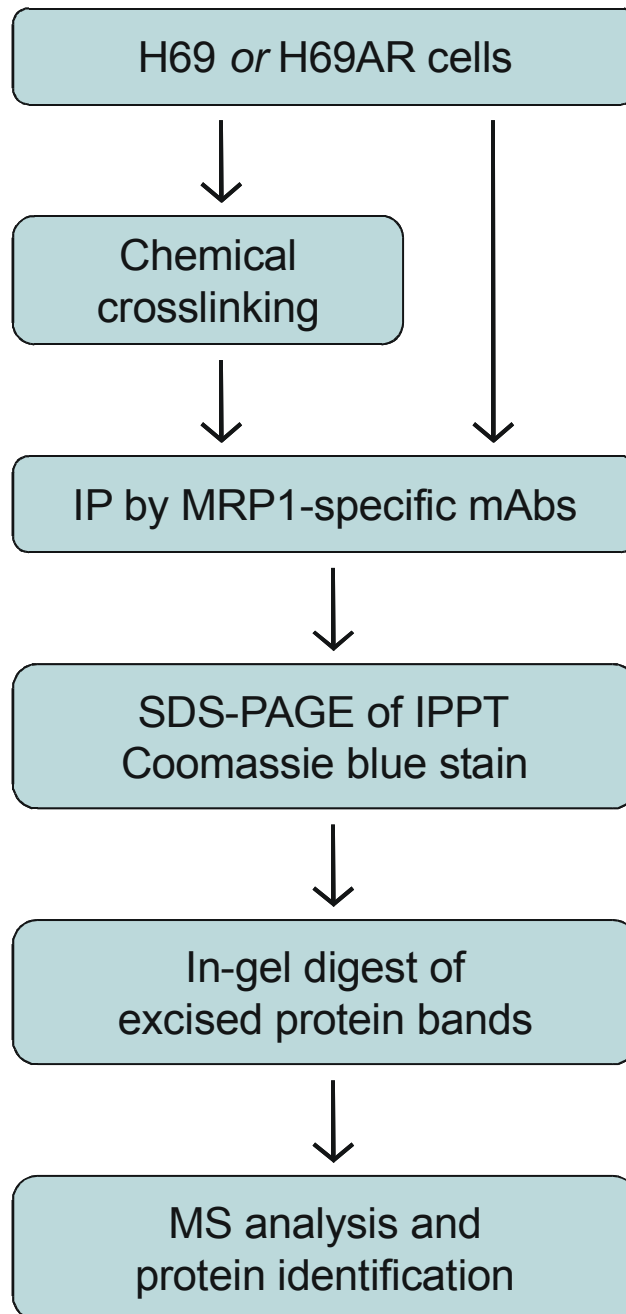


**Figure 3.1: Schematic outlining experimental approach of identifying interacting protein partners of MRP1.** IP, immunoprecipitation; IPPT, immunoprecipitate.

drebrin mAb (clone M2F6) was from MBL (Naka-ku, Nagoya, Japan). siGENOME SMART pool siRNA, containing a mixture of four siRNAs specific for human drebrin mRNA (NCBI no. NM\_004395) [165], and siGENOME non-targeting siRNA #3 were from Dharmacon (Lafayette, CO). Alexa Fluor<sup>®</sup> 488-conjugated F(ab')<sub>2</sub> fragment of goat anti-mouse IgG (H+L) was from Invitrogen (Eugene, OR). BioTrace<sup>™</sup>PVDF (polyvinylidene fluoride) membranes (0.45 µm pore size) were from Pall Corporation (Pensacola, FL). Horseradish peroxidase-conjugated goat anti-mouse IgG and horseradish peroxidase-conjugated goat anti-rat IgG were from Pierce (Edmonton, AB). Western Lightning<sup>™</sup> chemiluminescence reagent Plus was from Perkin Elmer Life Science, Inc. (Boston, MA). Progene<sup>®</sup> scientific autoradiography film was from Ultident Scientific (St. Laurent, QC). Lipofectamine<sup>™</sup> 2000 and Opti-MEM<sup>®</sup>I reduced serum medium were from Invitrogen (Carlsbad, CA).

### *3.2.2 Chemical Cross-linking of Cultured Cells*

The chemical cross-linking of cells was performed as previously described [166] with some modifications. The MRP1 overexpressing cell line H69AR cells were grown as suspension cultures in 500 ml glass bottles in RPMI 1640 medium containing 5% FBS as described previously [8, 11]. H69AR cells were washed twice with pre-warmed phosphate buffered saline (PBS) and then resuspended in PBS at a density of  $6 \times 10^6$  cells per ml. Freshly made DSP stock in DMSO (10 mM) was added to the cell suspension at a final concentration of 0.5 mM (5% DMSO) and incubated for 10 min at room temperature unless otherwise indicated. Cross-linking reactions were stopped by adding

~15-20 ml buffer containing 50 mM Tris-HCl (pH 7.4), 250 mM sucrose and 0.25 mM CaCl<sub>2</sub>. The cells were then collected by centrifugation and cell pellets were stored at -80 °C.

### 3.2.3 Immunoprecipitations

All immunoprecipitation steps were performed at 4 °C. Typically, lysates for immunoprecipitation were prepared by incubating H69AR cell pellets (with or without DSP treatment) and its drug sensitive parental cell line H69 (cultured under the same conditions as H69AR cells [8]) on ice in a buffer containing 1% CHAPS (w/v), 120 mM NaCl, 10 mM MgCl<sub>2</sub>, 0.5 mM PMSF, protease and phosphatase inhibitors in PBS (pH 7.4). In some experiments, the lysis buffer consisted of 1% Triton X-100 (v/v), 100 mM NaCl, 20 mM Tris (pH 7.4), 5 mM EDTA and protease inhibitors. The pellet was resuspended every 15 min by gentle agitation. After 1 h of solubilization, the sample was centrifuged (15,000 rpm for 15 min, ThermoIEC 21000R centrifuge) and the supernatant (cell lysate) was then incubated with 15 µl protein G-Sepharose beads for 1 h on a rotating shaker (Labquake<sup>®</sup>) as a pre-clearing step. Meanwhile, antibodies (10 µg) were incubated with 60 µl protein G-Sepharose beads on a shaker for 2 h, and the beads were then washed twice with 400 µl lysis buffer to remove any unbound antibodies. The pre-cleared cell lysates were then combined with antibody-bound beads and the mixture was rotated on a shaker for 3 h. Unbound proteins were removed by extensive washings (4-5 times) with 500 µl lysis buffer (micro-centrifugation for 1 min at 15,000 rpm). Bound proteins were then eluted by incubating with 60 µl Laemmli sample buffer containing

DTT (100 mM final concentration) and left at room temperature for 1 h before subjecting the sample to electrophoretic separation.

#### *3.2.4 Immunoblotting and Coomassie Blue Staining*

Samples derived from the immunoprecipitations above were separated on a 7% SDS-polyacrylamide minigel (10 x 7 cm, Bio-Rad). Protein gels for MS analysis were stained with Coomassie Brilliant blue (45% methanol (v/v), 10% acetic acid (v/v)) for 45 min at room temperature and then destained in a solution containing 40% (v/v) methanol and 7% (v/v) acetic acid until the protein bands were distinct and the background was clear. For immunoblotting, the protein gels were subjected to electrophoretic transfer (100 V for 1 h) to PVDF membranes. After blocking in 4% (w/v) skim milk at room temperature for 1 h, the membranes were incubated with appropriate antibodies diluted in blocking solution at room temperature for 1 h. After several washings with TBS-Tween solution (150 mM NaCl and 0.5% (v/v) Tween 20 in 10 mM Tris, pH 7.5), the blot was incubated with horseradish peroxidase-conjugated goat anti-mouse IgG or horseradish peroxidase-conjugated goat anti-rat IgG diluted in blocking solution for 1 h at room temperature. Binding of the conjugates was detected using Western Lightning<sup>TM</sup> chemiluminescence reagent and the blot then exposed to Progene<sup>®</sup> scientific autoradiography film. The relative levels of protein expression were determined by densitometry of exposed films using Image J software (<http://rsb.info.nih.gov/ij/>).

### *3.2.5 In-gel Digestion and Peptide Extraction*

In-gel digestion of the Coomassie-stained protein bands was performed by Dr. Yi-min She (Department of Chemistry, Queen's University, Kingston, ON, Canada). The excised protein bands were crushed into small pieces and destained with 100 mM  $\text{NH}_4\text{HCO}_3$ /acetonitrile (ACN) (1:1, v/v) until completely colorless. The gel particles were then dried by SpeedVac centrifugation. The proteins in the gel pieces were reduced with 10 mM DTT (in 100 mM  $\text{NH}_4\text{HCO}_3$ ) and incubated at 56 °C for 1 h. The DTT solution was then removed by centrifugation. Free sulfhydryl groups were blocked by incubating with 55 mM iodoacetamide at room temperature for 45 min. The solution was then removed and the gel particles completely dried by SpeedVac centrifugation. The proteins were then digested with 10 ng sequencing grade trypsin (Calbiochem) in 25 mM  $\text{NH}_4\text{HCO}_3$  (pH 7.6) (5 ng/ $\mu\text{l}$ ) at 37 °C overnight. The proteolytic peptides were sequentially extracted with the aid of sonication using 0.1% trifluoroacetic acid (TFA), 0.1% TFA in 60% ACN, and finally 100% ACN. Finally, the fractions from each extraction step were combined and dried by SpeedVac centrifugation. They were further purified for MALDI/TOF MS and MS/MS analyses by passage through C18 ZipTips (Millipore) filters.

### *3.2.6 Mass Spectrometry Analysis and Protein Identification*

MALDI data were acquired at the Department of Chemistry, Queen's University (Kingston, ON, Canada) using an Applied Biosystems / MDS Sciex QStar XL quadrupole time-of-flight (QqTOF) MS equipped with an oMALDI II source and a

nitrogen laser operating at 337 nm. Samples to be analyzed were prepared at a ratio of 1:1 (v/v) peptide digest to matrix (i.e. 2,5-dihydroxybenzoic acid), and subsequently dried on a stainless steel MALDI plate. After MALDI MS mapping, the peptide sequencing of selected ions was determined by MALDI QqTOF MS/MS measurements using argon as the collision gas.

The peptide fingerprinting masses were analyzed by MS-Fit program against the NCBI database using ProteinProspector at the University of California San Francisco (UCSF) web site (<http://prospector.ucsf.edu>), whereas the MS/MS ions search on each tandem mass spectrum were performed using the Mascot search engine (Matrix Science, London, UK, <http://www.matrixscience.com>) against the NCBI database of Homo sapiens taxonomy. These searches were set up to take into account up to two missed trypsin cleavage sites. Several common side chain modifications were also considered, such as methionine oxidation, carbamidomethylation, asparagine and glutamine deamidation to aspartate acid and glutamic acid, as well as NH<sub>2</sub>-terminal pyroglutamation. The mass tolerance between calculated and observed masses used for the database search was set at a range of  $\pm 100$  ppm for the MS peaks and  $\pm 0.2$  Da for the MS/MS fragment ions.

### *3.2.7 NanoLC-ESI MS/MS Analysis and Data Processing*

The nanoLC/MS/MS analyses of the tryptic digests were performed by Dr. Yi-min She (Department of Chemistry, Queen's University, Kingston, ON, Canada). The experiments were carried out on the same type of QStar XL instrument with a nanospray<sup>®</sup>

II source designed by MDS Sciex (Concord, ON, Canada). An Agilent 1100 capillary HPLC system was coupled on-line to LC MS/MS analysis, and 2.5  $\mu$ l of the sample was injected each time. Peptides were separated on a C18 PepMap100 analytical column (75  $\mu$ m i.d. x 15 cm, particle size 3  $\mu$ m, pore size 100 $\text{\AA}$ ). Gradient LC elution of the peptides was achieved through a gradient ranging from 5% to 90% of solvent B (98% ACN containing 0.1% formic acid (v/v)) mixed with solvent A (0.1% formic acid) for 60 min at a flow rate of 500 nl/min. The LC MS/MS analysis was performed in Information Dependent Acquisition (IDA) mode, where MS scan and MS/MS data were obtained using a 1 sec survey scan followed by three consecutive 2 sec product ion scans.

LC MS/MS spectra were processed by Applied Biosystems BioAnalyst<sup>TM</sup> 1.1 software, and the resulting MS/MS data sets were then searched against the NCBI database of Homo sapiens taxonomy using the Mascot search engine (<http://www.matrixscience.com/>). The peptide sequences and protein identifications were further manually validated by visual inspection of individual MS/MS spectra.

### *3.2.8 Preparation of Subcellular Fractions and Whole Cell Lysates*

The cytosolic and nuclear fractions of H69 and H69AR cells were prepared as described previously [167]. First, cells ( $1 \times 10^7$ ) were washed once with PBS and collected by centrifugation (900 x g for 5 min). The cell pellet was then resuspended in 150  $\mu$ l buffer A (30 mM Tris-HCl (pH 7.5), 1.5 mM MgCl<sub>2</sub>, 10 mM KCl, 1% Triton X-100 (v/v), 10  $\mu$ g benzamidine and protease inhibitors). The sample was vortexed and placed on ice for 5 min. The supernatant (crude cytosolic/membrane fraction) (135  $\mu$ l)

was then removed after centrifugation (13,000 x g for 1.5 min). Fifteen  $\mu\text{l}$  10 x DNase/RNase (5 mg/ml DNase I, 2.5 mg/ml RNase A) and 17  $\mu\text{l}$  2% SDS/100 mM DTT were added to the supernatant and the mixture was incubated for 1 h at 4 °C. The pellet (crude nuclear fraction) was resuspended in 135  $\mu\text{l}$  buffer B (50 mM Tris-HCl (pH 7.5), 5 mM  $\text{MgCl}_2$ , 0.1 mg/ml DNase I, 0.25 mg/ml RNase A, 10  $\mu\text{g}$  benzamidine and protease inhibitors) and incubated for 1 h at 4 °C. Both the cytosolic/membrane and nuclear fractions were vortexed briefly every 15 min during the 1 h incubation.

To prepare whole cell lysates,  $10^6$  cells were washed two times with PBS, pelleted by centrifugation (900 x g for 5 min), and then resuspended in 150  $\mu\text{l}$  solubilization buffer (1% CHAPS (w/v), 0.5 mM PMSF, 10 mM  $\text{MgCl}_2$  and protease inhibitors in PBS) and fully mixed by pipetting up and down several times. One  $\mu\text{l}$  DNase I (5 mg/ml) was added if the solution appeared viscous. Protein concentrations in all the cellular preparations were determined using a Bio-Rad  $D_c$  protein assay according to the manufacturer's instructions.

### 3.2.9 siRNA Knockdown of Drebrin

Drebrin knockdown by siRNA was performed as previously described [168]. Briefly, H69AR cells were seeded in 6-well tissue culture plates at a density of  $0.75 \times 10^6$  cells per well on day 0. On day 1, the first siRNA transfection was performed. Prior to transfection, 5  $\mu\text{l}$  Lipofectamine<sup>TM</sup> 2000 was added to 50  $\mu\text{l}$  Opti-MEM<sup>®</sup>I, and the mixture was incubated at room temperature for 5-10 min. A second solution containing 7.5  $\mu\text{l}$  of 20  $\mu\text{M}$  siRNA and 100  $\mu\text{l}$  Opti-MEM<sup>®</sup>I was then added to the first mixture, and

incubated together at room temperature for 15-20 min. Then 1.34 ml Opti-MEM<sup>®</sup>I was added to the siRNA/Lipofectamine<sup>™</sup> 2000 mixture to make a final volume of 1.5 ml with final siRNA concentration of 100 nM. The cells were washed with Opti-MEM<sup>®</sup>I once and the siRNA/Lipofectamine<sup>™</sup> 2000 mixture was added to the well. Four h after transfection, an additional 1.5 ml of pre-warmed fresh RPMI/5% FBS were added to each well and the cells were incubated at 37 °C overnight. On day 2, the cell medium was replaced with 3 ml of pre-warmed fresh RPMI/5% FBS. For immunofluorescence experiments, the cells were removed from the well by trypsinization and seeded in two wells of the 6-well tissue culture plate on glass coverslips (22 x 22 mm) at the end of day 2. The second transfection was performed on day 3 followed the same procedure as the first one. The media were again changed on day 4 and cells were trypsinized and collected on day 5. Whole cell lysates were prepared and protein quantified as described in Section 3.2.8.

### *3.2.10 Confocal Fluorescence Microscopy*

Cells were seeded on a glass coverslip in a 6-well tissue culture plate at a density of approximately  $10^6$  cells per well. The cells were washed twice with PBS and fixed with 4% paraformaldehyde at room temperature for 10 min, followed by permeabilization with 0.1% Triton X-100 in PBS for 5 min at room temperature. Fixed and permeabilized cells were then incubated in a blocking solution containing 0.1% bovine serum albumin (BSA) and 0.1% skim milk at room temperature for 1 h. The cells were then incubated with primary antibodies for 1 h at room temperature. After several washes with PBS,

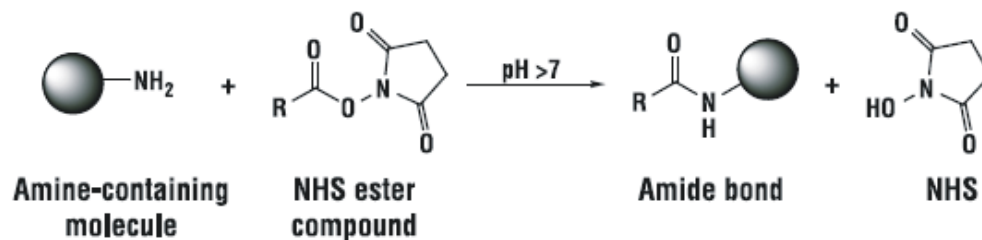
cells were incubated with Alexa 488-conjugated secondary antibodies for 30 min at room temperature in the dark. Cell nuclei were counterstained by adding DAPI (100  $\mu$ l mounting solution with 0.1  $\mu$ l of DAPI). The coverslips were then mounted on glass slides before viewing. Confocal fluorescence microscopy was performed by Matt Gordon and Jeff Mewburn in the cytometry and imaging facility of Queen's University, Division of Cancer Biology and Genetics. Fluorescence images were collected using a Leica TCS SP2 multi-photon confocal microscope (Heidelberg, Germany) equipped with a PL APO 100X/1.40 oil immersion lens (Leica). Images were collected at an 8-bit depth and 1024 x 1024 pixel resolution using LCS software (Leica).

### **3.3 Results**

#### *3.3.1 In vivo chemical cross-linking of H69AR cells*

As illustrated in Figure 3.1, an experimental approach involving *in vivo* chemical cross-linking and MS measurements was used for identifying proteins associated with MRP1. To cross-link adjacent proteins, a protocol employing DSP that has previously been used to determine the oligomerization state of CFTR [166] was adopted. DSP is a homobifunctional, thiol cleavable, and membrane permeable amine-reactive cross-linking agent. It contains an amine-reactive NHS ester at each end of an 8-carbon spacer arm (12.0 Å) (Fig. 3.2B) which reacts with primary amines at pH 7-9 to form stable amide bonds (Fig. 3.2A). To examine the cross-linking effect and determine the optimal reaction conditions in H69AR cells, several experimental parameters, such as the incubation time, DSP concentration and reaction temperature, were investigated. Figure

**A**



**B**

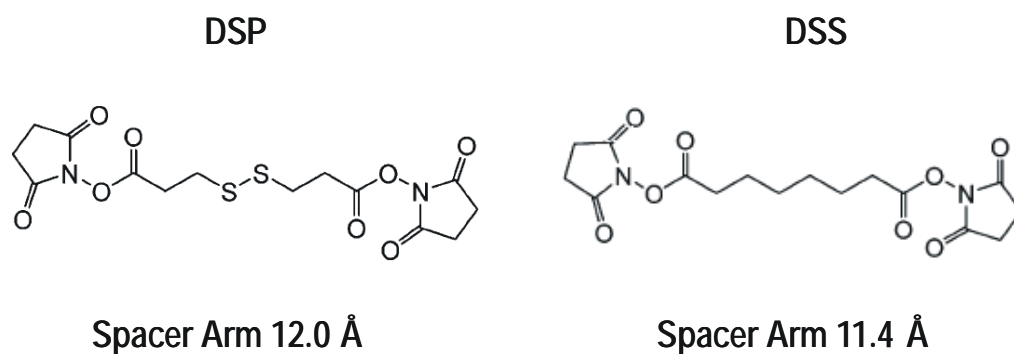
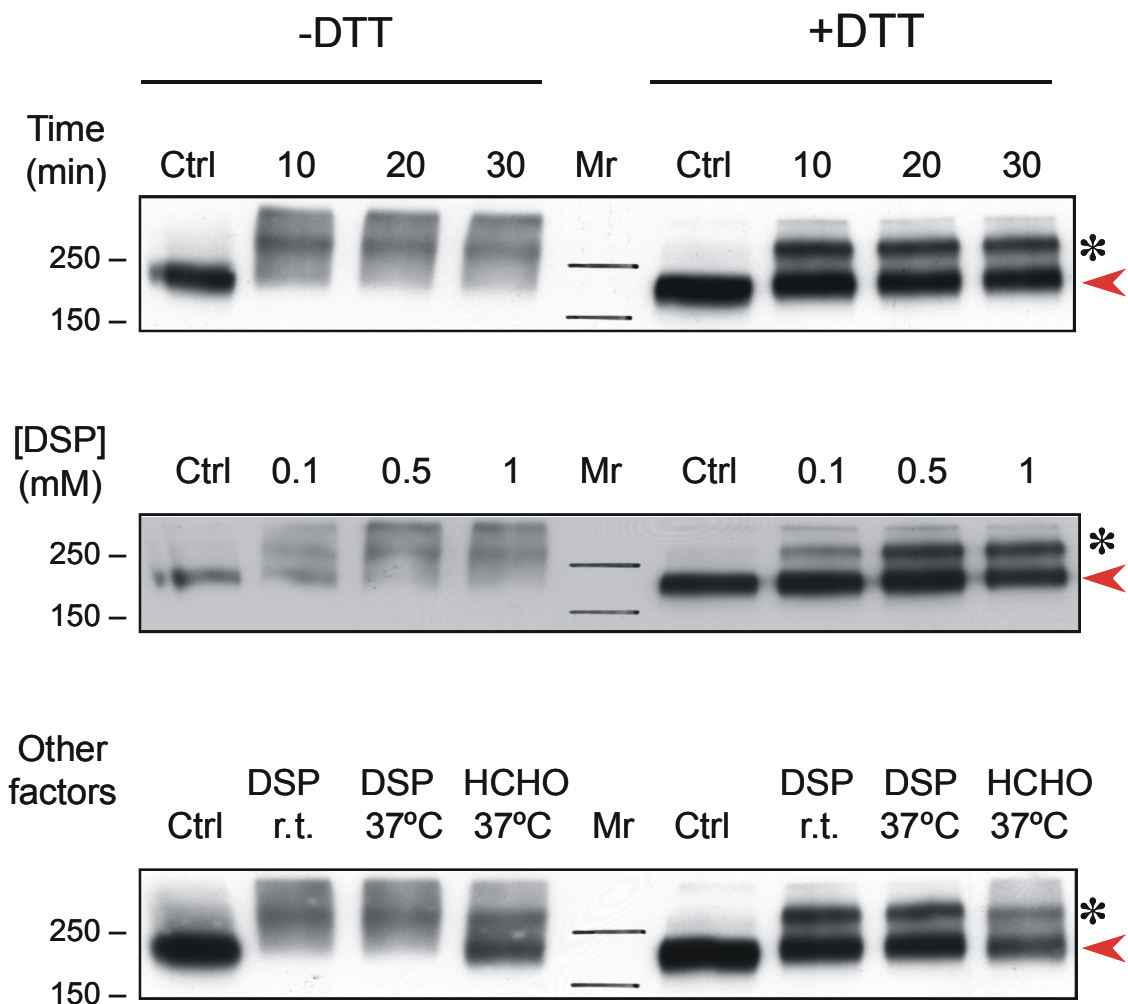


**Figure 3.2: Reaction scheme of NHS-ester and chemical structure of NHS-ester cross-linkers.** (A) Reaction scheme of NHS-ester functional group reacts with a primary amine which forms a covalent amide bond and free NHS. (B) Chemical structures of NHS-ester crosslinking agent DSS and its thiol-cleavable derivative DSP (adapted from Pierce crosslinking reagents technical handbook).

3.3 shows an immunoblot of lysates prepared from H69AR cells cross-linked under various conditions. When probed with MRP1-specific mAb MRPr1, all DSP-treated samples appeared as smears, and no clear band was detected unless the sample was subsequently incubated with DTT (Fig. 3.3). After reduction by DTT, two immunoreactive bands were apparent. The lower band was full-length MRP1 according to the molecular weight standard and comparison with the control (no cross-linker). The upper band, which was present in all cross-linked samples but not in the control, had a molecular weight > 250 kDa. The intensity of this upper band seemed to increase as the concentration of DSP increased (Fig. 3.3, middle blot). The aggregation observed in the cross-linked samples not incubated with DTT suggested that either intra- or inter-molecular cross-linking had occurred. The higher molecular weight immunoreactive band revealed by incubating with DTT may be the cross-linked product. Since the efficiency of cross-linking did not change after 10 min of incubation with 0.5 mM DSP at room temperature (Fig. 3.3), subsequent experiments were carried out using these conditions.

The cross-linked complexes were affinity purified using a mixture of four well-characterized MRP1-specific mAbs (QCRL-1 to -4) [23, 25, 164]. The complexes were then dissociated with DTT and separated by SDS-PAGE. Coomassie Brilliant blue staining of proteins copurified with MRP1 showed that the recovery of proteins in DSP-treated H69AR cells was greatly reduced compared with untreated cells (Fig. 3.4). In the cross-linked sample, even the predominant MRP1 band was of low intensity. Several DSP cross-linking reaction conditions tested in this study did not improve the yield (data

**Figure 3.3: *In vivo* cross-linking of H69AR cells with DSP.** H69AR cells were incubated with DSP (1 mM) at room temperature for various times (top blot); or with various concentrations of DSP at room temperature for 30 min (middle blot); or with DSP (1 mM) or formaldehyde (1%) at different temperatures for 30 min (bottom blot). The control (denoted as Ctrl) was H69AR cells with no cross-linker added. Cell lysates were prepared and DTT (100 mM final concentration, 30 min, room temperature) was added to half of the samples before resolving protein by 7% SDS-PAGE. Protein were then electrotransferred from the gel to PVDF membrane, and immunoblotted with rat MRP1-specific mAb MRPr1 (1:5,000). Arrows indicate the 190 kDa full-length MRP1. Asterisks indicate a higher molecular weight immunoreactive band found in all DTT-treated samples.



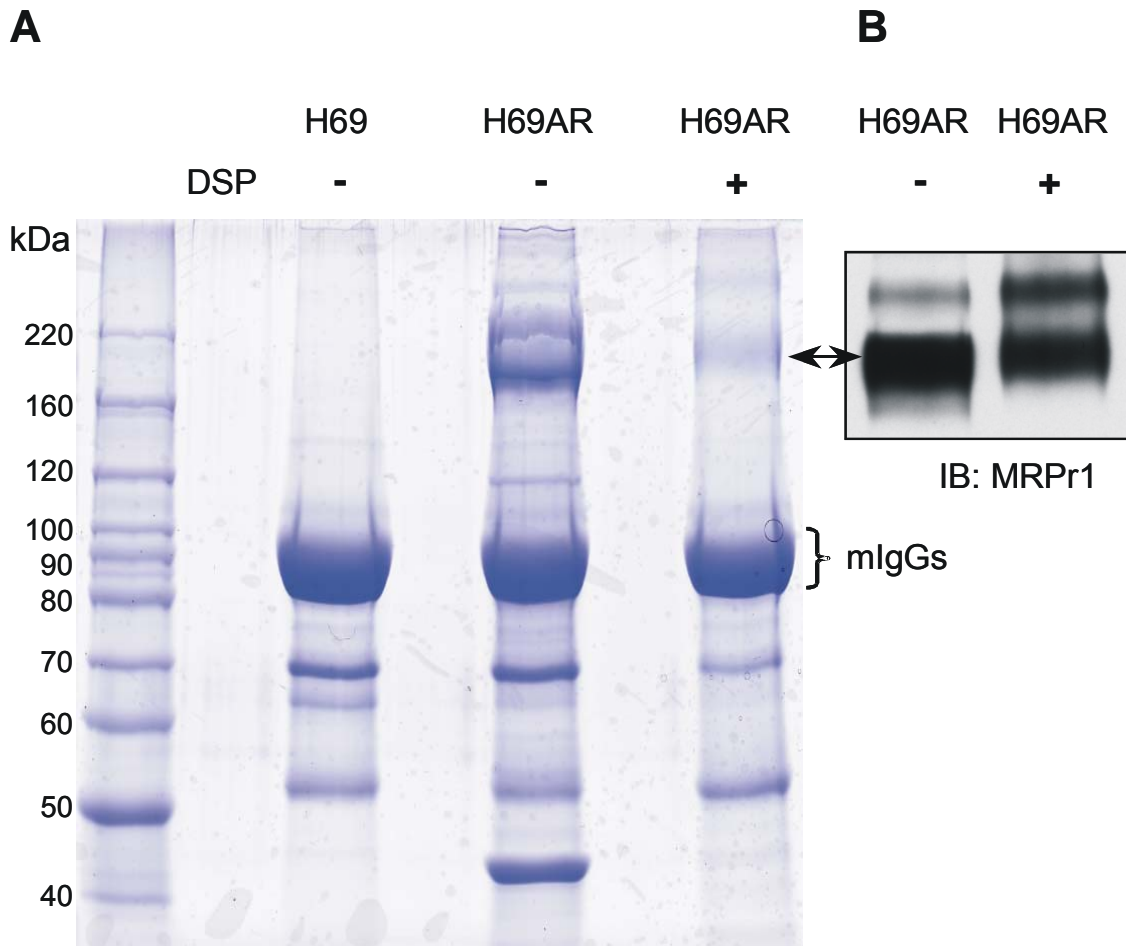


**Figure 3.4: Immunoaffinity purification of MRP1 and potential interacting proteins from H69, H69AR, and H69AR cells treated with DSP.** (A) Lysates prepared from H69, H69AR, or DSP-treated (0.5 mM, 10 min, room temperature) H69AR cells were affinity purified using a mixture of MRP1-specific mAbs (QCRL-1, QCRL-2, QCRL-3, and QCRL-4). The immunoprecipitates were separated by 7% SDS-PAGE and stained with Coomassie Brilliant Blue. The intense diffuse bands at ~90 kDa are mouse IgG heavy chain dimers as noted. (B) The H69AR samples from (A) were immunoblotted with mAb MRPr1 (1:5,000). The arrow indicates the 190 kDa full-length MRP1.

not shown). Unfortunately, the amount of MRP1-containing complex recovered from DSP-cross-linked cells was too low to generate accurate protein identification by MS. The reason for the low protein yield is unclear, but it may be caused by the modification of the mAb epitopes due to excessive cross-linking. Whatever the reason, the DSP cross-linking approach was not successful under the conditions tested. However, the Coomassie stain revealed several protein bands that co-immunoprecipitated with MRP1 and were present in H69AR (MRP1 overexpressing) cells but not in H69 (very low MRP1 expression) cells (Fig. 3.4). Whether any of these proteins have specific associations with MRP1 is unknown.

### *3.3.2 Identification of proteins co-immunoprecipitated with MRP1 by MS*

To identify the proteins that were associated with MRP1 by co-immunoprecipitation, sufficient amounts of the MRP1-containing complexes needed to be purified to allow MS analysis. The MRP1-containing protein complexes were affinity purified from batches of  $2 \times 10^8$  H69AR cells and separated by SDS-PAGE. Coomassie Brilliant blue staining of gel revealed numerous protein bands. Six major bands (Fig. 3.5) were excised and digested with trypsin. Tryptic peptides were extracted, separated by nanoflow LC, and introduced into the qTOF mass spectrometer. MS/MS analysis and database searching of the sequenced peptides resulted in the identification of six proteins in addition to MRP1, each of which matched to at least two unique peptide sequences (Table 3.1). All proteins that were identified had a Mowse score higher than the

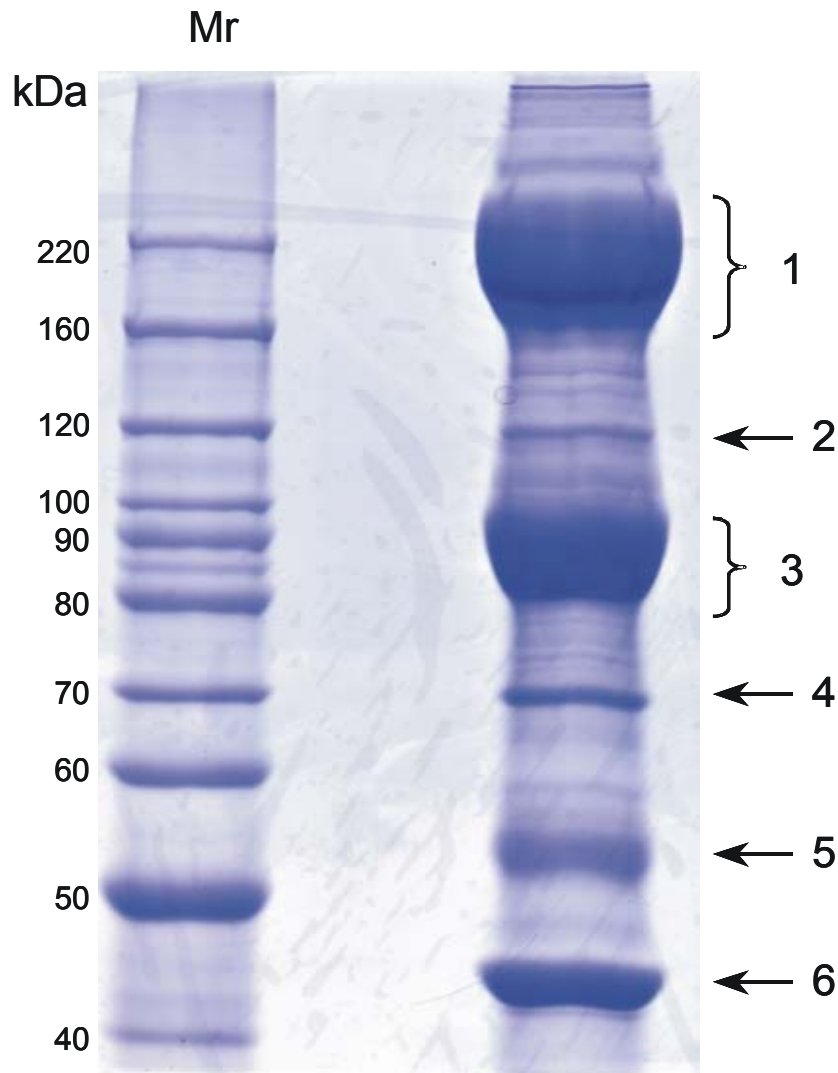


**Figure 3.5: SDS-PAGE and Coomassie staining of proteins obtained by co-immunoprecipitation with MRP1.** MRP1 and its putative associated protein partners were copurified using a mixture of MRP1-specific mAbs (QCRL-1 to 4). The immunoprecipitate was separated by SDS-PAGE (7%, 1 mm gel) and stained with Coomassie Brilliant Blue. The number 1-6 to the right of the gel denote major protein bands excised and analyzed by MS. Band 1: myosin, MRP1; Band 2: drebrin; Band 3: mouse IgG; Band 4: fusion, ribophorin I; Band 5:  $\beta$ -tubulin; Band 6:  $\alpha$ -actin.

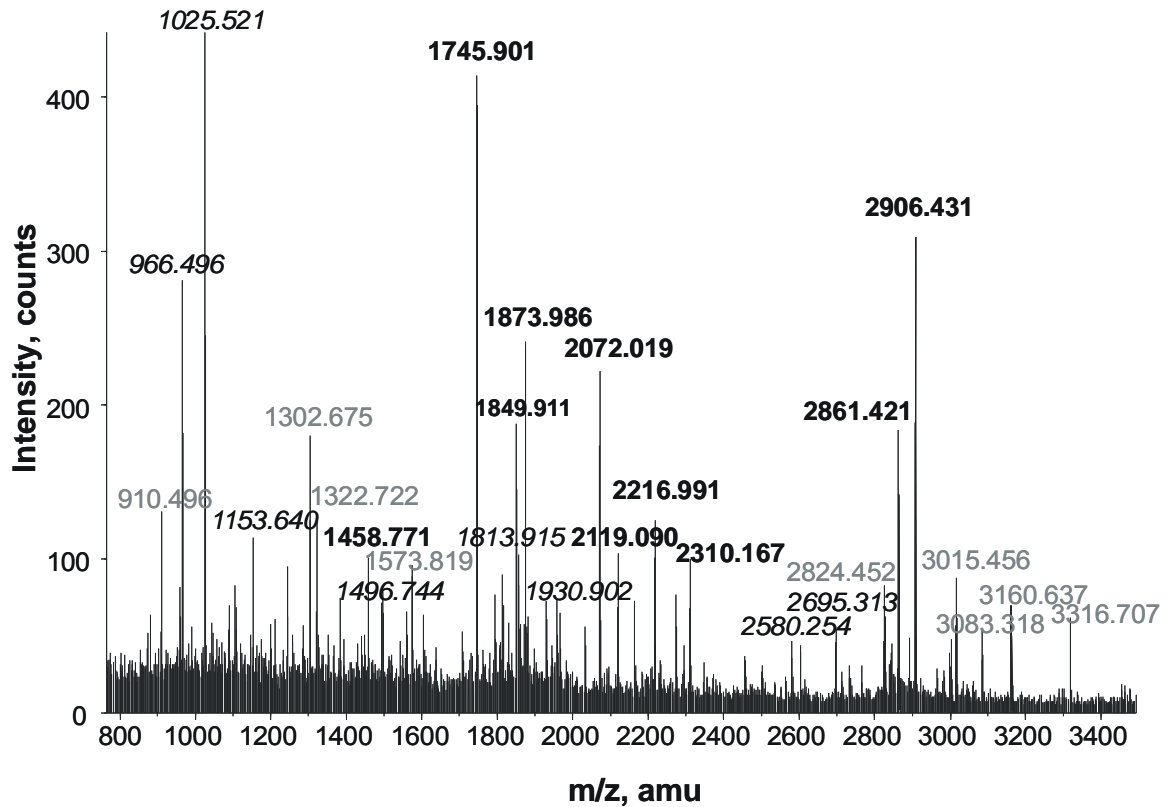
statistically significant threshold [169]. Some gel bands (Fig. 3.5, band 1 and 4) contained more than one protein.

To test for reproducibility, a total of three independent experiments were carried out in which two were ESI-based MS analysis and one was MALDI-TOF MS analysis. The LC coupled MS analysis is a fully automatic data collection process and best for identifying a mixture of proteins whereas MALDI MS analysis is operated manually and thus has a higher accuracy with respect to identifying the protein of interest. Figure 3.6 shows a representative MALDI MS spectrum of a tryptic peptide derived from the protein band with an estimated mass of 120 kDa (Fig. 3.5, band 2). Subsequent MS/MS analysis identified the major protein as human drebrin isoform E with a Mowse score of 608 (Fig. 3.6). The reason for the remarkably slow migration of drebrin in the SDS polyacrylamide gel is not known. However, biochemical studies have shown that drebrin is highly serine/threonine phosphorylated *in vivo* [170, 171]. Peptides from most protein bands other than ribophorin I (band 4) were identified in all three experiments with significant Mowse scores (Table 3.1), whereas the peptide derived from ribophorin I was observed in only one experiment using LC-MS/MS analysis.

### *3.3.3 Protein-protein association by reciprocal co-immunoprecipitation*

The protein MS analysis revealed six proteins from H69AR cell lysates that co-immunoprecipitated with MRP1 using anti-MRP1 antibodies (Fig. 3.5). The reported cellular function and subcellular localization of these six proteins are listed in Table 3.1. Myosin is an actin-based motor protein that utilizes the energy from ATP hydrolysis at

**Figure 3.6: MALDI-MS spectrum of drebrin E tryptic fragments.** A representative MALDI-MS spectrum of tryptic peptides extracted from gel band 2 (Fig. 3.5) with an estimated molecular weight of 120 kDa. The extracted tryptic peptides were analyzed using MS-Fit program against the NCBI database. The  $m/z$  ions representing drebrin are in boldface type. The  $m/z$  ions representing MRP1 are indicated in italics. The tandem mass spectrum of each drebrin-derived  $m/z$  ions was analyzed using the Mascot search engine. The Mowse score and sequence coverage are indicated with the matched sequences in boldface type.



**Drebrin E      Score 608      21% sequence coverage**

MAGVSFSGHR	LELLAAYEEV	IREESAADWA	LYTYEDGSDD	LKLAASGEGG	LQELSGHFEN
QKVMYGFCSV	KDSQAALPKY	VLINWVGEDV	PDARKCACAS	HVAKVAEFFQ	GVDVIVNASS
VEDIDAGAIG	QRLSNGLARL	SSPVLHRLRL	REDENAEPVG	TTYQKTDAAV	EMKRINREQF
WEQAKKEEEL	RKEEERKKAL	DERLRFEQER	MEQERQEQEE	RERRYREREQ	QIEEHRKQQ
<b>TLEAEEAKRR</b>	<b>LKEQSIFGDH</b>	<b>RDEEEETHMK</b>	<b>KSESEVEEAA</b>	<b>AIIAQRPDNP</b>	<b>REFFKQQERV</b>
ASASAGSCDV	PSPFNHRPGS	HLDSHRMAP	TPIPTRSPSD	SSTASTPVAE	QIERALDEVT
SSQPPPLPPP	PPPAQETQEP	SPILDSEETR	AAAPQAWAGP	MEEPPQAQAP	PRGPGSPAED
LMFMESAEQA	VLAAPVEPAT	ADATEVHDAA	DTIETDTATA	DTTVANNVPP	AATSLIDLWP
GNGEGASTLQ	GEPRAPTPPS	GTEVTLA EVP	LLDEVAPEPL	LPAGEGCATL	LNFDELPEPP
ATFCDPEEVE	GEPLAAPQTP	TLPSALEELE	QEQEPEPHLL	TNGETTQKEG	TQASEGYFSQ
SQEEFAQSE	ELCAKAPPPV	FYNKPPEIDI	TCWDADPVPE	EEEGFEGGD	

**Table 3.1: Summary of LC- MS/MS analysis of proteins co-immunoprecipitated with MRP1 <sup>a</sup>**

Band <sup>b</sup>	Protein	Accession no. <sup>c</sup>	Calculated mass (kDa) <sup>d</sup>	Actual mass (kDa) <sup>e</sup>	Mowse Score <sup>f</sup>	Peptide sequenced <sup>g</sup>	Function	Subcellular localization	Ref.
1	Myosin	NP_002464	227.6	NA	726	104	Motor protein	Cytosol	172
1	MRP1	AAB83983	163.7	190	511	57	ABC transporter	Plasma membrane	11
2	Drebrin	Q16643	71.8	120	68	4	F-actin binding protein	Cytosol	176
3	Anti-human mAb IgG heavy chain	CAD88275	52.0	~90	440	7			
4	Fusion	AAH26062	53.3	68	77	8	RNA-binding protein	Nucleus	174
4	Ribophorin I	NP_002941	68.6	68	46	2	OST complex member	Rough ER	177
5	$\beta$ -Tubulin	NP_001060	50.3	55	252	18	Cytoskeleton component	Cytosol	173
6	$\alpha$ -Actin	BAD96645	42.0	42	608	12	Cytoskeleton component	Cytosol	173

NA: not available

- <sup>a</sup>. Results listed are the better of two independent LC-MS/MS experiments.
- <sup>b</sup>. Band numbers – see Figure 3.5
- <sup>c</sup>. The accession number refers to the protein with the highest number of hits when the MS/MS spectra were searched against the NCBI database.
- <sup>d</sup>. The calculated molecular mass is based on amino acid sequence (obtained from the Mascot search engine) and does not take into account any post-translational modifications.
- <sup>e</sup>. Molecular mass according to SDS-PAGE.
- <sup>f</sup>. The probability based molecular weight search (Mowse) scores were assigned by Mascot search engine. A Mowse score of 45 or higher was considered statistically significant when searched against the NCBI database of Homo sapiens taxonomy. With the exception of Band 3, the MS/MS spectra were searched against the NCBI database for all species and the statistically significant threshold value was 57. The protein identified was *Mus musculus* origin.
- <sup>g</sup>. The number of peptides identified by MS/MS that have the sequences matching the particular protein.

the motor domain to move along the actin filaments [172]. Tubulin and actin are major cytoskeleton components [173]. Fusion (FUS) is an RNA-binding protein and contributes to the reciprocal chromosomal translocation t(12;16)(q13;p11) in myxoid-round cell liposarcoma [174, 175]. Drebrin (neuron-specific developmentally regulated brain protein) is an F actin-binding protein and is found mainly in neurons [176]. Ribophorin I is a part of the oligosaccharyltransferase (OST) complex which catalyzes the *N*-glycosylation of newly synthesized polypeptides in the rough ER [177].

Three of the six proteins, FUS, drebrin and actin, were selected for further study to determine if they interacted directly with MRP1. FUS was selected because of its reported oncogenic properties [174, 175]. Drebrin and actin were selected because drebrin binds to actin so that they may function as scaffolding proteins close to the plasma membrane, as reported for the gap junction protein connexin-43 (Cx43) [178].

Protein-protein interactions between MRP1 and FUS, drebrin and actin were studied by reciprocal co-immunoprecipitation, where a physical interaction between two proteins can be verified by immunoprecipitation of either protein in the complex. However, this verification is based on the assumption that the antibodies used do not disrupt particular protein-protein interactions and the epitopes recognized by the antibodies are not blocked by the physical association [179]. The anti-FUS, anti-drebrin and anti-actin mAbs used in the present study were obtained from commercial suppliers. The mouse anti-FUS mAb (clone 4H11) was raised against a fusion protein corresponding to the COOH-terminus of human FUS. The mouse anti-drebrin mAb (clone M2F6) was raised against purified chicken drebrin E, which reacts with both

drebrin E and A isoforms on immunoblotting. The mouse anti-actin mAb (clone AC-40) recognizes an epitope located on the COOH-terminal end of actin, which is conserved in all actin isoforms.

When using a solubilization buffer containing 1% CHAPS as detergent, MRP1, drebrin and actin were able to pull down each other by using antibodies specific to either protein (Fig. 3.7B, lane 4, 6 and 8). Furthermore, this phenomenon was only observed in lysates from MRP1 overexpressing H69AR cells but not in lysates from H69 cells (Fig. 3.7B, lane 3-8). No detectable MRP1 was pulled down by anti-FUS mAb under the conditions used (Fig. 3.7B, lane 10). When another commonly used solubilization condition containing 1% Triton X-100 was applied (Fig. 3.8A), in general, more proteins were recovered than with 1% CHAPS (Fig. 3.7A). However, the immunoprecipitation profile did not change much for MRP1, where all three selected candidate proteins were co-immunoprecipitated with MRP1 under either set of conditions (Fig. 3.7B, lane 8; Fig. 3.8B, lane 6). Also, drebrin and actin seemed to copurify when either one was present (Fig. 3.7B, lane 4, 6 and 8; Fig. 3.8B, lane 3-10). However, the immunoprecipitation profiles for some mAbs were altered by using a different lysis buffer. Thus use of the 1% Triton X-100 buffer allowed the FUS mAb to pull down MRP1 from the H69AR cell lysate (Fig. 3.8B, lane 4, empty arrow) but this was not the case for the mAbs specific for drebrin and actin (Fig. 3.8B, lane 8 and 10).

**Figure 3.7: Co-immunoprecipitations of MRP1 and potential interacting proteins in H69 and H69AR cells.** H69 and H69AR (denoted as AR) cells were lysed in CHAPS-containing lysis buffer and immunoprecipitations were carried out as described in Section 3.2.3. (A) SDS-PAGE and Coomassie blue staining of proteins obtained after each immunoprecipitation. Arrows (from top to bottom) indicate the approximate molecular weights for MRP1 (190 kDa), drebrin (120 kDa), FUS (68 kDa), tubulin (55 kDa) and actin (42 kDa). The presence of any of these proteins needs to be confirmed by immunoblotting. (B) Immunoblotting of proteins obtained after each immunoprecipitation. Equal volumes of samples (5  $\mu$ l of inputs and 3  $\mu$ l of immunoprecipitates) were loaded in each lane. The membrane was stripped and reprobed several times with the different mAbs against the proteins indicated on the left. Horseradish peroxidase conjugated goat anti-mouse IgG (H+L) (1:10,000) was used to detect mouse IgGs that were used in each immunoprecipitation (denoted as mIgGs). Rat mAb MRPr1 (1:5,000) was used to detect MRP1. Mouse mAb clone M2F6 (1:5,000) was used to detect drebrin. Mouse mAb clone 4H11 (1:5,000) was used to detect FUS. Mouse mAb clone AC-40 (1:5,000) was used to detect actin. Empty arrows indicate the presence of MRP1.

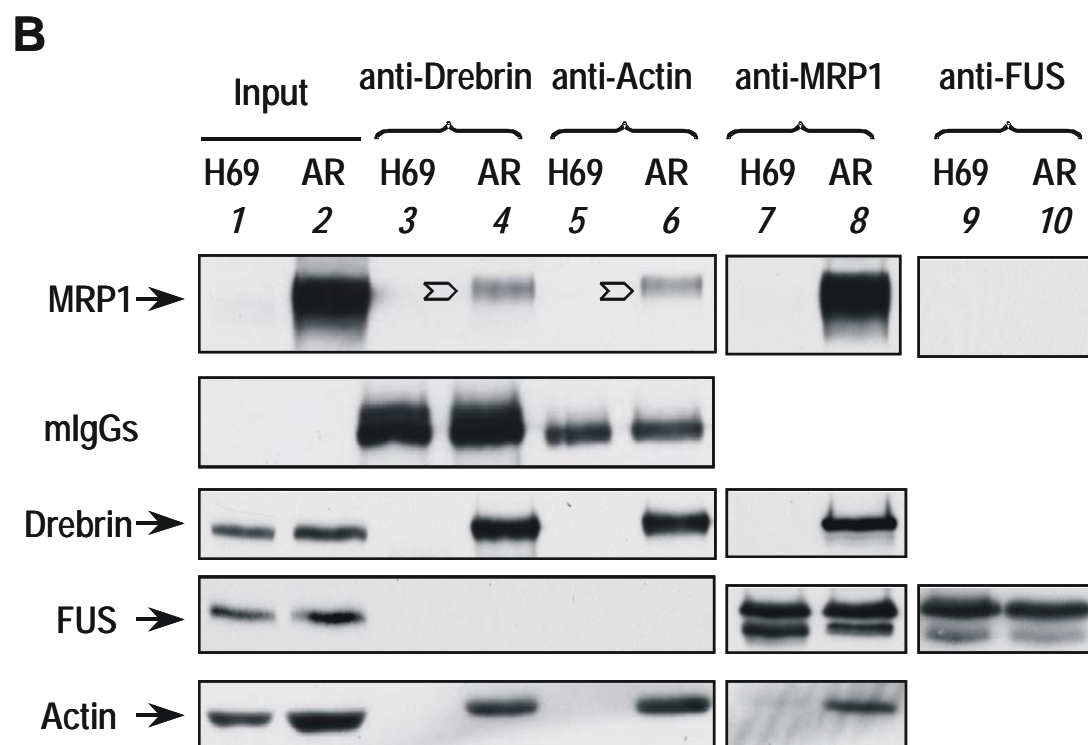
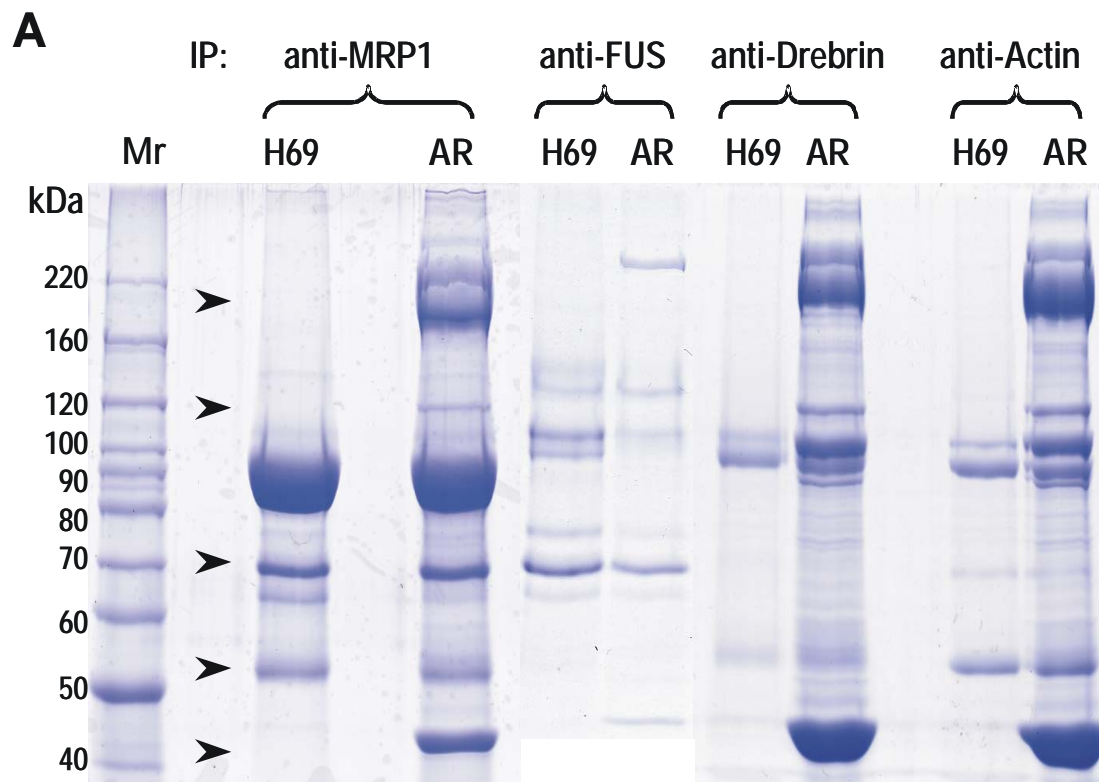
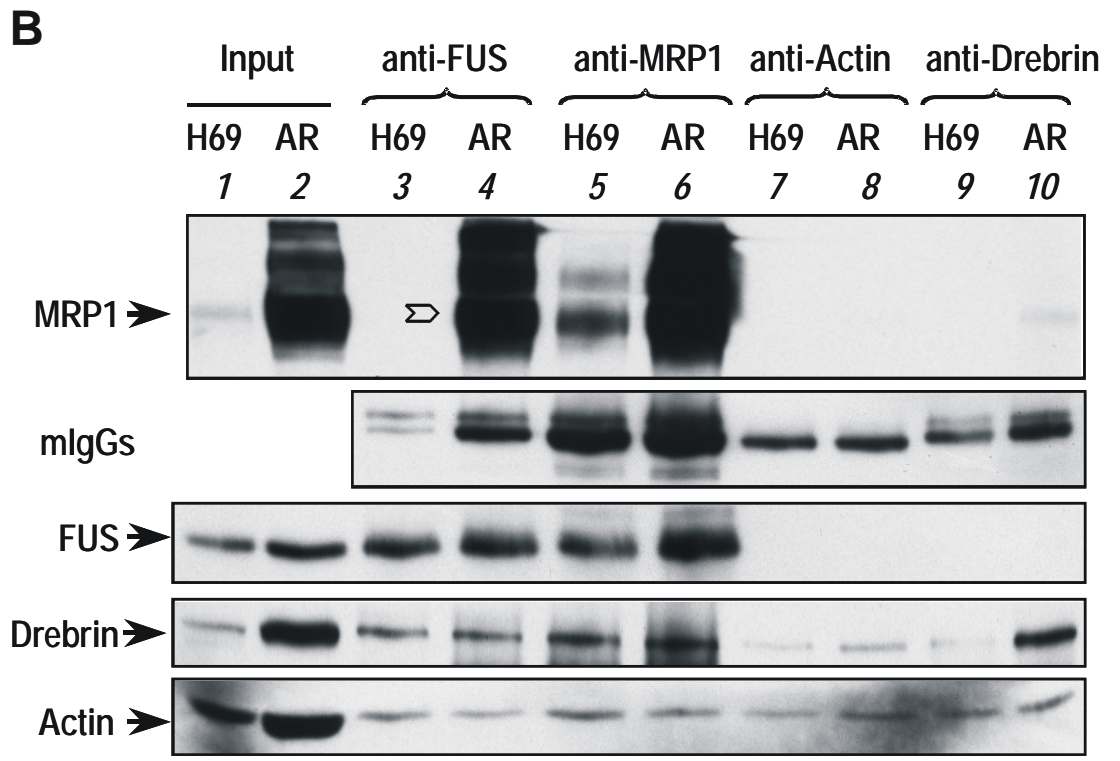
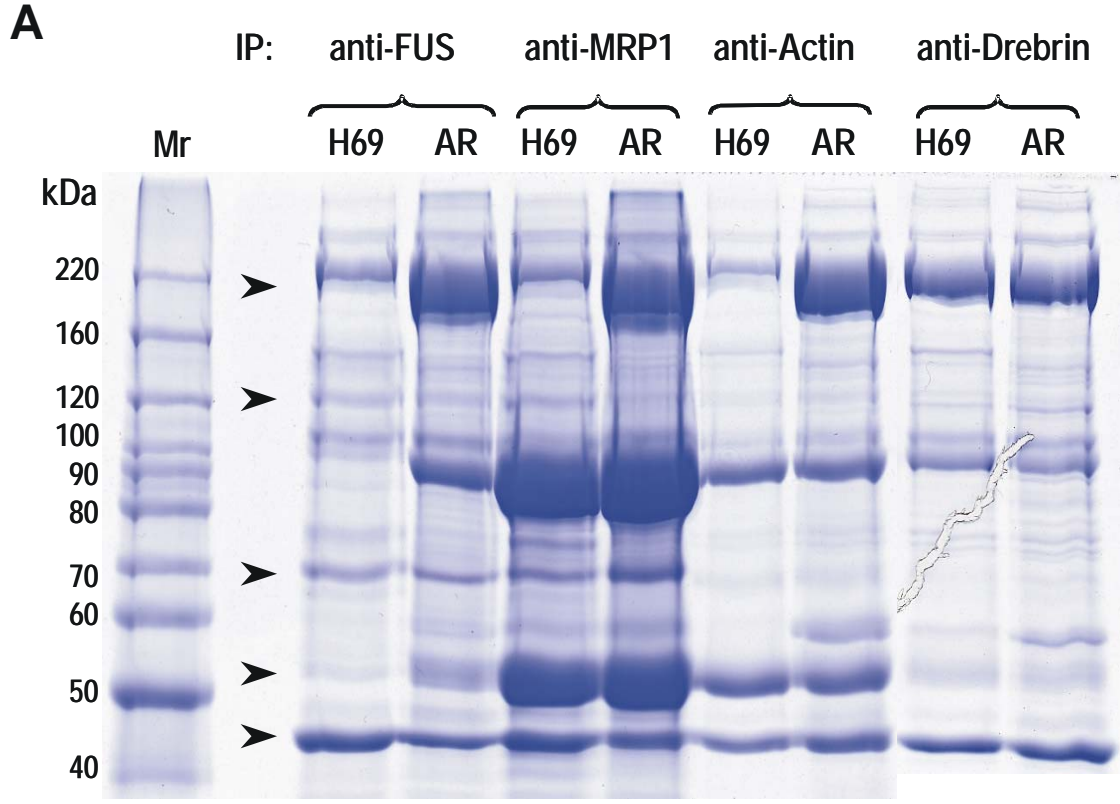


**Figure 3.8: Co-immunoprecipitations of MRP1 and its potential interacting proteins in H69 and H69AR cell lysates containing 1% Triton X-100.** H69 and H69AR (denoted as AR) cells were lysed in lysis buffer containing 1% Triton X-100 (v/v) and immunoprecipitations were carried out as described in Section 3.2.3. (A) SDS-PAGE and Coomassie blue staining of proteins obtained after each immunoprecipitation. Arrows (from top to bottom) indicate the approximate molecular weights for MRP1 (190 kDa), drebrin (120 kDa), FUS (68 kDa), tubulin (55 kDa) and actin (42 kDa). The presence of any of these proteins needs to be confirmed by immunoblotting. (B) Immunoblotting of proteins obtained after each immunoprecipitation. Equal volumes of samples (5  $\mu$ l of inputs and 3  $\mu$ l of immunoprecipitates) were loaded in each lane. The membrane was stripped and reprobed several times with the different mAbs against the proteins indicated on the left. Horseradish peroxidase conjugated goat anti-mouse IgG (H+L) (1:10,000) was used to detect mouse IgGs that were used in each immunoprecipitation (denoted as mIgGs). Rat mAb MRPr1 (1:5,000) was used to detect MRP1. Mouse mAb clone M2F6 (1:5,000) was used to detect drebrin. Mouse mAb clone 4H11 (1:5,000) was used to detect FUS. Mouse mAb clone AC-40 (1:5,000) was used to detect actin. Empty arrow indicates the presence of MRP1.



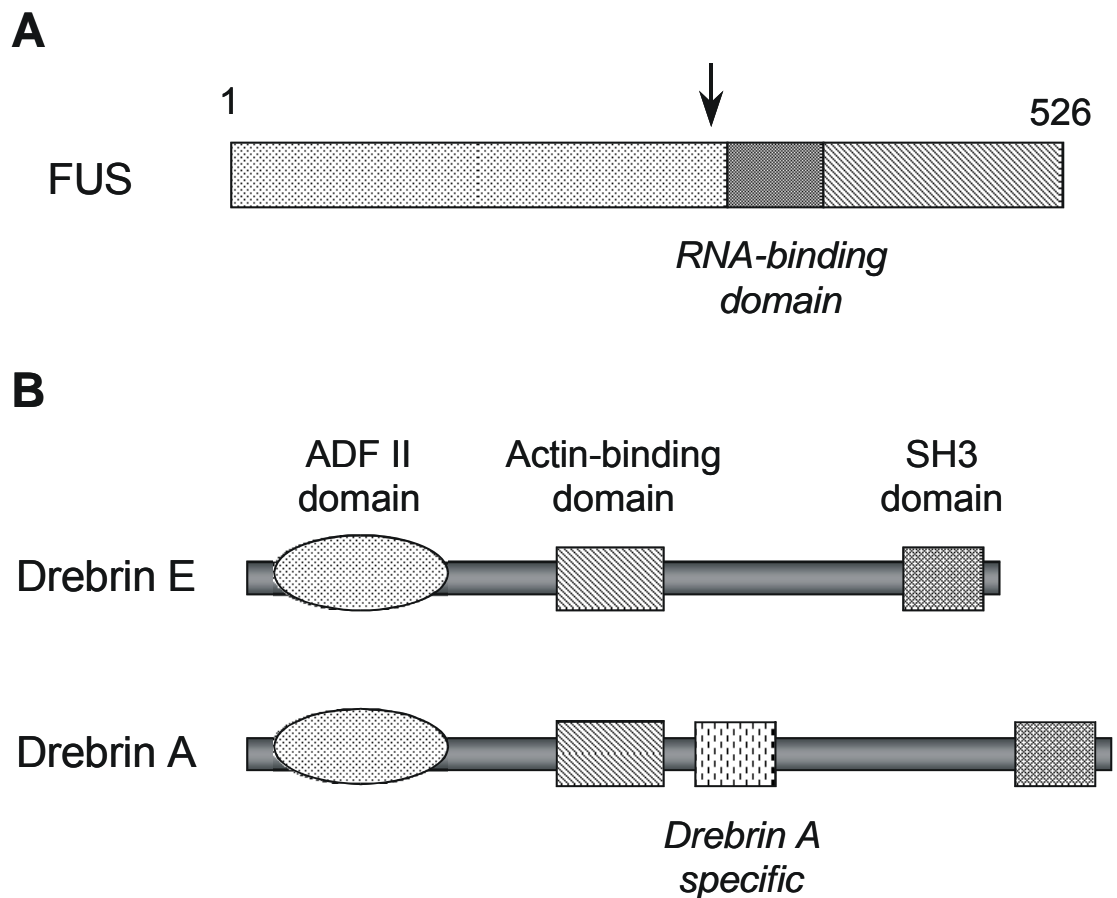
### *3.3.4 Cellular localization of FUS*

FUS is a 526-amino acid protein that contains an RNA-recognition motif (Fig. 3.9A) and is a component of nuclear riboprotein complexes which function like a chaperone for RNA in the nucleus [174, 175, 180]. In this study, FUS was one of the proteins identified in the co-immunoprecipitate with MRP1 when a mixture of MRP1-specific antibodies was used. Moreover, the anti-FUS mAb was able to pull down MRP1 in a reciprocal co-immunoprecipitation experiment.

To further investigate the potential interaction between FUS and MRP1, the cellular localization of FUS in MRP1 expressing cell lines was determined by subcellular fractionation and immunofluorescence microscopy. In agreement with previous reports [174, 175, 180], FUS was found mainly in nuclear extracts whereas MRP1 was found in cytosolic/membrane extracts of H69AR cells (Fig. 3.10A). Moreover, FUS was equally abundant in H69 and H69AR cells (Fig. 3.10A, whole cell lysate samples). When examined by confocal microscopy, FUS had a very distinctive nuclear localization in both H69AR cells and HEK cells transiently transfected with wild-type MRP1 cDNA whereas MRP1 was located in the plasma membrane as expected (Fig. 3.10B). Based on its apparently exclusive nuclear localization, FUS seems unlikely to have a direct interaction with MRP1.

### *3.3.5 Consequences of Drebrin siRNA knock-down*

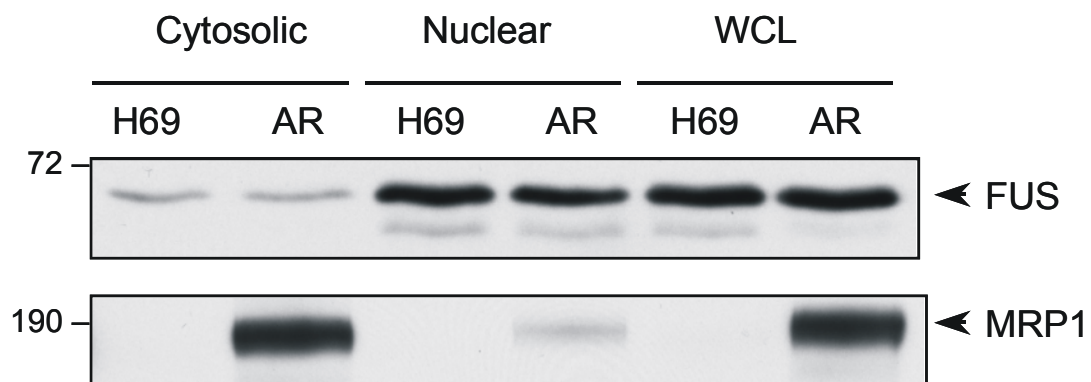
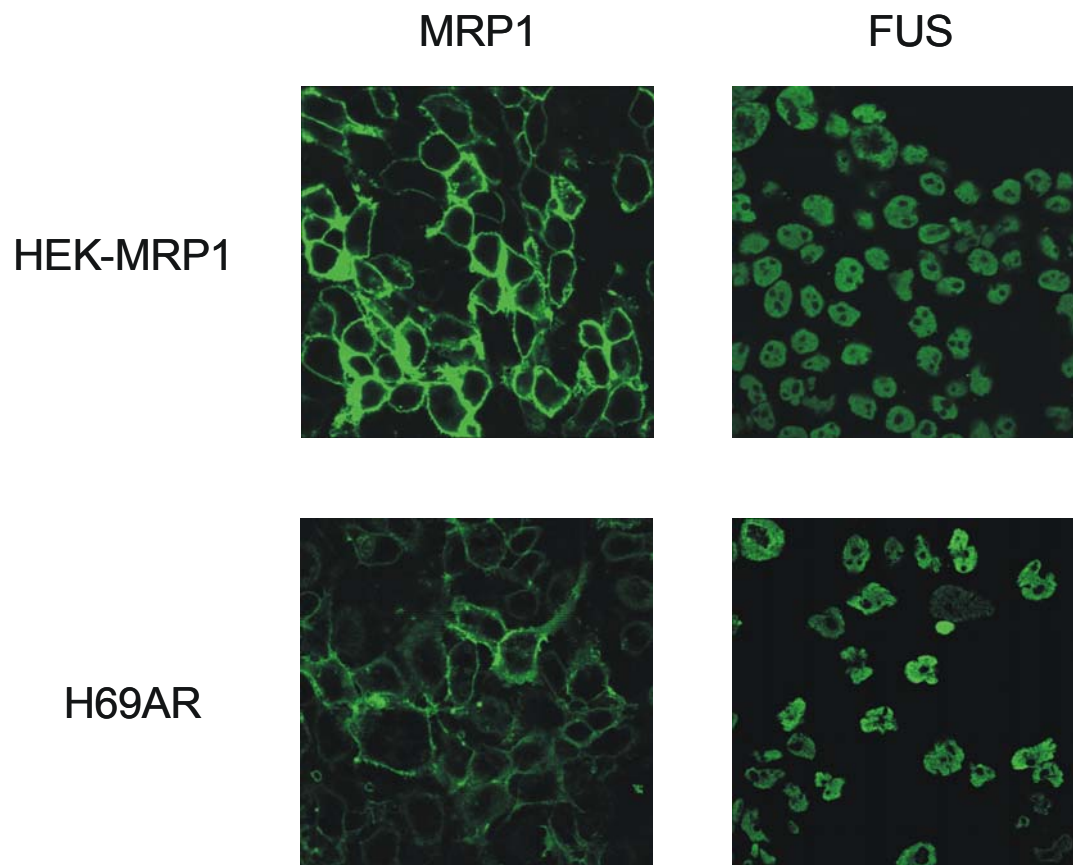
Drebrin and actin both showed a physical association with MRP1 by reciprocal co-immunoprecipitation of H69AR cell lysates prepared using 1% CHAPS solubilization



**Figure 3.9: Domain structures of FUS, and drebrin E and A proteins.** (A) Shown is the domain structure of the 526-amino acid FUS protein. The myxoid-round cell liposarcoma exhibits the characteristic chromosomal translocation  $t(12;16)(q13;p11)$  that fuses the 5' part of the FUS gene (right before the RNA-binding motif, indicated by an arrow) with the complete coding region of transcription factor DDIT3 [174, 175]. (B) The drebrin E (embryonic) and A (adult) refer to the different isoforms of drebrin that arise from alternative splicing. Drebrin A protein differs from drebrin E by an internal 46 amino acid insertion indicated by the hatched box [191]. ADF II, actin-depolymerizing factor homology domain.

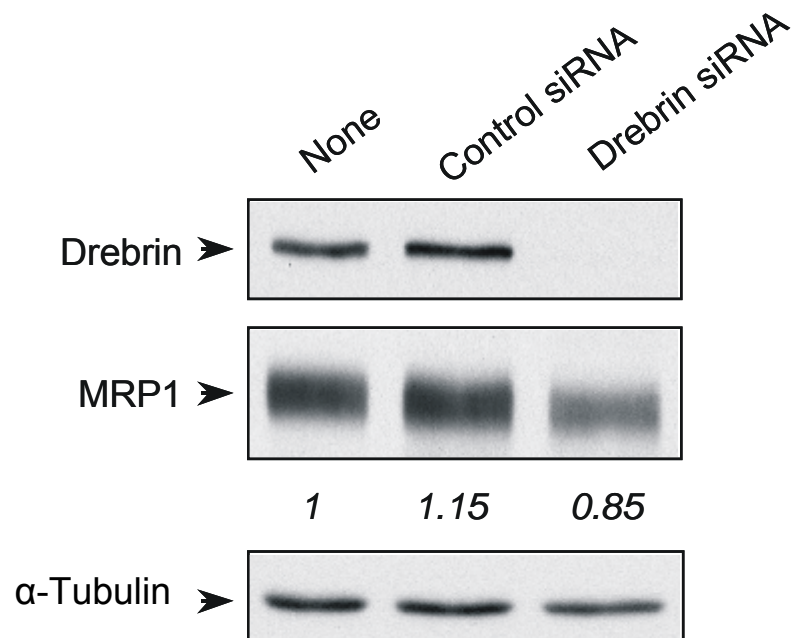
**Figure 3.10: Subcellular localization of FUS in various MRP1 expressing cell lines.**

(A) Immunoblot analysis of cytosolic and nuclear fractions as well as whole cell lysates (denoted as WCL) from H69 and H69AR (denoted as AR) cells. Cellular fractions (15  $\mu$ g) prepared from H69 and H69AR cells were subjected to 7% SDS-PAGE, and then electrotransferred to a PVDF membrane. The membrane was probed with mouse anti-FUS mAb (1:5,000). The same membrane was stripped and reprobed with mouse MRP1-specific mAb QCRL-1 (1:10,000). (B) Immunofluorescence staining for MRP1 and FUS in HEK293T cells transfected with MRP1 cDNA expression vector (denoted as HEK-MRP1) and H69AR cells. Cells were plated and fixed as described in Section 3.2.10. Each confocal microscopy image was single stained by either mouse anti-FUS mAb (1:200) or mouse MRP1-specific mAb QCRL-3 (1:2,500), and Alexa 488-conjugated goat anti-mouse IgG was used as the secondary antibody in all samples.

**A****B**

buffer (Fig. 3.7B, lane 4 and 6). Drebrin has been previously reported to be a cytosolic protein that associates with the gap junction protein Cx43 at the plasma membrane of the cell-cell interface [178]. Thus, the cellular localization of drebrin makes it conceivable that it could interact with MRP1 directly at the sub-plasma membrane region. If so, it is also possible that it might stabilize the expression of MRP1 at the plasma membrane.

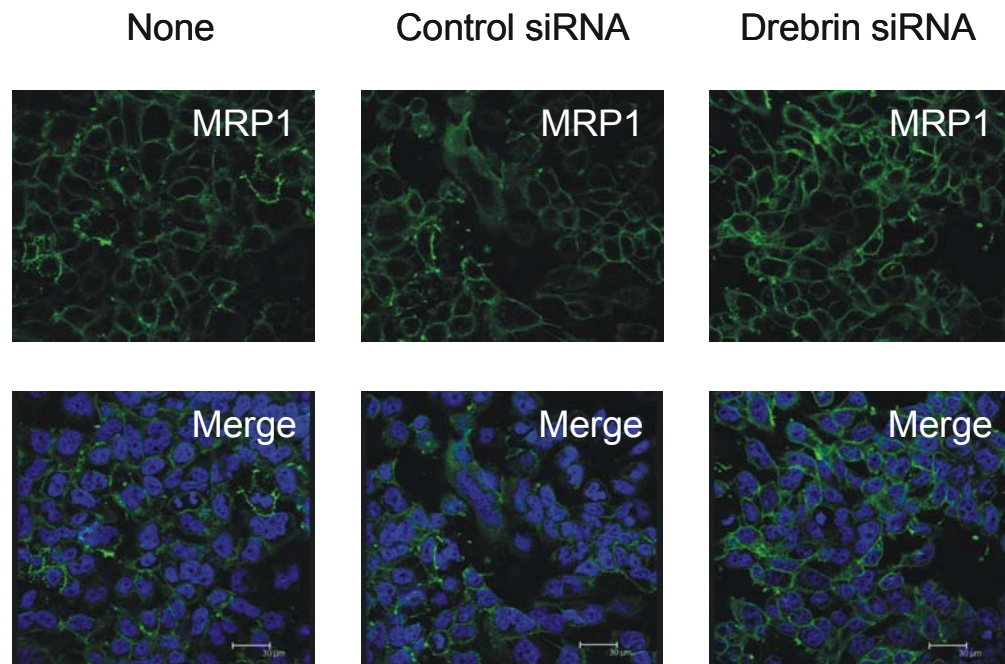
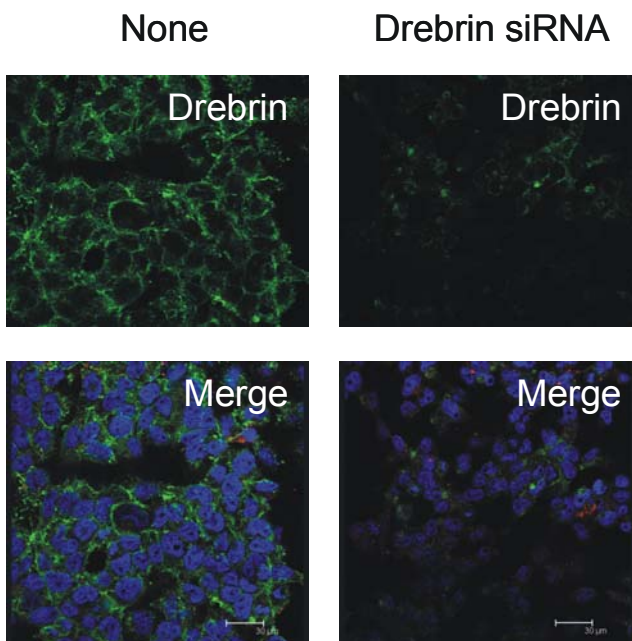
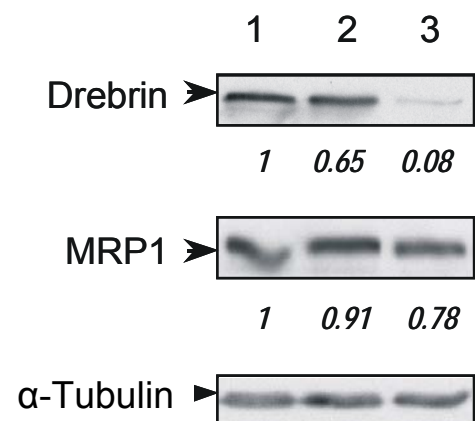
To determine if drebrin levels affect plasma membrane expression of MRP1 in H69AR cells, drebrin was knocked down with a SMART pool siRNA reagent containing a mixture of four siRNAs specific for human drebrin mRNA [165]. For more efficient knock-down, the cells were transfected with drebrin siRNA twice over five days of continuous culture. Cells were then analyzed by immunoblotting and immunofluorescent staining. Using this protocol, drebrin could be reduced to an almost undetectable level by immunoblotting (Fig. 3.11). As a consequence of drebrin knock-down, the overall level of MRP1 appeared to be downregulated by approximately 30% compared with control siRNA knock-down as indicated by immunoblotting (average of three independent experiments) (Fig. 3.11). Cells transfected with drebrin siRNA were also plated on glass slides and immunostained separately with anti-drebrin and anti-MRP1 antibodies. At least three images were taken at different areas of the coverslip for each immunostaining and a representative image of each condition is shown in Figure. 3.12A. The staining pattern of MRP1 did not seem to change after the drebrin knock-down and MRP1 remained mainly at the plasma membrane as in the control siRNA treated cells (Fig. 3.12A). On the other hand, there was barely any fluorescence detected in the drebrin knock-down cells stained with the anti-drebrin mAb (Fig. 3.12B). Immunoblotting



**Figure 3.11: Expression of MRP1 in H69AR cells treated with drebrin siRNA.**

Immunoblots of total proteins (15  $\mu$ g) after treatment of H69AR cells with control and drebrin siRNA. H69AR cells treated with transfection reagent only (denoted as none) were used as a control. The relative levels of MRP1 and drebrin are indicated in italics under the blot (normalized to  $\alpha$ -tubulin level which was used as a loading control).

**Figure 3.12: MRP1 expression and localization in H69AR cells treated with drebrin siRNA.** (A) Immunofluorescence staining for MRP1 (green) in H69AR cells treated with transfection reagent only (denoted as none), with control siRNA, and with drebrin-specific siRNAs. H69AR cells were sequentially transfected with siRNAs against drebrin (or control siRNA) twice over five days of continuous culture. All the samples were fixed, stained and examined by confocal microscopy on day 5. Cells were plated and fixed as described in Section 3.2.10. Each confocal microscopy image shows staining with MRP1-specific mouse mAb QCRL-3 (1:2,500), and Alexa 488-conjugated goat anti-mouse IgG was used as the secondary antibody. Cellular DNA was stained with DAPI (blue). Scale bar, 30  $\mu$ m. (B) Immunofluorescence staining for drebrin (mouse anti-drebrin mAb, 1:200) in H69AR cells treated with transfection reagent only (denoted as none), and H69AR cells treated with drebrin-specific siRNAs. The siRNA transfection and confocal microscopy preparation conditions were the same as in Panel A. Scale bar, 30  $\mu$ m. (C) Immunoblot of total proteins (8  $\mu$ g) after treatment of cells with control (lane 2) and drebrin siRNA (lane 3). Lane 1, H69AR cells treated with transfection reagent only. The relative drebrin and MRP1 levels are indicated in italics under each blot (normalized to  $\alpha$ -tubulin level which was used as a loading control).

**A****B****C**

showed that in this experiment, the drebrin knock down in H69AR cells was approximately 88% and MRP1 levels were reduced by approximately 14% compared with control siRNA knock-down (Fig. 3.12C, lane 2 and 3).

### **3.4 Discussion**

Chemical cross-linking is a tool that can maintain protein associations, especially noncovalent and transient interactions, by covalently connecting them as stable complexes. For amine-reactive chemical cross-linkers like DSP, the cross-linking reaction depends on the number and location of lysine residues within the interacting surfaces of the proteins [181]. These primary amine pairs must also be accessible to the agent and within the distance spanned by the cross-linker spacer arms [181]. Ideally, the cross-linker should covalently link associated proteins that are in close proximity to the protein of interest. However, the cross-linking reaction often results in some unwanted and nonspecific cross-linking events, such as self-conjugation, intramolecular cross-linking and polymerization. Therefore, the cross-linker concentration, reaction times, and buffer conditions need to be optimized to achieve optimal yields of cross-linked product, while at the same time, not disrupting the protein structures by introducing too many inter- and intra-molecular cross-links.

In the present study, several pieces of evidence indicate the presence of cross-linking, such as the smear observed in all cross-linker treated samples in the absence of DTT, as well as the higher molecular weight band resolved after DTT treatment (Fig. 3.3). There are several cross-linking possibilities that could account for this distinctive

band. First, this could represent intermolecular cross-linking between MRP1 and associated protein(s). Secondly, this could be the result of self-conjugation by intramolecular cross-linking of MRP1. Thirdly, this could be the dimerization of two MRP1 monomers. However, the size of the upper band (just over 250 kDa) suggests it is not likely to be a MRP1 dimer which would be expected to be around 380 kDa. Also, the region above 250 kDa was excised and analyzed by MS, and only MRP1 fragments were identified so far. Thus, this MRP1 immunoreactive band is most likely to be a self-conjugated MRP1. The intramolecular cross-linking could put MRP1 in a constrained conformation causing it to migrate more slowly in the gel. Since large membrane proteins like MRP1 cannot tolerate extensive heating (unpublished observations), the treatment conditions with DTT have to be relatively mild which in turn, may result in the thiol groups in the cross-linked MRP1 not being fully reduced.

Several chemical cross-linking reaction conditions were tested and the intensity of the higher molecular band increased only as the concentration of DSP increased from 0.1 to 0.5 mM (Fig. 3.3, middle blot). This may be due to the rapid hydrolysis of the highly reactive NHS-ester which competes with the primary amine reaction of DSP. However, despite the short-lived DSP solution, the most challenging problem encountered was the poor yield of proteins after DSP cross-linking (Fig. 3.4). This may be due to rapid non-specific cross-linking, which could modify the epitopes so that none of the MRP1-specific mAb could bind efficiently during the affinity purification step. Also, since cross-linking is a relatively empirical process, multiple cross-linkers with different spacer arms and/or with different reactivity may need to be employed. However, the use of 1%

formaldehyde as cross-linker did not change the cross-linking pattern in the present study (Fig. 3.3, bottom blot). Finally, the possibility that the cell system used in the present study is just not suitable for *in vivo* chemical cross-linking reactions cannot be ruled out.

One of the oldest, but still powerful, techniques to study protein-protein interaction is the use of classic protein purification methods, such as immunoprecipitation, to isolate protein complexes containing the protein of interest, followed by identification of the proteins in the complex. A major pitfall associated with this approach is that the number of false positives tends to be high, which results from the formation of non-physiological protein-protein interactions after cell lysis, or because of the cross-reactivity and nonspecific binding of the antibody to other cellular proteins [179]. To eliminate or minimize the number of false positives, several precautions were taken in this study. First, four well-characterized mAbs (QCRL-1 to -4) which recognize different regions of MRP1 were used [23, 25, 164] (Fig. 1.2). Secondly, normal mouse IgGs and normal rat IgGs were used for negative control immunoprecipitations. Reassuringly, none of the candidate MRP1-associated proteins were present in the negative controls (data not shown). Thirdly, drug-sensitive H69 cells which express little or no MRP1 were used to confirm that the observed interactions were MRP1-specific. Lastly, the whole cell lysates were pre-cleared by incubation with protein G-Sepharose before immunoprecipitation, together with extensive washings of the immunoprecipitates. By applying these precautions, six proteins were identified within the MRP1-containing immunoprecipitates, none of which are considered to be common background proteins, such as metabolic enzymes (e.g., pyruvate kinase) or heat shock proteins [182].

The physical interaction between FUS, drebrin and actin with MRP1 was confirmed by reciprocal co-immunoprecipitation. Since the solubilization buffer can interfere with certain protein-protein interactions, not all antibodies are expected to have the same co-immunoprecipitation profile under different experimental conditions [183]. This may be the reason that drebrin and actin appeared to associate with MRP1 in co-immunoprecipitations using CHAPS (Fig. 3.7B, lane 4 and 6, empty arrows) but not Triton X-100 (Fig. 3.8B, lane 8 and 10). Further biochemical measurements, such as fluorescence resonance energy transfer (FRET), are needed to corroborate the physical association observed in reciprocal co-immunoprecipitations. Furthermore, the massive disruption of cellular compartmentalization during cell lysis provides an opportunity for proteins that might not normally ever be in the same subcellular location to form nonphysiological complexes. This might be the case for FUS which was only detectable in the nucleus but nevertheless associated with MRP1 in co-immunoprecipitations (Fig. 3.8B, lane 4, empty arrow). However, an interaction between nuclear DNA topoisomerase II and the predominantly plasma membrane protein phospholipid scramblase 1 (PLSCR1) has been reported that is explained by the fact that a small amount of the latter protein can shuttle into the nucleus where it can act as a transcription factor [184]. Similarly, it may be that a small amount of FUS might reside in the cytosol in certain circumstances, and in this way make an interaction between FUS and MRP1 conceivable.

The FUS gene was first identified in myxoid-round cell liposarcoma as part of the t(12;16)(q13;p11) chromosomal translocation gene fusion product [174, 175]. FUS also

participates in gene fusions linked to other types of cancer, such as angiomatoid fibrous histiocytoma [185], low grade fibromyxoid sarcoma [186] and acute myeloid leukemia [187]. FUS contributes its NH<sub>2</sub>-terminal domain, just before its RNA-binding domain, to the gene fusion product (Fig. 3.9A) which then functions as a transcriptional activation domain [174, 175, 185-188]. The anti-FUS mAb used in this study is raised against a fusion protein corresponding to the COOH-terminus of human FUS. Therefore, only full-length FUS is detected but not the possible gene fusion products. In future studies, not only the possible association of FUS with MRP1 under some rare circumstances, but also its oncogenic properties could be examined further in the SCLC cell lines.

An important aspect of the present study was to determine whether MRP1 expression or function is modulated by its potential interactions with drebrin and actin. Drebrin is an actin-binding protein which influences actin filament assembly and arrangement by competitively inhibiting the actin-binding of several actin-bundling proteins, including tropomyosin, fascin and  $\alpha$ -actinin [189, 190]. In mammals, drebrins exist as two isoforms which are generated by alternative splicing of a single gene (Fig. 3.9B) [191]. The drebrin identified in this study is the E (embryonic) type (Fig. 3.6) which is more ubiquitously expressed than drebrin A (adult) type, including in some non-neuronal cells [191, 192]. In addition to its role in morphogenesis, patterning and maintenance of dendritic spines in neurons, a novel role for drebrin in the stabilization of gap junctions has been reported [178]. Drebrin E interacts with Cx43 at its COOH-terminal domain, and the depletion of drebrin by siRNA results in impaired cell-cell coupling and internalization of Cx43 [178]. In the present study, both drebrin and actin

were found to be co-immunoprecipitated with MRP1. However, it is not known which of the two proteins is directly associated with MRP1 since drebrin always copurifies with actin (Fig. 3.7B, lane 4, 6 and 8; Fig. 3.8B, lane 3-10).

By immunofluorescence microscopy, drebrin showed a punctate cytosolic expression pattern in H69AR cells and membrane-like staining in some regions (presumably cell-cell interface) (Fig. 3.12B). Thus, drebrin would be expected to colocalize with MRP1 in H69AR cells if double staining conditions can be implemented. Even though the overall MRP1 level revealed by immunoblotting, showed a moderate decrease after almost complete drebrin knock-down (Fig. 3.11), the membrane localization of MRP1 did not appear to change significantly (Fig. 3.12A). The drebrin knock-down reagent used in this experiment proved to be very specific and highly efficient. The same set of siRNA reagent was used previously by Peitsch *et al.* [165] for studying the role of drebrin in cell migration. They showed that the drebrin knock-down (up to 95%) did not affect the mobility nor change the pattern and expression levels of actin and some actin binding proteins in human fibroblasts [165]. Based on the present observations, drebrin does not seem critical for maintaining the membrane stability of MRP1. Future studies could examine the possible reasons for the 30% reduction in MRP1 overall expression level upon the depletion of drebrin and whether the reduction of MRP1 has any effect on substrate transport in H69AR cells.

Ribophorin I and myosin (non-muscle class II, MyH9) were also identified as potential interacting partners in this study. Ribophorin I is part of the OST complex and abundant in ER membrane [193]. OST catalyzes the covalent attachment of high-

mannose oligosaccharide group from the dolicholpyrophosphate (donor) to nascent polypeptides (acceptor) at asparagine (Asn) residues with consensus sequence Asn-X-Ser/Thr in rough ER [177]. Mammalian OST has a very elaborate composition with at least seven subunits, among which only STT3 carries the transferase activity [194]. Ribophorin I has ER retention information present in its luminal domain and has been shown to enhance the efficiency of *N*-glycosylation by presenting the acceptor substrate to the catalytic core [195, 196]. MRP1 is known to be *N*-glycosylated at Asn<sup>19</sup>, Asn<sup>23</sup> and Asn<sup>1006</sup> [22]. It would be of interest to know if ribophorin I is involved in MRP1 glycosylation.

The myosin family of actin filament-based motor proteins consists of over 20 classes and they are involved in a variety of cellular functions, including cell migration and adhesion, signal transduction, membrane trafficking, as well as protein, RNA and organelle localization [197]. CFTR (ABCC7) is known to interact with a complex of proteins containing myosin VI and clathrin at the apical membrane [198]. Thus myosin VI facilitates the endocytosis of CFTR where displacement of endogenous myosin VI with a dominant-negative recombinant tail domain (i.e., without the motor domain) reduces CFTR endocytosis and increases CFTR expression in the plasma membrane [198]. The role of myosin Vb in assisting the recycling of CFTR was discovered by the same group using a similar approach [199]. Myosin II was first studied for its role in muscle contraction, but it also functions in non-muscle cells, with possible roles in tension generation, adhesion, endo- and exocytosis [200]. It will be of interest to

determine if the non-muscle class II myosin identified in this study has roles in endocytosis or recycling of MRP1 as is reported for CFTR.

The major drawback for using immunoprecipitation to study protein-protein interaction is the likelihood of the interference of weak protein associations by non-denaturing detergents as well as by the use of stringent washing conditions [179, 183]. This may be the reason that only six MRP1-associated proteins were identified in this study. On the other hand, this method can provide information on the strength of the protein-protein interaction *in vitro* under a particular solubilization condition. Furthermore, some low abundance proteins are likely to be missed because of poor separation by 1D gel analysis and because of low recovery of peptides from in-gel digestions. Modern MS technology, with enhanced sensitivity, mass accuracy and tolerance towards sample heterogeneity, has become a powerful tool for identification of interaction partners and structural characterization of protein-protein interactions [201]. Most notable is the successful development of multidimensional protein identification technology (MudPIT) that multidimensional peptide separation techniques, such as strong cation exchange (SCX) LC together with reverse phase (RP)  $\mu$ LC, are implemented [202]. This method allows better separation of highly complex mixtures, thus increasing the ability to detect low-abundance protein components. Wang *et al.* [203] used this high-throughput approach and generated a CFTR interactome with more than 200 potential interactors identified. MudPIT could be the ultimate experimental approach for identification of the MRP1 interactome. However, there are some alternative proteomic approaches in a smaller scale that could be applied in the more immediate future, such as

pull down assays using recombinant polypeptides corresponding to only part of MRP1 (e.g., the cytoplasmic loops or the COOH-terminus) where intercellular protein-protein interactions are likely to reside. Also, the protein preparations from subcellular fractions (i.e., membrane fractions) could be used instead of whole cell lysates in the pull-down assays and/or immunoprecipitations, which would help avoid possible artifacts due to compartmentalization.

In summary, protein-protein interactions of MRP1 have been investigated in this study using immunoaffinity chromatography and MS-based protein identification. This method was found to be effective in purifying MRP1 and its associated protein complexes from cultured tumor cells. Six potential interacting proteins were identified and the associations of MRP1 with FUS and drebrin were examined in the subsequent biochemical analyses. However, FUS seems unlikely to be an important binding partner of MRP1 *in vivo*, because of its essentially exclusive nuclear localization. Drebrin does not seem critical for maintaining the membrane stability of MRP1 as revealed by unchanged MRP1 expression pattern upon drebrin siRNA knock-down. In the present study, only two of the six candidate interacting proteins were studied. More extensive work is definitely needed in the future for understanding MRP1 regulation by interactions with other cellular modulators.

## References

1. Ling, V. 1997. Multidrug resistance: molecular mechanisms and clinical relevance. *Cancer Chemother. Pharmacol.* **40**:S3-8.
2. Scagliotti, G.V., Novello, S., and Selvaggi, G. 1999. Multidrug resistance in non-small-cell lung cancer. *Ann. Oncol.* **10**:83-6.
3. Juszczynski, P., Niewiarowski, W., Krykowski, E., Robak, T., and Warzocha, K. 2002. Expression of the multidrug resistance-associated protein (mrp) gene in chronic lymphocytic leukemia. *Leuk. Lymphoma* **43**:153-8.
4. Triller, N., Korosec, P., Kern, I., Kosnik, M., and Debeljak, A. 2006. Multidrug resistance in small cell lung cancer: expression of P-glycoprotein, multidrug resistance protein 1 and lung resistance protein in chemo-naïve patients and in relapsed disease. *Lung Cancer* **54**:235-40.
5. Alexander, D., Yamamoto, T., Kato, S., and Kasai, S. 1999. Histopathological assessment of multidrug resistance in gastric cancer: expression of P-glycoprotein, multidrug resistance-associated protein, and lung-resistance protein. *Surg. Today* **29**:401-6.
6. Juliano, R.L., and Ling, V. 1976. A surface glycoprotein modulating drug permeability in Chinese hamster ovary cell mutants. *Biochim. Biophys. Acta* **455**:152-62.
7. Gottesman, M.M., and Ling, V. 2006. The molecular basis of multidrug resistance in cancer: the early years of P-glycoprotein research. *FEBS Lett.* **580**:998-1009.
8. Mirski, S.E., Gerlach, J.H., and Cole, S.P.C. 1987. Multidrug resistance in a human small cell lung cancer cell line selected in adriamycin. *Cancer Res.* **47**:2594-8.
9. Cole, S.P.C., Chanda, E.R., Dicke, F.P., Gerlach, J.H., Mirski, S.E. 1991. Non-P-glycoprotein-mediated multidrug resistance in a small cell lung cancer

cell line: evidence for decreased susceptibility to drug-induced DNA damage and reduced levels of topoisomerase II. *Cancer Res.* **51**: 3345-52.

10. Cole, S.P.C. 1990. Patterns of cross-resistance in a multidrug-resistant small-cell lung carcinoma cell line. *Cancer Chemother. Pharmacol.* **26**:250-6.
11. Cole, S.P.C., Bhardwaj, G., Gerlach, J.H., Mackie, J.E., Grant, C.E., Almquist, K.C., Stewart, A.J., Kurz, E.U., Duncan, A.M., and Deeley, R.G. 1992. Overexpression of a transporter gene in a multidrug-resistant human lung cancer cell line. *Science* **258**:1650-4.
12. Borst, P., Evers, R., Kool, M., and Wijnholds, J. 2000. A family of drug transporters: the multidrug resistance-associated proteins. *J. Natl. Cancer Inst.* **92**:1295-302.
13. Higgins, C.F., Hiles, I.D., Whalley, K., and Jamieson, D.J. 1985. Nucleotide binding by membrane components of bacterial periplasmic binding protein-dependent transport systems. *EMBO J.* **4**:1033-9.
14. Higgins, C.F., Hiles, I.D., Salmond, G.P., Gill, D.R., Downie, J.A., Evans, I.J., Holland, I.B., Gray, L., Buckel, S.D., Bell, A.W., and Hermodson, M.A. 1986. A family of related ATP-binding subunits coupled to many distinct biological processes in bacteria. *Nature* **323**:448-50.
15. Walker, J.E., Saraste, M., Runswick, M.J., and Gay, N.J. 1982. Distantly related sequences in the  $\alpha$ - and  $\beta$ -subunits of ATP synthase, myosin, kinases and other ATP-requiring enzymes and a common nucleotide binding fold. *EMBO J.* **1**:945-51.
16. Higgins, C.F. 1992. ABC transporters: from microorganisms to man. *Annu. Rev. Cell Biol.* **8**:67-113.
17. Dean, M., Rzhetsky, A., and Allikmets, R. 2001. The human ATP-binding cassette (ABC) transporter superfamily. *Genome Res.* **11**:1156-66.

18. Toyoda, Y., Hagiya, Y., Adachi, T., Hoshijima, K., Kuo, M.T., and Ishikawa, T. 2008. MRP class of human ATP binding cassette (ABC) transporters: historical background and new research directions. *Xenobiotica* **38**:833-62.
19. Riordan, J.R., Rommens, J.M., Kerem, B., Alon, N., Rozmahel, R., Grzelczak, Z., Zielenski, J., Lok, S., Plavsic, N., and Chou, J.L. 1989. Identification of the cystic fibrosis gene: cloning and characterization of complementary DNA. *Science* **245**:1066-73.
20. Aguilar-Bryan, L., Nichols, C.G., Wechsler, S.W., Clement, J.P 4<sup>th</sup>., Boyd, A.E 3<sup>rd</sup>., Gonzalez, G., Herrera-Sosa, H., Nguy, K., Bryan, J., and Nelson, D.A. 1995. Cloning of the  $\beta$  cell high-affinity sulfonyleurea receptor: a regulator of insulin secretion. *Science* **268**:423-6.
21. Bakos, E., Hegedüs, T., Holló, Z., Welker, E., Tusnády, G.E., Zaman, G.J., Flens, M.J., Váradi, A., and Sarkadi, B. 1996. Membrane topology and glycosylation of the human multidrug resistance-associated protein. *J. Biol. Chem.* **271**:12322-6.
22. Hipfner, D.R., Almquist, K.C., Leslie, E.M., Gerlach, J.H., Grant, C.E., Deeley, R.G., and Cole, S.P.C. 1997. Membrane topology of the multidrug resistance protein (MRP). A study of glycosylation-site mutants reveals an extracytosolic NH<sub>2</sub> terminus. *J. Biol. Chem.* **272**:23623-30.
23. Hipfner, D.R., Almuist, K.C., Stride, B.D., Deeley, R.G., and Cole, S.P.C. 1996. Location of a protease-hypersensitive region in the multidrug resistance protein (MRP) by mapping of the epitope of MRP-specific monoclonal antibody QCRL-1. *Cancer Res.* **56**:3307-14.
24. Hipfner, D.R., Gao, M., Scheffer, G., Scheper, R.J., Deeley, R.G, and Cole, S.P.C. 1998. Epitope mapping of monoclonal antibodies specific for the 190-kDa multidrug resistance protein (MRP). *Br. J. Cancer* **78**:1134-40.
25. Hipfner, D.R., Mao, Q., Qiu, W., Leslie, E.M., Gao, M., Deeley, R.G., and Cole, S.P.C. 1999. Monoclonal antibodies that inhibit the transport function of the 190-kDa multidrug resistance protein, MRP. Localization of their epitopes to the nucleotide-binding domains of the protein. *J. Biol. Chem.* **274**:15420-6.

26. Koike, K., Deeley, R.G., and Cole, S.P.C. 2004. Mapping of the MRPm5 epitope to the cytosolic region between transmembrane helices 13 and 14 in the drug and organic anion transporter, MRP1 (ABCC1). *Biochem. Biophys. Res. Commun.* **315**:719-25.
27. Kast, C., and Gros, P. 1997. Topology mapping of the amino-terminal half of multidrug resistance-associated protein by epitope insertion and immunofluorescence. *J. Biol. Chem.* **272**:26479-87.
28. Kast, C., and Gros, P. 1998. Epitope insertion favors a six transmembrane domain model for the carboxy-terminal portion of the multidrug resistance-associated protein. *Biochemistry* **37**:2305-13.
29. Bakos, E., Evers, R., Szakács, G., Tusnády, G.E., Welker, E., Szabó, K., de Haas, M., van Deemter, L., Borst, P., Váradi, A., Sarkadi, B. 1998. Functional multidrug resistance protein (MRP1) lacking the *N*-terminal transmembrane domain. *J. Biol. Chem.* **273**:32167-75.
30. Qian, Y.M., Qiu, W., Gao, M., Westlake, C.J., Cole, S.P.C., and Deeley, R.G. 2001. Characterization of binding of leukotriene C<sub>4</sub> by human multidrug resistance protein 1: evidence of differential interactions with NH<sub>2</sub>- and COOH-proximal halves of the protein. *J. Biol. Chem.* **276**:38636-44.
31. Bakos, E., Evers, R., Calenda, G., Tusnády, G.E., Szakács, G., Váradi, A., and Sarkadi, B. 2000. Characterization of the amino-terminal regions in the human multidrug resistance protein (MRP1). *J. Cell Sci.* **113**:4451-61.
32. Westlake, C.J., Qian, Y.M., Gao, M., Vasa, M., Cole, S.P.C., and Deeley, R.G. 2003. Identification of the structural and functional boundaries of the multidrug resistance protein 1 cytoplasmic loop 3. *Biochemistry* **42**:14099-113.
33. Rosenberg, M.F., Mao, Q., Holzenburg, A., Ford, R.C., Deeley, R.G., and Cole, S.P.C. 2001. The structure of the multidrug resistance protein 1 (MRP1/ABCC1). Crystallization and single-particle analysis. *J. Biol. Chem.* **276**:16076-82.

34. Rosenberg, M.F., Kamis, A.B., Aleksandrov, L.A., Ford, R.C., and Riordan, J.R. 2004. Purification and crystallization of the cystic fibrosis transmembrane conductance regulator (CFTR). *J. Biol. Chem.* **279**:39051-7.
35. Rosenberg, M.F., Callaghan, R., Modok, S., Higgins, C.F., and Ford, R.C. 2005. Three-dimensional structure of P-glycoprotein: the transmembrane regions adopt an asymmetric configuration in the nucleotide-bound state. *J. Biol. Chem.* **280**:2857-62.
36. DeGorter, M.K., Conseil, G., Deeley, R.G., Campbell, R.L., and Cole, S.P.C. 2008. Molecular modeling of the human multidrug resistance protein 1 (MRP1/ABCC1). *Biochem. Biophys. Res. Commun.* **365**:29-34.
37. Dawson, R.J., and Locher, K.P. 2006. Structure of a bacterial multidrug ABC transporter. *Nature* **443**:180-5.
38. Dawson, R.J., and Locker, K.P. 2007. Structure of the multidrug ABC transporter Sav1866 from *Staphylococcus aureus* in complex with AMP-PNP. *FEBS Lett.* **581**:935-8.
39. Zolnerciks, J.K., Wooding, C., and Linton, K.J. 2007. Evidence for a Sav1866-like architecture for the human multidrug transporter P-glycoprotein. *FASEB J.* **21**:3937-48.
40. Loo, T.W., and Clarke, D.M. 2000. The packing of the transmembrane segments of human multidrug resistance P-glycoprotein is revealed by disulfide cross-linking analysis. *J. Biol. Chem.* **275**:5253-6.
41. Flens, M.J., Zaman, G.J., van der Valk, P., Izquierdo, M.A., Schroeijers, A.B., Scheffer, G.L., van der Groep, P., de Haas, M., Meijer, C.J., and Scheper, R.J. 1996. Tissue distribution of the multidrug resistance protein. *Am. J. Pathol.* **148**:1237-47.
42. Nagashige, M., Ushigome, F., Koyabu, N., Hirata, K., Kwabuchi, M., Hirakawa, T., Satoh, S., Tsukimori, K., Nakano, H., Uchiumi, T., Kuwano,

- M., Ohtani, H., and Sawada, Y. 2003. Basal membrane localization of MRP1 in human placental trophoblast. *Placenta* **24**:951-8.
43. Roelofsen, H., Vos, T.A., Schippers, I.J., Kuipers, F., Koning, H., Moshage, H., Jansen, P.L., and Muller, M. 1997. Increased levels of the multidrug resistance protein in lateral membranes of proliferating hepatocyte-derived cells. *Gastroenterology* **112**:511-21.
44. Ros, J.E., Libbrecht, L., Geuken, M., Jansen, P.L., and Roskams, T.A. 2003. High expression of MDR1, MRP1, and MRP3 in the hepatic progenitor cell compartment and hepatocytes in severe human liver disease. *J. Pathol.* **200**:553-60.
45. Evers, R., Zaman, G.J., van Deemter, L., Jansen, H., Calafat, J., Oomen, L.C., Oude Elferink, R.P., Borst, P., and Schinkel, A.H. 1996. Basolateral localization and export activity of the human multidrug resistance-associated protein in polarized pig kidney cells. *J. Clin. Invest.* **97**:1211-8.
46. Wright, S.R., Boag, A.H., Valdimarsson, G., Hipfner, D.R., Campling, B.G., Cole, S.P.C., and Deeley, R.G. 1998. Immunohistochemical detection of multidrug resistance protein in human lung cancer and normal lung. *Clin. Cancer Res.* **4**:2279-89.
47. Leslie, E.M., Deeley, R.G., and Cole, S.P.C. 2005. Multidrug resistance proteins: role of P-glycoprotein, MRP1, MRP2, and BCRP (ABCG2) in tissue defense. *Toxicol. Appl. Pharmacol.* **204**:216-37.
48. Nies, A.T., Jedlitschky, G., Konig, J., Herold-Mende, C., Steiner, H.H., Schmitt, H.P., and Keppler, D. 2004. Expression and immunolocalization of the multidrug resistance proteins, MRP1-MRP6 (ABCC1-ABCC6), in human brain. *Neuroscience* **129**:349-60.
49. Zhang, Y., Schuetz, J.D., Elmquist, W.F., Miller, D.W. 2004. Plasma membrane localization of multidrug resistance-associated protein homologs in brain capillary endothelial cells. *J. Pharmacol. Exp. Ther.* **311**:449-55.

50. Grant, C.E., Valdimarsson, G., Hipfner, D.R., Almquist, K.C., Cole, S.P., and Deeley, R.G. 1994. Overexpression of multidrug resistance-associated protein (MRP) increases resistance to natural product drugs. *Cancer Res.* **54**:357-61.
51. Cole, S.P.C., and Deeley, R.G. 2006. Transport of glutathione and glutathione conjugates by MRP1. *Trends Pharmacol. Sci.* **27**:438-46.
52. Deeley, R.G., and Cole, S.P.C. 2006. Substrate recognition and transport by multidrug resistance protein 1 (ABCC1). *FEBS Lett.* **580**:1103-11.
53. Loe, D.W., Almquist, K.C., Deeley, R.G., and Cole S.P.C. 1996. Multidrug resistance protein (MRP)-mediated transport of leukotriene C<sub>4</sub> and chemotherapeutic agents in membrane vesicles. Demonstration of glutathione-dependent vincristine transport. *J. Biol. Chem.* **271**:9675-82.
54. Loe, D.W., Almquist, K.C., Cole, S.P.C., and Deeley, R.G. 1996. ATP-dependent 17 $\beta$ -estradiol 17-( $\beta$ -D-glucuronide) transport by multidrug resistance protein (MRP). Inhibition by cholestatic steroids. *J. Biol. Chem.* **271**:9683-9.
55. Loe, D.W., Deeley, R.G., and Cole, S.P.C. 1998. Characterization of vincristine transport by the *Mr* 190,000 multidrug resistance protein (MRP): Evidence for cotransport with reduced glutathione. *Cancer Res.* **58**:5130-6.
56. Morrow, C.S., Peclak-Scott, C., Bishwokarma, B., Kute, T.E., Smitherman, P.K., and Townsend, A.J. 2006. Multidrug resistance protein 1 (MRP1, ABCC1) mediates resistance to mitoxantrone via glutathione-dependent drug efflux. *Mol. Pharmacol.* **69**:1499-505.
57. Qian, Y.M., Song, W.C., Cui, H., Cole, S.P.C., and Deeley, R.G. 2001. Glutathione stimulates sulfated estrogen transport by multidrug resistance protein 1. *J. Biol. Chem.* **276**:6404-11.
58. Leslie, E.M., Ito, K., Upadhyaya, P., Hecht, S.S., Deeley, R.G., and Cole, S.P.C. 2001. Transport of the beta-*O*-glucuronide conjugates of the tobacco-specific carcinogen 4-(methylnitrosamino)-1-(3-pyridyl)-1-butanol (NNAL)

by the multidrug resistance protein 1 (MRP1). Requirement for glutathione or a non-sulfur-containing analog. *J. Biol. Chem.* **276**:27846-54.

59. Peklak-Scott, C., Townsend, A.J., and Morrow, C.S. 2005. Dynamics of glutathione conjugation and conjugate efflux in detoxification of the carcinogen, 4-nitroquinoline 1-oxide: contributions of glutathione, glutathione S-transferase, and MRP1. *Biochemistry* **44**:4426-33.
60. Loe, D.W., Deeley, R.G., and Cole, S.P.C. 2000. Verapamil stimulates glutathione transport by the 190-kDa multidrug resistance protein 1 (MRP1). *J. Pharmacol. Exp. Ther.* **293**:530-8.
61. Leslie, E.M., Deeley, R.G., and Cole, S.P.C. 2003. Bioflavonoid stimulation of glutathione transport by the 190-kDa multidrug resistance protein 1 (MRP1). *Drug Metab. Dispos.* **31**:11-5.
62. Bakos, E., Evers, R., Sinkó, E., Váradi, A., Borst, P., and Sarkadi, B. 2000. Interactions of the human multidrug resistance proteins MRP1 and MRP2 with organic anions. *Mol. Pharmacol.* **57**:760-8.
63. Lorico, A., Rappa, G., Finch, R.A., Yang, D., Flavell, R.A., and Sartorelli, A.C. 1997. Disruption of the murine MRP (multidrug resistance protein) gene leads to increased sensitivity to etoposide (VP-16) and increased levels of glutathione. *Cancer Res.* **57**:5238-42.
64. Wijnholds, J., Evers, R., van Leusden, M.R., Mol, C.A., Zaman, G.J., Mayer, U., Beijnen, J.H., van der Valk, M., Krimpenfort, P., and Borst, P. 1997. Increased sensitivity to anticancer drugs and decreased inflammatory response in mice lacking the multidrug resistance-associated protein. *Nat. Med.* **3**:1275-9.
65. Wijnholds, J., Scheffer, G.L., van der Valk, M., van der Valk, P., Beijnen, J.H., Scheper, R.J., and Borst, P. 1998. Multidrug resistance protein 1 protects the oropharyngeal mucosal layer and the testicular tubules against drug-induced damage. *J. Exp. Med.* **188**:797-808.

66. Thiebaut, F., Tsuruo, T., Hamada, H., Gottesman, M.M., Pastan, I., and Willingham, M.C. 1987. Cellular localization of the multidrug-resistance gene product P-glycoprotein in normal human tissues. *Proc. Natl. Acad. Sci. USA* **84**:7735-8.
67. Kartenbeck, J., Leuschner, U., Mayer, R., and Keppler, D. 1996. Absence of the canalicular isoform of the MRP gene-encoded conjugate export pump from the hepatocytes in Dubin-Johnson syndrome. *Hepatology* **23**:1061-6.
68. Maliapaard, M., Scheffer, G.L., Faneyte, I.F., van Gastelen, M.A., Pijnenborg, A.C., Schinkel, A.H., van De Vijver, M.J., Scheper, R.J., and Schellens, J.H. 2001. Subcellular localization and distribution of the breast cancer resistance protein transporter in normal human tissues. *Cancer Res.* **61**:3458-64.
69. Cole, S.P.C., Downes, H.F., Mirski, S.E., Clements, D.J. 1990. Alterations in glutathione and glutathione-related enzymes in a multidrug-resistance small cell lung cancer cell line. *Mol. Pharmacol.* **37**:192-7.
70. Jungsuwadee, P., Cole, M.P., Sultana, R., Joshi, G., Tangpong, J., Butterfield, D.A., St Clair, D.K., and Vore, M. 2006. Increase in Mrp1 expression and 4-hydroxy-2-nonenal adduction in heart tissue of Adriamycin-treated C57BL/6 mice. *Mol. Cancer Ther.* **5**:2851-60.
71. Renes, J., de Vries, E.E., Hooiveld, G.J., Krikken, I., Jansen, P.L., and Müller, M. 2000. Multidrug resistance protein MRP1 protects against the toxicity of the major lipid peroxidation product 4-hydroxynonenal. *Biochem. J.* **350**:555-61.
72. Berger, W., Setinek, U., Hollaus, P., Zidek, T., Steiner, E., Elbling, L., Cantonati, H., Attems, J., Gsur, A., and Micksche, M. 2005. Multidrug resistance markers P-glycoprotein, multidrug resistance protein 1, and lung resistance protein in non-small cell lung cancer: prognostic implications. *J. Cancer Res. Clin. Oncol.* **131**:355-63.
73. Oshika, Y., Nakamura, M., Tokunaga, T., Fukushima, Y., Abe, Y., Ozeki, Y., Yamazaki, H., Tamaoki, N., and Ueyama, Y. 1998. Multidrug resistance-associated protein and mutant p53 protein expression in non-small cell lung cancer. *Mod. Pathol.* **11**:1059-63.

74. Filipits, M., Pohl, G., Rudas, M., Dietze, O., Lax, S., Grill, R., Pirker, R., Zielinski, C.C., Hausmaninger, H., Kubista, E., Samonigg, H., and Jakesz, R. 2005. Clinical role of multidrug resistance protein 1 expression in chemotherapy resistance in early-stage breast cancer: the Austrian Breast and Colorectal Cancer Study Group. *J. Clin. Oncol.* **23**:1161-8.
75. van Brussel, J.P., and Mickisch, G.H. 2003. Multidrug resistance in prostate cancer. *Onkologie* **26**:175-81.
76. Kourti, M., Vavatsi, N., Gombakis, N., Sidi, V., Tzimagiorgis, G., Papageorgiou, T., Koliouskas, D., and Athanassiadou, F. 2007. Expression of multidrug resistance 1 (MDR1), multidrug resistance-related protein 1 (MRP1), lung resistance protein (LRP), and breast cancer resistance protein (BCRP) genes and clinical outcome in childhood acute lymphoblastic leukemia. *Int. J. Hematol.* **86**:166-73.
77. Pajic, M., Norris, M.D., Cohn, S.L., and Haber, M. 2005. The role of the multidrug resistance-associated protein 1 gene in neuroblastoma biology and clinical outcome. *Cancer Lett.* **228**:241-6.
78. Gottesman, M.M., Fojo, T., and Bates, S.E. 2002. Multidrug resistance in cancer: role of ATP-dependent transporters. *Nat. Rev. Cancer* **2**:48-58.
79. Gottesman, M.M. 2002. Mechanisms of cancer drug resistance. *Annu. Rev. Med.* **53**:615-27.
80. Hopfner, K.P., Karcher, A., Shin, D.S., Craig, L., Arthur, L.M., Carney, J.P., and Tainer, J.A. 2000. Structural biology of Rad50 ATPase: ATP-driven conformational control in DNA double-strand break repair and the ABC-ATPase superfamily. *Cell* **101**:789-800.
81. Moody, J.E., Millen, L., Binns, D., Hunt, J.F., and Thomas, P.J. 2002. Cooperative, ATP-dependent association of the nucleotide binding cassettes during the catalytic cycle of ATP-binding cassette transporters. *J. Biol. Chem.* **277**:21111-4.

82. Smith, P.C., Karpowich, N., Millen, L., Moody, J.E., Rosen, J., Thomas, P.J., and Hunt, J.F. 2002. ATP binding to the motor domain from an ABC transporter drives formation of a nucleotide sandwich dimer. *Mol. Cell* **10**:139-49.
83. Davidson, A.L., and Chen, J. 2004. ATP-binding cassette transporters in bacteria. *Annu. Rev. Biochem.* **73**:241-68.
84. Hung, L.W., Wang, I.X., Nikaido, K., Liu, P.Q., Ames, G.F., and Kim, S.H. 1998. Crystal structure of the ATP-binding subunit of an ABC transporter. *Nature* **396**:703-7.
85. Chen, J., Lu, G., Lin, J., Davidson, A.L., and Quioco, F.A. 2003. A tweezers-like motion of the ATP-binding cassette dimer in an ABC transport cycle. *Mol. Cell* **12**:651-61.
86. Yuan, Y.R., Blecker, S., Martsinkevich, O., Millen, L., Thomas, P.J., and Hunt, J.F. 2001. The crystal structure of the MJ0796 ATP-binding cassette. Implications for the structural consequences of ATP hydrolysis in the active site of an ABC transporter. *J. Biol. Chem.* **276**:32313-21.
87. Verdon, G., Albers, S.V., Dijkstra, B.W., Driessen, A.J., and Thunnissen, A.M. 2003. Crystal structures of the ATPase subunit of the glucose ABC transporter from *Sulfolobus solfataricus*: nucleotide-free and nucleotide-bound conformations. *J. Mol. Biol.* **330**:343-58.
88. Gao, M., Cui, H.R., Loe, D.W., Grant, C.E., Almquist, K.C., Cole, S.P.C., and Deeley, R.G. 2000. Comparison of the functional characteristics of the nucleotide binding domains of multidrug resistance protein 1. *J. Biol. Chem.* **275**:13098-108.
89. Hou, Y., Cui, L., Riordan, J.R., and Chang, X. 2000. Allosteric interactions between the two non-equivalent nucleotide binding domains of multidrug resistance protein MRP1. *J. Biol. Chem.* **275**:20280-7.
90. Hou, Y.X., Cui, L., Riordan, J.R., and Chang, X.B. 2002. ATP binding to the first nucleotide-binding domain of multidrug resistance protein MRP1

increases binding and hydrolysis of ATP and trapping of ADP at the second domain. *J. Biol. Chem.* **277**:5110-9.

91. Payen, L.F., Gao, M., Westlake, C.J., Cole, S.P.C., and Deeley, R.G. 2003. Role of carboxylate residues adjacent to the conserved core Walker B motifs in the catalytic cycle of multidrug resistance protein 1 (ABCC1). *J. Biol. Chem.* **278**:38537-47.
92. Yang, R., McBride, A., Hou, Y.X., Goldberg, A., and Chang, X.B. 2005. Nucleotide dissociation from NBD1 promotes solute transport by MRP1. *Biochim. Biophys. Acta* **1668**:248-61.
93. Ren, X.Q., Furukawa, T., Haraguchi, M., Sumizawa, T., Aoki, S., Kobayashi, M., and Akiyama, S. 2004. Function of the ABC signature sequences in the human multidrug resistance protein 1. *Mol. Pharmacol.* **65**:1536-42.
94. Hou, Y.X., Cui, L., Riordan, J.R., and Chang, X.B. 2002. ATP binding to the first nucleotide-binding domain of multidrug resistance protein MRP1 increases binding and hydrolysis of ATP and trapping of ADP at the second domain. *J. Biol. Chem.* **277**:5110-9.
95. Buyse, F., Hou, Y.X., Vigano, C., Zhao, Q., Ruyschaert, J.M., and Chang, X.B. 2006. Replacement of the positively charged Walker A lysine residue with a hydrophobic leucine residue and conformational alteration caused by this mutation in MRP1 impair ATP binding and hydrolysis. *Biochem. J.* **397**:121-30.
96. Payen, L., Gao, M., Westlake, C., Theis, A., Cole, S.P.C., and Deeley, R.G. 2005. Functional interactions between nucleotide binding domains and leukotriene C<sub>4</sub> binding sites of multidrug resistance protein 1 (ABCC1). *Mol. Pharmacol.* **67**:1944-53.
97. Senior, A.E., al-Shawi, M.K., and Urbatsch, I.L. 1995. The catalytic cycle of P-glycoprotein. *FEBS Lett.* **377**:285-9.
98. Sauna, Z.E., Kim, I.W., Nandigama, K., Kopp, S., Chiba, P., and Ambudkar, S.V. 2007. Catalytic cycle of ATP hydrolysis by P-glycoprotein: evidence for

formation of the E.S. reaction intermediate with ATP- $\gamma$ -S, a nonhydrolyzable analogue of ATP. *Biochemistry* **46**:13787-99.

99. Smith, C.A., and Rayment, I. 1996. X-ray structure of the magnesium(II)·ADP·vanadate complex of the *Dictyostelium discoideum* myosin motor domain to 1.9 Å resolution. *Biochemistry* **35**:5404-17.
100. Urbatsch, I.L., Sankaran, B., Weber, J., and Senior, A.E. 1995. P-glycoprotein is stably inhibited by vanadate-induced trapping of nucleotide at a single catalytic site. *J. Biol. Chem.* **270**:19383-90.
101. Higgins, C.F., and Linton, K.J. 2004. The ATP switch model for ABC transporters. *Nat. Struct. Mol. Biol.* **11**:918-26.
102. Chang, X.B. 2007. A molecular understanding of ATP-dependent solute transport by multidrug resistance-associated protein MRP1. *Cancer Metastasis Rev.* **26**:15-37.
103. Slovak, M.L., Ho, J.P., Bhardwaj, G., Kurz, E.U., Deeley, R.G., and Cole, S.P.C. 1993. Localization of a novel multidrug resistance-associated gene in the HT1080/DR4 and H69AR human tumor cell lines. *Cancer Res.* **53**:3221-5.
104. Lee, J.T., Jr., Steelman, L.S., and McCubrey, J.A. 2004. Phosphatidylinositol 3'-kinase activation leads to multidrug resistance protein-1 expression and subsequent chemoresistance in advanced prostate cancer cells. *Cancer Res.* **64**:8397-404.
105. Zhu, H., Chen, X.P., Luo, S.F., Guan, J., Zhang, W.G., and Zhang, B.X. 2005. Involvement of hypoxia-inducible factor-1-alpha in multidrug resistance induced by hypoxia in HepG2 cells. *J. Exp. Clin. Cancer Res.* **24**:565-74.
106. Zhu, Q., and Center, M.S. 1994. Cloning and sequence analysis of the promoter region of the MRP gene of HL60 cells isolated for resistance to adriamycin. *Cancer Res.* **54**:4488-92.

107. Kurz, E.U., Cole, S.P.C., and Deeley, R.G. 2001. Identification of DNA-protein interactions in the 5' flanking and 5' untranslated regions of the human multidrug resistance protein (MRP1) gene: evaluation of a putative antioxidant response element/AP-1 binding site. *Biochem. Biophys. Res. Commun.* **285**:981-90.
108. Muredda, M., Nunoya, K., Burtch-Wright, R.A., Kurz, E.U., Cole, S.P.C., and Deeley, R.G. 2003. Cloning and characterization of the murine and rat mrp1 promoter regions. *Mol. Pharmacol.* **64**:1259-69.
109. Zhu, Q., and Center, M.S. 1996. Evidence that Sp1 modulates transcriptional activity of the multidrug resistance-associated protein gene. *DNA Cell Biol.* **15**:105-11.
110. Wang, Q., and Beck, W.T. 1998. Transcriptional suppression of multidrug resistance-associated protein (MRP) gene expression by wild-type p53. *Cancer Res.* **58**:5762-9.
111. Sullivan, G.F., Yang, J.M., Vassil, A., Yang, J., Bash-Babula, J., and Hait, W.N. 2000. Regulation of expression of the multidrug resistance protein MRP1 by p53 in human prostate cancer cells. *J. Clin. Invest.* **105**:1261-7.
112. Cripe, L.D., Gelfanov, V.M., Smith, E.A., Spigel, D.R., Phillips, C.A., Gabig, T.G., Jung, S.H., Fyffe, J., Hartman, A.D., Kneebone, P., Mercola, D., Burgess, G.S., and Boswell, H.S. 2002. Role for *c-jun* N-terminal kinase in treatment-refractory acute myeloid leukemia (AML): signaling to multidrug-efflux and hyperproliferation. *Leukemia* **16**:799-812.
113. Yamane, Y., Furuichi, M., Song, R., Van, N.T., Mulcahy, R.T., Ishikawa, T., and Kuo, M.T. 1998. Expression of multidrug resistance protein/GS-X pump and  $\gamma$ -glutamylcysteine synthetase genes is regulated by oxidative stress. *J. Biol. Chem.* **273**:31075-85.
114. Tatebe, S., Sinicrope, F.A., and Kuo, M.T. 2002. Induction of multidrug resistance proteins MRP1 and MRP3 and  $\gamma$ -glutamylcysteine synthetase gene expression by nonsteroidal anti-inflammatory drugs in human colon cancer cells. *Biochem. Biophys. Res. Commun.* **290**:1427-33.

115. Ma, L., Krishnamachary, N, and Center, M.S. 1995. Phosphorylation of the multidrug resistance associated protein gene encoded protein P190. *Biochemistry* **34**:3338-43.
116. Davis, P.B. 2006. Cystic fibrosis since 1938. *Am. J. Respir. Crit. Care Med.* **173**:475-82.
117. Riordan, J.R. 2005. Assembly of functional CFTR chloride channels. *Annu. Rev. Physiol.* **67**:701-18.
118. Guggino, W.B., and Stanton, B.A. 2006. New insights into cystic fibrosis: molecular switches that regulate CFTR. *Nat. Rev. Mol. Cell Biol.* **7**:426-36.
119. Cormet-Boyaka, E., Di, A., Chang, S.Y., Naren, A.P., Tousson, A., Nelson, D.J., and Kirk, K.L. 2002. CFTR chloride channels are regulated by a SNAP-23/syntaxin 1A complex. *Proc. Natl. Acad. Sci. USA* **99**:12477-82.
120. Chang, S.Y., Di, A., Naren, A.P., Palfrey, H.C., Kirk, K.L., and Nelson, D.J. 2002. Mechanisms of CFTR regulation by syntaxin 1A and PKA. *J. Cell Sci.* **115**:783-91.
121. Naren, A.P., Nelson, D.J., Xie, W., Jovov, B., Pevsner, J., Bennett, M.K., Benos, D.J., Quick, M.W., and Kirk, K.L. 1997. Regulation of CFTR chloride channels by syntaxin and Munc18 isoforms. *Nature* **390**:302-5.
122. Li, C., Naren, A.P. 2005. Macromolecular complexes of cystic fibrosis transmembrane conductance regulator and its interacting partners. *Pharmacol. Ther.* **108**:208-23.
123. Hegedus, T., Sessler, T., Scott, R., Thelin, W., Bakos, E., Vardi, A., Szabo, K., Homolya, L., Milgram, S.L., and Sarkadi, B. 2003. C-terminal phosphorylation of MRP2 modulates its interaction with PDZ proteins. *Biochem. Biophys. Res. Commun.* **302**:454-61.

124. Kocher, O., Comella, N., Gilchrist, A., Pal, R., Tognazzi, K., Brown, L.F., and Knoll, J.H. 1999. PDZK1, a novel PDZ domain-containing protein up-regulated in carcinomas and mapped to chromosome 1q21, interacts with cMOAT (MRP2), the multidrug resistance-associated protein. *Lab Invest.* **79**:1161-70.
125. Buechler, C., Boettcher, A., Bared, S.M., Probst, M.C., and Schmitz, G. 2002. The carboxyterminus of the ATP-binding cassette transporter A1 interacts with a  $\beta$ 2-syntrophin/utrophin complex. *Biochem. Biophys. Res. Commun.* **293**:759-65.
126. Hoque, M.T., and Cole, S.P. 2008. Down-regulation of  $\text{Na}^+/\text{H}^+$  exchanger regulatory factor 1 increases expression and function of multidrug resistance protein 4. *Cancer Res.* **68**:4802-9.
127. Rainbow, R.D., James, M., Hudman, D., Al Johi, M., Singh, H., Watson, P.J., Ashmole, I., Davies, N.W., Lodwick, D., and Norman, R.I. 2004. Proximal C-terminal domain of sulphonylurea receptor 2A interacts with pore-forming Kir6 subunits in KATP channels. *Biochem. J.* **379**:173-81.
128. Cui, N., Kang, Y., He, Y., Leung, Y.M., Xie, H., Pasyk, E.A., Gao, X., Sheu, L., Hansen, J.B., Wahl, P., Tsushima, R.G., and Gaisano, H.Y. 2004. H3 domain of syntaxin 1A inhibits KATP channels by its actions on the sulfonylurea receptor 1 nucleotide-binding folds-1 and -2. *J. Biol. Chem.* **279**:53259-65.
129. Wada, Y., Yamshita, T., Imai, K., Miura, R., Takao, K., Nishi, M., Takeshima, H., Asano, T., Morishita, R., Nishizawa, K., Kokubun, S., and Nukada, T. 2000. A region of the sulfonylurea receptor critical for a modulation of ATP-sensitive  $\text{K}^+$  channels by G-protein  $\beta\gamma$ -subunits. *EMBO J.* **19**:4915-25.
130. Sonveaux, N., Shapiro, A.B., Goormaghtigh, E., Ling, V., and Ruyschaert, J.M. 1996. Secondary and tertiary structure changes of reconstituted P-glycoprotein. A Fourier transform attenuated total reflection infrared spectroscopy analysis. *J. Biol. Chem.* **271**:24617-24.

131. Sonveaux, N., Vigano, C., Shapiro, A.B., Ling, V., and Ruyschaert, J.M. 1999. Ligand-mediated tertiary structure changes of reconstituted P-glycoprotein. A tryptophan fluorescence quenching analysis. *J. Biol. Chem.* **274**:17649-54.
132. Liu, R., Siemiarczuk, A., and Sharom, F.J. 2000. Intrinsic fluorescence of the P-glycoprotein multidrug transport: sensitivity of tryptophan residues to binding of drugs and nucleotides. *Biochemistry* **39**:14927-38.
133. Manciu, L., Chang, X.B., Riordan, J.R., and Ruyschaert, J.M. 2000. Multidrug resistance protein MRP1 reconstituted into lipid vesicles: secondary structure and nucleotide-induced tertiary structure changes. *Biochemistry* **39**:13026-33.
134. Manciu, L., Chang, X.B., Buyse, F., Hou, Y.X., Gustot, A., Riordan, J.R., and Ruyschaert, J.M. 2003. Intermediate structural states involved in MRP1-mediated drug transport. Role of glutathione. *J. Biol. Chem.* **278**:3347-56.
135. Vigano, C., Manciu, L., and Ruyschaert, J.M. 2005. Structure, orientation, and conformational changes in transmembrane domains of multidrug transporters. *Acc. Chem. Res.* **38**:117-26.
136. Wang, G., Pincheira, R., Zhang, M., and Zhang, J.T. 1997. Conformational changes of P-glycoprotein by nucleotide binding. *Biochem. J.* **328**:897-904.
137. Julien, M., and Gros, P. 2000. Nucleotide-induced conformational changes in P-glycoprotein and in nucleotide binding site mutants monitored by trypsin sensitivity. *Biochemistry* **39**:4559-68.
138. Mao, Q., Qiu, W., Weigl, K.E., Lander, P.A., Tabas, L.B., Shepard, R.L., Dantzig, A.H., Deeley, R.G., and Cole, S.P.C. 2002. GSH-dependent photolabeling of multidrug resistance protein MRP1 (ABCC1) by [<sup>125</sup>I]LY475776. Evidence of a major binding site in the COOH-proximal membrane spanning domain. *J. Biol. Chem.* **277**:28690-9.
139. Leslie, E.M., Létourneau, I.J., Deeley, R.G., and Cole, S.P.C. 2003. Functional and structural consequences of cysteine substitutions in the NH<sub>2</sub>

proximal region of the human multidrug resistance protein 1 (MRP1/ABCC1). *Biochemistry* **42**:5214-24.

140. Ren, X.Q., Furukawa, T., Nakajima, Y., Takahashi, H., Aoki, S., Sumizawa, T., Haraguchi, M., Kobayashi, M., Chijiwa, K., and Akiyama, S. 2005. GSH inhibits trypsinization of the C-terminal half of human MRP1. *J. Biol. Chem.* **280**:6231-7.
141. Rothnie, A., Callaghan, R., Deeley, R.G., and Cole, S.P.C. 2006. Role of GSH in estrone sulfate binding and translocation by the multidrug resistance protein 1 (MRP1/ABCC1). *J. Biol. Chem.* **281**:13906-14.
142. Rothnie, A., Conseil, G., Lau, A.Y., Deeley, R.G., and Cole, S.P.C. 2008. Mechanistic differences between GSH transport by MRP1 (ABCC1) and GSH modulation of MRP1-mediated transport. *Mol. Pharmacol.* **74**:1630-40.
143. Loo, T.W., and Clarke, D.M. 1995. Membrane topology of a cysteine-less mutant of human P-glycoprotein. *J. Biol. Chem.* **270**:843-8.
144. Taylor, A.M., Storm, J., Soceneantu, L., Linton, K.J., Gabriel, M., Martin, C., Woodhouse, J., Blott, E., Higgins, C.F., and Callaghan, R. 2001. Detailed characterization of cysteine-less P-glycoprotein reveals subtle pharmacological differences in function from wild-type protein. *Br. J. Pharmacol.* **134**:1609-18.
145. Loo, T.W., and Clarke, D.M. 1996. Inhibition of oxidative cross-linking between engineered cysteine residues at positions 332 in predicted transmembrane segments (TM) 6 and 975 in predicted TM12 of human P-glycoprotein by drug substrates. *J. Biol. Chem.* **271**:27482-7.
146. Loo, T.W., and Clarke, D.M. 1999. Determining the structure and mechanism of the human multidrug resistance P-glycoprotein using cysteine-scanning mutagenesis and thiol-modification techniques. *Biochim. Biophys. Acta* **1461**:315-25.

147. Loo, T.W., and Clarke, D.M. 2005. Recent progress in understanding the mechanism of P-glycoprotein-mediated drug efflux. *J. Membr. Biol.* **206**:173-85.
148. Stenham, D.R., Campbell, J.D., Sansom, M.S., Higgins, C.F., Kerr, I.D., and Linton, K.J. 2003. An atomic detail model for the human ATP binding cassette transporter P-glycoprotein derived from disulfide cross-linking and homology modeling. *FASEB J.* **17**:2287-9.
149. Yang, R., Cui, L., Hou, Y.X., Riordan, J.R., and Chang, X.B. 2003. ATP binding to the first nucleotide binding domain of multidrug resistance-associated protein plays a regulatory role at low nucleotide concentration, whereas ATP hydrolysis at the second plays a dominant role in ATP-dependent leukotriene C<sub>4</sub> transport. *J. Biol. Chem.* **278**:30764-71.
150. Lee, S.H., and Altenberg, G.A. 2003. Transport of leukotriene C<sub>4</sub> by a cysteine-less multidrug resistance protein 1 (MRP1). *Biochem. J.* **370**:357-60.
151. Falke, J.J., and Koshland, D.E.Jr. 1987. Global flexibility in a sensory receptor: a site-directed cross-linking approach. *Science* **237**:1596-600.
152. Ito, K., Olsen, S.L., Qiu, W., Deeley, R.G., and Cole, S.P.C. 2001. Mutation of a single conserved tryptophan in multidrug resistance protein 1 (MRP1/ABCC1) results in loss of drug resistance and selective loss of organic anion transport. *J. Biol. Chem.* **276**:15616-24.
153. Goodno, C.C. 1982. Myosin active-site trapping with vanadate ion. *Methods Enzymol.* **85** Pt B:116-23.
154. Dani, V.S., Ramakrishnan, C., and Varadarajan, R. 2003. MODIP revisited: re-evaluation and refinement of an automated procedure for modeling of disulfide bonds in proteins. *Protein Eng.* **16**:187-93.
155. Yu, X., and Egelman, E.H. 1992. Direct visualization of dynamics and cooperative conformational changes within RecA filaments that appear to be associated with the hydrolysis of adenosine 5'-O-(3-thiotriphosphate). *J. Mol. Biol.* **225**:193-216.

156. Neumann, L., Abele, R., and Tampé, R. 2002. Thermodynamics of peptide binding to the transporter associated with antigen processing (TAP). *J. Mol. Biol.* **324**:965-73.
157. Li, C., Krishnamurthy, P.C., Penmatsa, H., Marrs, K.L., Wang, X.Q., Zaccolo, M., Jalink, K., Li, M., Nelson, D.J., Schuetz, J.D., and Naren, A.P. 2007. Spatiotemporal coupling of cAMP transporter to CFTR chloride channel function in the gut epithelia. *Cell* **131**:940-51.
158. Kikuchi, S., Hata, M., Fukumoto, K., Yamane, Y., Matsui, T., Tamura, A., Yonemura, S., Yamagishi, H., Keppler, D., Tsukita, S., and Tsukita, S. 2002. Radixin deficiency causes conjugated hyperbilirubinemia with loss of Mrp2 from bile canalicular membranes. *Nat. Genet.* **31**:320-5.
159. Trakselis, M.A., Alley, S.C., and Ishmael, F.T. 2005. Identification and mapping of protein-protein interactions by a combination of cross-linking, cleavage, and proteomics. *Bioconj. Chem.* **16**:741-50.
160. Borch, J., Jorgensen, T.J., and Roepstorff, P. 2005. Mass spectrometric analysis of protein interactions. *Curr. Opin. Chem. Biol.* **9**:509-16.
161. Mao, Q., Leslie, E.M., Deeley, R.G., and Cole, S.P.C. 1999. ATPase activity of purified and reconstituted multidrug resistance protein MRP1 from drug-selected H69AR cells. *Biochim. Biophys. Acta* **1461**:69-82.
162. Mao, Q., Deeley, R.G., and Cole, S.P.C. 2000. Functional reconstitution of substrate transport by purified multidrug resistance protein MRP1 (ABCC1) in phospholipids vesicles. *J. Biol. Chem.* **275**:34166-72.
163. Wu, P., Oleschuk, C.J., Mao, Q., Keller, B.O., Deeley, R.G., and Cole, S.P.C. 2005. Analysis of human multidrug resistance protein 1 (ABCC1) by matrix-assisted laser desorption ionization/time of flight mass spectrometry: toward identification of leukotriene C<sub>4</sub> binding sites. *Mol. Pharmacol.* **68**:1455-65.

164. Hipfner, D.R., Gauldie, S.D., Deeley, R.G., and Cole, S.P.C. 1994. Detection of the Mr 190,000 multidrug resistance protein, MRP, with monoclonal antibodies. *Cancer Res.* **54**:5788-92.
165. Peitsch, W.K., Bulkescher, J., Spring, H., Hofmann, I., Goerdts, S., and Franke, W.W. 2006. Dynamics of the actin-binding protein drebrin in motile cells and definition of a juxtannuclear drebrin-enriched zone. *Exp. Cell Res.* **312**:2605-18.
166. Li, C., Roy, K., Dandridge, K., and Naren, A.P. 2004. Molecular assembly of cystic fibrosis transmembrane conductance regulator in plasma membrane. *J. Biol. Chem.* **279**:24673-84.
167. Feldhoff, P.W., Mirski, S.E., Cole, S.P.C., and Sullivan, D.M. 1994. Altered subcellular distribution of topoisomerase II alpha in a drug-resistant human small cell lung cancer cell line. *Cancer Res.* **54**:756-62.
168. Motley, A., Bright, N.A., Seaman, M.N., and Robinson, M.S. 2003. Clathrin-mediated endocytosis in AP-2-depleted cells. *J. Cell Biol.* **162**:909-18.
169. Pappin, D.J., Hojrup, P., and Bleasby, A.J. 1993. Rapid identification of proteins by peptide-mass fingerprinting. *Curr. Biol.* **3**:327-32.
170. Hayashi, K., Ishikawa, R., Kawai-Hirai, R., Takagi, T., Taketomi, A., and Shirao, T. 1999. Domain analysis of the actin-binding and actin-remodeling activities of drebrin. *Exp. Cell Res.* **253**:673-80.
171. Grønberg, M., Kristiansen, T.Z., Stensballe, A., Andersen, J.S., Ohara, O., Mann, M., Jensen, O.N., and Pandey, A. 2002. A mass spectrometry-based proteomic approach for identification of serine/threonine-phosphorylated proteins by enrichment with phosphor-specific antibodies: identification of a novel protein, Frigg, as a protein kinase A substrate. *Mol. Cell Proteomics.* **1**:517-27.
172. Cross, R.L. 2004. Molecular motors: turning the ATP motor. *Nature* **427**:407-8.

173. Erickson, H.P. 2007. Evolution of the cytoskeleton. *Bioessays* **29**:668-77.
174. Crozat, A., Aman, P., Mandahl, N., and Ron, D. 1993. Fusion of CHOP to a novel RNA-binding protein in human myxoid liposarcoma. *Nature* **363**:640-4.
175. Rabbitts, T.H., Forster, A., Larson, R., and Nathan, P. 1993. Fusion of the dominant negative transcription regulator CHOP with a novel gene FUS by translocation t(12;16) in malignant liposarcoma. *Nat. Genet.* **4**:175-80.
176. Shirao, T., Kojima, N., Kato, Y., and Obata, K. 1988. Molecular cloning of a cDNA for the developmentally regulated brain protein, drebrin. *Brain Res.* **464**:71-4.
177. Kelleher, D.J., and Gilmore, R. 2006. An evolving view of the eukaryotic oligosaccharyltransferase. *Glycobiology* **16**:47R-62R.
178. Butkevich, E., Hulsmann, S., Wenzel, D., Shirao, T., Duden, R., and Majoul, I. 2004. Drebrin is a novel connexin-43 binding partner that links gap junctions to the submembrane cytoskeleton. *Curr. Biol.* **14**:650-8.
179. Golemis, E.A., and Adams, P.D. 2005. "Protein-protein interactions-A molecular cloning manual", 2nd edition, CSHL press, Cold Spring Harbor, New York. pp.55-62
180. Calvio, C., Neubauer, G., Mann, M., and Lamond, A.I. 1995. Identification of hnRNP P2 as TLS/FUS using electrospray mass spectrometry. *RNA* **1**:724-33.
181. Sinz, A. 2006. Chemical cross-linking and mass spectrometry to map three-dimensional protein structures and protein-protein interactions. *Mass Spectrom. Rev.* **25**:663-82.
182. Kock, S., Maehr, R., Overkleeft, H.S., Wang, E.W., Iyer, L.K., Lennon-Dumenil, A.M., Ploegh, H.L., and Kessler, B.M. 2003. Functional proteomics

of the active cysteine protease content in *Drosophila* S2 cells. *Mol. Cell Proteomics* **2**:1188-97.

183. Elion, E.A. 2007. Detection of protein-protein interactions by coprecipitation. *Curr. Protoc. Immunol.* Chapter 8:Unit 8.7.
184. Wyles, J.P., Wu, Z., Mirski, S.E., and Cole, S.P.C. 2007. Nuclear interactions of topoisomerase II alpha and beta with phospholipids scramblase 1. *Nucleic Acids Res.* **35**:4076-85.
185. Waters, B.L., Panagopoulos, I., and Allen, E.F. 2000. Genetic characterization of angiomatoid fibrous histiocytoma identifies fusion of the FUS and ATF-1 genes induced by a chromosomal translocation involving bands 12q13 and 16p11. *Cancer Genet. Cytogenet.* **121**:109-16.
186. Storlazzi, C.T., Mertens, F., Nascimento, A., Isaksson, M., Wejde, J., Brosjo, O., Mandahl, N., and Panagopoulos, I. 2003. Fusion of the FUS and BFB2H7 genes in low grade fibromyxoid sarcoma. *Hum. Mol. Genet.* **12**:2349-58.
187. Panagopoulos, I., Aman, P., Fioretos, T., Hoglund, M., Johansson, B., Mandahl, N., Heim, S., Behrendtz, M., and Mitelman, F. 1994. Fusion of the FUS gene with ERG in acute myeloid leukemia with t(16;21)(p11;q22). *Genes Chromosomes Cancer* **11**:256-62.
188. Pérez-Losada, J., Sánchez-Martín, M., Rodríguez-García, M.A., Pérez-Mancera, P.A., Pintado, B., Flores, T., Battaner, E., and Sánchez-García, I. 2000. Liposarcoma initiated by FUS/TLS-CHOP: the FUS/TLS domain plays a critical role in the pathogenesis of liposarcoma. *Oncogene* **19**:6015-22.
189. Ishikawa, R., Hayashi, K., Shirao, T., Xue, Y., Takagi, T., Sasaki, Y., and Kohama, K. 1994. Drebrin, a development-associated brain protein from rat embryo, causes the dissociation of tropomyosin from actin filaments. *J. Biol. Chem.* **269**:29928-33.
190. Sasaki, Y., Hayashi, K., Shirao, T., Ishikawa, R., and Kohama, K. 1996. Inhibition by drebrin of the actin-bundling activity of brain fascin, a protein localized in filopodia of growth cones. *J. Neurochem.* **66**:980-8.

191. Jin, M., Tanaka, S., Sekino, Y., Ren, Y., Yamazaki, H., Kawai-Hirai, R., Kojima, N., and Shirao, T. 2002. A novel, brain-specific mouse drebrin: cDNA cloning, chromosomal mapping, genomic structure, expression, and functional characterization. *Genomics* **79**:686-92.
192. Peitsch, W.K., Hofmann, I., Bulkescher, J., Hergt, M., Spring, H., Bleyl, U., Goerdts, S., Franke, W.W. 2005. Drebrin, an actin-binding, cell-type characteristic protein: induction and localization in epithelial skin tumors and cultured keratinocytes. *J. Invest. Dermatol.* **125**:761-74.
193. Marcantonio, E.E., Amar-Costesec, A., and Kreibich, G. 1984. Segregation of the polypeptide translocation apparatus to regions of the endoplasmic reticulum containing ribophorins and ribosomes. II. Rat liver microsomal subfractions contain equimolar amounts of ribophorins and ribosomes. *J. Cell Biol.* **99**:2254-9.
194. Yan, Q., and Lennarz, W.J. 2002. Studies on the function of oligosaccharyl transferase subunits. Stt3p is directly involved in the glycosylation process. *J. Biol. Chem.* **277**:47692-700.
195. Fu, J., and Kreibich, G. 2000. Retention of subunits of the oligosaccharyltransferase complex in the endoplasmic reticulum. *J. Biol. Chem.* **275**:3984-90.
196. Wilson, C.M., Roebuck, Q., and High, S. 2008. Ribophorin I regulates substrate delivery to the oligosaccharyltransferase core. *Proc. Natl. Acad. Sci. USA* **105**:9534-9.
197. Krendel, M., and Mooseker, M.S. 2005. Myosins: tails (and heads) of functional diversity. *Physiology* **20**:239-51.
198. Swiatecka-Urban, A., Boyd, C., Coutermarsh, B., Karlson, K.H., Barnaby, R., Aschenbrenner, L., Langford, G.M., Hasson, T., and Stanton, B.A. 2004. Myosin VI regulates endocytosis of the cystic fibrosis transmembrane conductance regulator. *J. Biol. Chem.* **279**:38025-31.

199. Swiatecka-Urban, A., Talebian, L., Kanno, E., Moreau-Marquis, S., Coutermarsh, B., Hansen, K., Karlson, K.H., Barnaby, R., Cheney, R.E., Langford, G.M., Fukuda, M., and Stanton, B.A. 2007. Myosin Vb is required for trafficking of the cystic fibrosis transmembrane conductance regulator in Rab11a-specific apical recycling endosomes in polarized human airway epithelial cells. *J. Biol. Chem.* **282**:23725-36.
200. Eddinger, T.J., and Meer, D.P. 2007. Myosin II isoforms in smooth muscle: heterogeneity and function. *Am. J. Physiol. Cell Physiol.* **293**:C-493-508.
201. Borch, J., Jorgensen, T.J., and Roepstorff, P. 2005. Mass spectrometric analysis of protein interactions. *Curr. Opin. Chem. Biol.* **9**:509-16.
202. Washburn, M.P., Wolters, D., and Yates, J.R., 3<sup>rd</sup>. 2001. Large-scale analysis of the yeast proteome by multidimensional protein identification technology. *Nat. Biotechnol.* **19**:242-7.
203. Wang, X., Venable, J., LaPointe, P., Hutt, D.M., Koulov, A.V., Coppinger, J., Gurkan, C., Kellner, W., Matteson, J., Plutner, H., Riordan, J.R., Kelly, J.W., Yates, J.R.3<sup>rd</sup>, and Balch, W.E. 2006. Hsp90 cochaperone Aha1 downregulation rescues misfolding of CFTR in cystic fibrosis. *Cell* **127**:803-15.